This is to certify that the
thesis entitled

USE OF QCM TECHNOLOGY FOR MEASURING BARRIER
PROPERTIES OF BIODEGRADABLE PACKAGING
MATERIAL

presented by

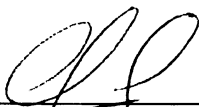NITIN GULATI

has been accepted towards fulfillment
of the requirements for the

Master of Science	degree in	Packaging

_____
Major Professor's Signature

O2 - 11 - O8
_____
Date

PLACE IN RETURN BOX to remove this checkout from your record.
TO AVOID FINES return on or before date due.
MAY BE RECALLED with earlier due date if requested.

DATE DUE	DATE DUE	DATE DUE

6/07 p:/CIRC/DateDue.indd-p.1

USE OF QCM TECHNOLOGY FOR MEASURING BARRIER PROPERTIES OF
BIODEGRADABLE PACKAGING MATERIAL

BY

NITIN GULATI

A THESIS

Submitted to
Michigan State University
in partial fulfillment of the requirements
for the degree of

MASTER OF SCIENCE

School of Packaging

2008

ABSTRACT

USE OF QCM TECHNOLOGY FOR MEASURING BARRIER PROPERTIES OF BIODEGRADABLE PACKAGING MATERIAL
By

NITIN GULATI

For measuring the sorption of water vapor on PLA for three different temperatures with relative humidity ranging from 20 % to 80 %, a new system based on quartz crystal microbalance (QCM) was built. For this purpose 1 % wt/v PLA was dissolved in THF at 35°C, and the polymer film was produced on the surface of the crystal using spin coating. After spin coating the polymer on the crystal, coated crystals were kept in a vacuum oven for 5 hours at 60 °C. Polymer films having a thickness of 1.25±0.29 μm were obtained with a crystallinity of 21.3 ± 2.3 %, glass transition temperature of 62.3 ± 1.4°C and melting point temperature of 151.5 ± 1.0° C. Then, coated crystals were kept in flow cells housed in a peltier chamber and water vapors generated by a computer control humidity generator were allowed to enter into the flow cells. Water vapor diffusion coefficients (D) in the range of 2.6 to 5.67 x 10^{-15} m^2 / sec , solubility coefficient (S) in the range of 0.33 to 11.0 x 10^{-2} Kg/m^3-Pa and permeability coefficient (P) in the range of 0.07 to 3.17 x 10^{-16} (Kg-m/m^2-sec-Pa) were obtained at temperatures of 10, 23 & 40 °C for relative humidity ranging from 20 to 80 %.

Equilibration time required for determining barrier properties of polymer was reduced significantly with this technique as compared to traditional methods. QCM technology was successful to measure water sorption in PLA.

To my parents and friends

Acknowledgements

Table of contents

List of Tables

List of Figures

viii

1 INTRODUCTION

As a product is packaged, it starts undergoing a series of dynamic changes, such as exchange of small molecule compounds from the external environment into the package and from the package to external environment. These molecular exchanges between the product and the package are termed as mass transfer interactions and they extend through out the shelf life of the package. These interactions play a crucial role in preserving the quality of the products stored inside the package. Since plastic based packaging materials are permeable to smaller molecules such as water vapor, organic vapors and liquids, the extent of mass transfer interactions can have a significant effect on the barrier performance of plastic based packaging materials. Therefore, it becomes necessary to understand the mass transfer process or the interactions to predict the barrier performance of the packaging materials and for optimizing the product shelf life.

Mass transfer interactions in polymers are categorized as diffusion of compounds through the polymer membrane, sorption of compounds by the polymer and migration from the polymer into the product. Diffusion can be defined as the movement of molecules from the area of high chemical potential or concentration to low chemical potential or concentration. As the permeant molecules diffuse through the polymer structure, they move within the free volume available in the amorphous regions of the polymer. Diffusion is a concentration–gradient controlled process and may avail reactants for chemical reactions between the product and the permeant, which can deteriorate the quality of the product.

Sorption is the uptake of moisture, flavor compounds or organic vapors by the packaging material. The extent of the sorption process mainly depends on the affinity

1

between the sorbate molecule and the polymeric material. In rubbery polymers, for low

concentration of permeants, sorption can be explained by the Henry's law of solubility,

which is expressed as

$$C = S*p \qquad (1-1)$$

where C is the concentration of the permeant, p is the partial vapor pressure and S is the

solubility coefficient.

Permeation is defined as the movement of organic vapors, gases across

homogenous polymeric packaging materials excluding the movement through the

pinholes, cracks or perforations present in the packaging material. Permeation involves

the dissolution of the permeant molecule followed by the transfer through the polymeric

membrane. Permeation process mainly depends on the mobility factor (diffusion of the

permeant in the polymer structure) and the solubility, which is the ratio of equilibrium

permeant concentration inside the polymer and the penetrant partial pressure. Diffusion

coefficient (D) and solubility coefficient (S) are used to calculate permeability coefficient

(P) when the Henry's law is obeyed

$$P = D*S \qquad (1-2)$$

Permeability coefficient (P) is a measure of the ability of the polymer to

allow transport of permeants through it; low barrier polymers are highly permeable where

as high barrier polymers are less permeable. Even though some polymeric packaging

materials act as a better barrier to specific compounds and they might be poor barrier to

other compounds. Barrier performance of polymer is significantly affected by the product

– package compatibility and the external environmental conditions. Mass transfer

interactions between the packaging material and product on a very small level can

2

accelerate further changes such as flavor loss, oxidation of the product, morphological changes in polymer and its degradation. As food items and drugs are items of direct consumption, any deterioration in their quality due to mass transfer interactions may be highly dangerous and have serious consequences. So, it becomes very important to properly understand mass transfer process and the impact of external environmental conditions on the barrier performance of the polymer.

Several conventional methods such as isostatic, quasi-isostatic, gravimetric technique, isopiestic technique, thermal stripping and desorption have been developed to determine barrier characteristics of polymers [1-4]. Studies measuring the sorption phenomenon of various compounds in glassy polymers, using these conventional methods have produced reliable and accurate results. The challenge involved with using these techniques is their tendency to become inaccurate at low vapor pressures or at low concentration of permeants and long equilibration times required to reach the steady state [4-7].

Quartz crystal microbalance (QCM), which works on the principle of piezoelectricity, offers excellent sensitivity, accuracy and simplicity to measure changes taking place on the surface of a crystal. QCM is an excellent mass sensor because of its capability to measure sub-nanogram changes at the solid-air and solid-liquid interfaces. It has already been used as an *in situ* mass detector to study a wide variety of materials and for sorption measurements [8-10].

With the increasing focus on using biodegradable polymeric materials in commercial packaging applications, polylactide (PLA), a biodegradable polymer made from corn starch has emerged as an alternate to the petroleum-based polymers. Growing

demand for PLA in the marketplace as a packaging material in short lived and commercial food packaging applications, which were initially served by the petroleum-based polymers such as polyethylene terepthalate (PET), required characterization of barrier properties of PLA. Water vapor permeability coefficient (P) for PLA was found lower than polystyrene (PS) but higher than those of polyethylene terepthalate (PET) [11]. Sorption isotherms for PLA films stored at temperatures of 5, 23 and 40 °C and water activity (a_w) ranging from 0.11 to 0.94 were studied, but no values were generated as the water absorption in those films was lower than the equipment sensitivity [12].

Another emerging issue with the advancement in processing technologies for producing high barrier polymers is that, it has become more difficult to assess their barrier characteristics using conventional methods. Therefore, it becomes necessary to utilize a technique or methodology which has a measurement range of mass uptake lower than above mentioned methods and shorten the equilibration times in permeation measurements while maintaining excellent sensitivity and accuracy [13, 14].

As water vapor sorption on PLA has been reported to be lower than 100 ppm, which is lower than the sensitivity range of most of the instruments available. QCM provides a new alternative for measuring the low levels of water vapor sorption in PLA. QCM offers the advantage of reducing the equilibration times for reaching the steady state; it can collectively be used as a tool to derive diffusion coefficient (D), solubility coefficient (S) and permeability coefficient (P) from the data generated from the measurements.

The objective of this thesis was to determine the water vapor barrier properties of PLA at 10, 23 and 40 °C at relative humidity ranging from 20 to 80 % using QCM.

2 LITERATURE REVIEW

2.1 Introduction

The first part of this chapter presents an overview of the process, to determine diffusion (D), solubility (S) and permeability (P) coefficients using the lag-time method. The second part of this chapter focuses on Quartz Crystal Microbalance (QCM) as a technique for mass sorption sensing, research done by using QCM, and problems faced and solutions to those problems. The last part of this chapter focuses on poly(lactide) as a commercial packaging polymer, its barrier properties and the problems associated in measuring its barrier properties.

2.2 Overview of permeation process

Packaging interactions in packaging systems start from the moment the packaging material and the product come in contact with each other and the external environment during its production, processing, packaging and storage. These interactions extend through out the life of the package. For a permeation process to take place through the polymeric packaging material, the permeant molecule should be first absorbed at the interacting phase between the polymer and the surrounding environment and then diffuse through the polymer structure. The main driving force for a permeation process to occur is the tendency of the permeant molecule to equilibrate its chemical activity. This results in the transfer of the permeant molecule from a region of high chemical activity or high concentration to low chemical activity or low concentration. Therefore, any molecular

species which are not in thermodynamic equilibrium will tend to equilibrate their chemical potential.
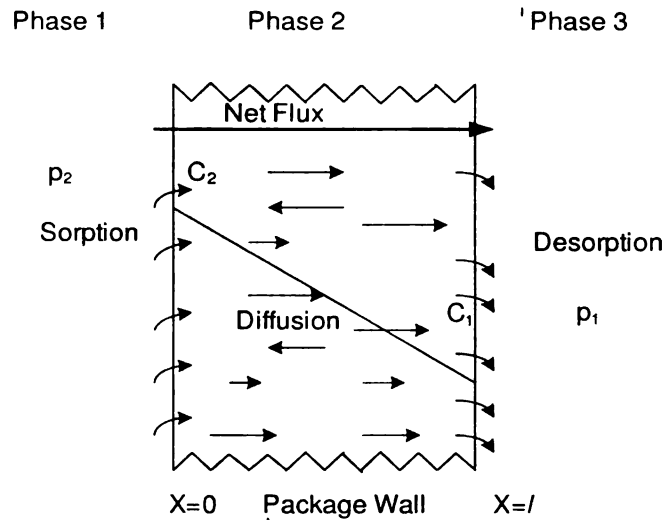
Figure 2-1 Sorption, desorption and diffusion process across a plastic sheet

Permeation process can be described as a three step procedure which are sorption, diffusion and desorption as shown in figure 2-1, which involves the adsorption of permeant molecule at high concentration side (p2). The concentration of the permeant at this interface may be determined by the Henry's Law of solubility which is

$$C = S.p \qquad (2\text{-}1)$$

where S is the solubility coefficient and p is the partial pressure. Solubility coefficient is a function of partial pressure of the vapor or the gas in the contacting phase. Henry's law of solubility holds well for real solutions as long as they are dilute and there is no interaction between the polymer and the penetrant molecule [15]. For strong interaction between the penetrant and the polymer, different models explaining the solubility can be found elsewhere [15].

After the permeant is adsorbed on the polymer interface, it starts to diffuse through the polymer film until the concentration of the penetrant becomes equal at both

7

sides. The ability of the permeant molecule to diffuse through the polymer film is greatly influenced by the physical and chemical structure of the polymer. After diffusing through the polymer film, the permeant molecule reaches the low concentration side (p1) and is desorbed from the polymer interface into the contacting media.

The rate of transfer of permeant and the amount of permeant transferred through the polymer film can be derived from Fick's first law of diffusion, which is based on the hypothesis that the rate of transfer of diffusing substance through unit area of a section is proportional to the concentration gradient measured normal to the section [5]. Fick's first law of diffusion can be expressed as

$$F = -D \frac{\partial c}{\partial x} \qquad (2\text{-}2)$$

where F is the rate of transfer per unit area, C is the concentration of the diffusing substance, x is the distance in direction of diffusion and D is the diffusion coefficient. As the Fick's first law describes the rate of transfer of the permeant diffusing through a polymeric material of certain thickness during steady state, the diffusion coefficient can be assumed to be independent of penetrant concentration and polymer relaxations. For unsteady or transient state, the rate of flow of permeant can be described by Fick's second law which can be written as

$$\frac{\partial c}{\partial t} = D \frac{\partial^2 c}{\partial x^2} \qquad (2\text{-}3)$$

where t is the time. Mass sorbed on the polymer film as a function of time provides the necessary information to calculate the diffusion coefficient of the permeant in the polymer and the mass uptake at the equilibrium state provides the solubility of the

8

penetrant in the polymer [16]. Commonly, the diffusion coefficient is calculated from the half time method, in which sorption reaches 50 % of its extent and can be calculated as

$$D = 0.049 \frac{l^2}{t_{1/2}}$$ (2-4)

But the main disadvantage associated with determining D with this method is that, if there is any deviations from the ideal conditions, significant errors can be introduced which can not be corrected by using this method. Duda et al [17] calculated the diffusion coefficient by integrating Fick's second law under the assumption of constant diffusivity and derived the following expression for determining the diffusion coefficient (D)

$$D = \frac{\pi l^2}{4} \left[\frac{\partial (M_t / M_\infty)}{\partial t^{1/2}} \right]^2$$ (2-5)

where M_t represents the mass of the penetrant at time t, M_∞ is the mass uptake at steady state, l is the thickness of the polymer film. Since the fractional mass uptake M_t/M_∞ almost follows a linear trend for region less than 0.4, mass sorbed on the polymer as a function of sqrt(time)/thickness of film can be used to determine the diffusion coefficient of permeant in the polymer film. This method for determining the diffusion coefficient is valid only for diffusion from two sides of the polymer film.

The solubility coefficient can be calculated by dividing the mass uptake at the steady state (t = ∞) by the volume of the polymer sample and the vapor pressure at respective partial pressure

$$S = \frac{M_\infty}{v.p}$$ (2-6)

where M_∞ is the total amount (mass) of vapor absorbed by the polymer at equilibrium for a given temperature, v is the volume of the polymer sample, and p is the penetrant driving force in units of concentration or pressure. The units of S used are $kg/m^3.Pa$. After that, a procedure based on the sum of squares technique described by Barr[18] can be utilized to determine the best estimated diffusion coefficient value. Using the value of permeant flow at steady state F_∞, the permeability coefficient P (in $kg.m/m^2.s.Pa$), can be determined by the expression

P=D*S (2-7)

Hence, diffusion (D) and solubility (S) coefficients for different temperature and relative humidity conditions can be obtained, which can be further used to calculate the permeability coefficients using P=D'S at respective temperature and relative humidity conditions

2.3 Quartz Crystal Microbalance

Quartz crystal microbalance (QCM) technology is becoming a promising technology these days because of its excellent sensitivity to detect small changes on the surface of a quartz crystal and is already being used for probing adhesion of visco-elastic polymer films, in situ studies of proteins and for electrolytic solutions. The excellent sensitivity and accuracy of the quartz crystal can also be used for studying the sorption of permeants on polymers at a nano-gram level. A QCM consists of a thin quartz crystal

10

with gold electrodes plated on its both sides. Figure 2-2 represents the front and the back electrodes of a quartz crystal used in QCM.
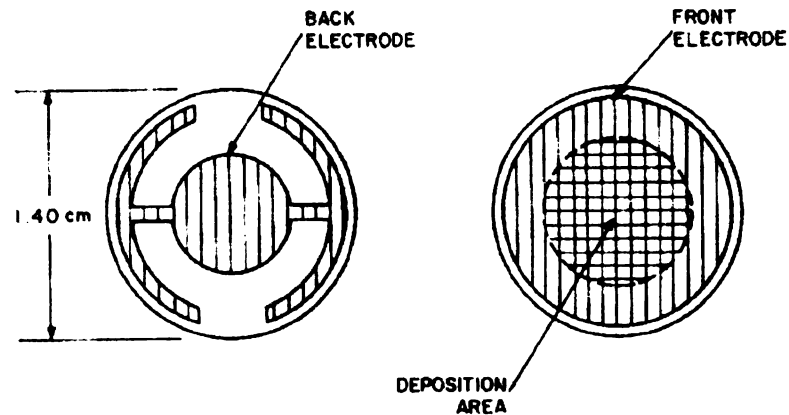
Figure 2-2 Back and front electrodes on the opposite sides of the crystal. Figure adapted from Lu and Lewis (1972) [19]

When an alternating electric field is applied across the opposite sides of a quartz crystal, by the virtue of piezoelectricity an internal mechanical stress is produced which results in a shear acoustic wave propagating normally to surface of the quartz crystal. If a quartz crystal is coupled with non- rigid materials such as polymer films, the amplitude and the phase of the acoustic wave can be influenced by mechanical properties of material As the resonant frequency of quartz crystal is affected both by mass and liquid loadings, measurement of the resonant frequency alone can not distinguish changes in surface mass from changes in solution properties .On the other side, electrical characteristics can be measured over a range of frequencies; it becomes very convenient to use a circuit model to describe the electrical behavior of quartz crystal, which can relate the circuit elements to physical properties of QCM as well as the surface mass layer and contacting liquid.

11

Butterworth-Van Dyke (BVD) equivalent circuit model can be used to describe an unloaded (without any mass or liquid loading) and loaded quartz crystal as a network of electrical parameters such as resistance (R), inductance (L) and capacitance (C) [20, 21]. The BVD circuit for a loaded crystal as shown in figure 2-3 has two arms–static arm with static capacitance (C_o), the capacitance that arises between the electrodes on the opposite sides of the crystal representing the shunt capacitance of the crystal electrodes and a motional arm in parallel with the static arm, which arises due to the electromechanical and piezoelectric coupling of the quartz crystal. Inductor (L) in the motional arm, represents the inertial component of the oscillation (related to the displacement of mass during the vibration of the crystal), capacitance (C_m) is related to the energy stored during the oscillation due to the elasticity of crystal and the surrounding medium and resistor (R) which corresponds to energy dissipated due to oscillation and from external mounting and the medium in contact.

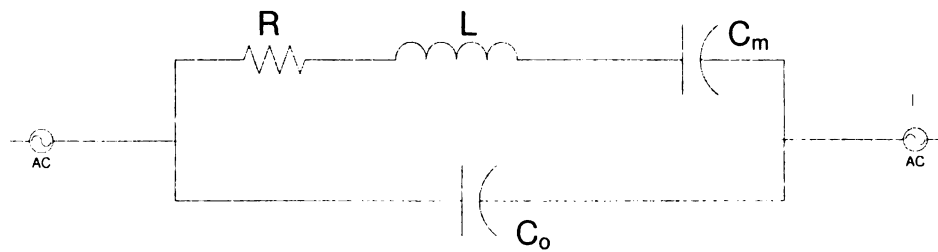Figure 2-3. Electrical equivalent circuit of a quartz crystal

The motional arm in the BVD circuit comes into play when there is a mass loading on the surface of the quartz crystal. As an electric field is applied across the sides of the crystal, fully charged capacitor (C_m) in the motional arm begins to discharge, resulting in a flow of current through the inductor (L). By the virtue of self-induction, the

12

inductor (L) resists the current flowing through it , until all of the current flowing through the inductor (L) is used to charge up the capacitor (C$_m$) again in the opposite polarity [22]. Once the current becomes zero, the capacitor (C$_m$) begins to discharge again using the energy gained by charging in the opposite polarity. If the resistance to the flow of current through the resistor (R) is zero, this process of charging and discharging of capacitor (C$_m$) continues resulting in oscillation of the crystal indefinitely. If R > 0, resistance to the flow of current will result in damping of amplitude of the oscillation and with the time, the crystal will stop oscillating. The static capacitance dominates the admittance away from the resonance, while the motional admittance dominates near the resonance which implies that the motional arm in the BVD equivalent circuit model comes into effect when an additional layer is deposited on the surface of the quartz crystal. When the static arm dominates, the crystal continues to oscillate without any dampening of the amplitude of oscillation. Details regarding calculating the physical properties of the surface layer and the contacting liquid from the electrical measurements of the quartz crystal can be found elsewhere [19, 23, 24].

As deposition of an additional mass on the surface of the quartz crystal leads to a decrease in its resonant frequency of oscillation, this frequency shift is proportional to the additional mass deposited on its surface. In 1957 Sauerbrey [25] postulated that for small mass change (up to 20 µg/cm^2), addition of foreign mass can be treated as a mass change on the surface of quartz crystal, so the resonant frequency shift obeys the relation :

$$\frac{df_q}{f_q} = -\frac{dm}{m_q} \qquad (2\text{-}8)$$

dm in equation 2-8 is the amount of additional mass deposited over the crystal surface, m_q is the mass of the quartz crystal, f_q is the resonant frequency of the unloaded crystal and

13

df_q is the shift in the resonant frequency of the crystal as a result of mass loading. Equation 2-8 can also be written as:

$$m_f = m_q (f_c - f_q) / f \qquad (2\text{-}9)$$

where m_f is the mass of the film, f_c is resonant frequency of the quartz crystal with deposited film and m_f is the mass of polymer film deposited on surface of quartz crystal. If the density of film deposited on the quartz crystal is known, the film thickness can be determined by using equation 2-10.

$$\rho_f t_f = (\rho_q t_q / f_q)(f_c - f_q) \qquad (2\text{-}10)$$

where ρ_q is the density of the quartz crystal, ρ_f is the density of polymer film, t_q is the thickness of quartz crystal, t_f is the thickness of the polymer film coated on the surface of quartz crystal.

As predicted in equation 2-10, the shift in the resonant frequency of the quartz crystal is linearly proportional to the mass deposited and is not affected by the mechanical properties of the film. Stockbridge [26] applied Rayleigh perturbation analysis to justify this fact and obtained the same frequency- mass relationship as in equation 2-10. The basic assumption in this equation was that there is no potential energy stored in the mass added on the surface of the crystal during its oscillation, which further implied that the mechanical energy of the crystal did not have any impact on the crystal oscillation. This approach for determining the mass frequency relationship was termed as "frequency measurement technique" [25].The maximum frequency shift allowed by the "frequency measurement technique" was only about 2 % of the original frequency for measuring the thickness of the layer deposited with reasonable accuracy. Lu et al reported that accuracy in mass determinations can be minimized to an error of less than 2 % if the

mass loading of the crystal is kept less than 2 µg/cm² [9, 27]. However, when the mass of the deposited material becomes appreciable and forms a uniform layer of finite thickness, the basic assumption that acoustic waves do not propagate in the film becomes less acceptable and errors in mass determination become less tolerable.

With improved crystal design and attempts to improve the mass loading capability of quartz crystal, a new theory termed as "period oscillation technique" was introduced in 1971 by Behrndt [28, 29] which correlates the change in period of oscillation and the deposited mass as

$$\frac{\tau_f - \tau_q}{\tau_q} = \frac{\Delta M}{M_q} \tag{2-11}$$

τ_f and τ_q in equation 2-11 are the oscillation periods for QCM before and after mass loading respectively. Equation 2-11 when compared with equation 2-10 is remarkably accurate and makes more sense mathematically as the deposited mass is now linearly proportional to the change in period of oscillations where as Sauerbrey's equation is based on an inverse proportionality .

$$\frac{\Delta M_q}{M_q} = \frac{\Delta l_q}{l_q} = \frac{\Delta \tau_q}{\tau_q} = -\frac{\Delta f_q}{f_q} \tag{2-12}$$

By using "period oscillation technique" for measuring the frequency shift, more than 10 % of the resonant frequency could be measured. However, the elastic properties of the deposited material were not considered into this mass frequency relationship. Lu et al suggested a different approach for improving the accuracy of QCM, and stated that the resonant frequency of a composite system of quartz crystal and film can also be

determined by considering the acoustic properties of the film and derived the following

equation:

$$\tan(\pi.f_c / f_q) = -(1/Z)\tan(\pi.f_c / f_f)$$ (2-13)

where $$Z = \frac{Z_q}{Z_f} = \rho_q \upsilon_q / \rho_f \upsilon_f$$ (2-14)

Z_q is the acoustic impedance of quartz crystal, Z_f is the acoustic impedance of polymer

film, υ_f and υ_q are the shear wave velocity in coated film and in the crystal. By solving

equation (2-13) algebraically, it can be reduced to

$$\frac{\Delta M}{M} = -\frac{1}{Z}.\frac{f_q}{\pi f}\arctan(Z.\tan\frac{\pi f}{f_q})$$ (2-15)

where ΔM is the mass change, Z is the shear mode acoustic impedance ratio between the

quartz crystal and film deposited on the quartz's surface. Equation 2-15 was termed as Z-

match equation [22, 30-32], and it considers the acoustic impedance of the deposited film

and quartz crystal for determining the mass uptake on the polymer film deposited on the

quartz crystal. The only drawback of using this technique is the fact that information

regarding the shear modulus of different polymer films is not always readily available.

These polymer films coated on crystal surface may result in deviations in the frequency

shift predicted from the Sauerbrey equation and introduce non-gravimetric behavior in

the measurements. Carsten et al [33] demonstrated a method for quickly determining the

shear modulus of the polymer films coated on a crystal surface.

Gas sorption in glassy polymers is traditionally studied by using conventional methods like gravimetric techniques, pressure decay method and inverse gas chromatography [10]. The results obtained from traditional measuring methods regarding the solubility of sorbents in glassy polymers have been found accurate and can be further utilized for investigating pure gas diffusion measurements [4-6]. The main disadvantage associated with using these techniques is that they become inaccurate at low vapor pressures which tend to increase the equilibration times required to reach the steady state, which can be extended up to weeks or more . QCM technique has been reported as a very accurate, rapid and reliable technique for measuring the gas sorption phenomenon in polymers as it significantly reduces the equilibration times required to reach the steady state [10, 34-37].

Various studies have been done for studying the sorption of gases and organic vapors in glassy polymers using QCM technique, and this technique has been established as a valuable tool for assessment of solubility and diffusion parameters in rubbery polymer systems [16]. Zhang et al [38] explored the fundamental phenomenon associated with the sorption of carbon dioxide in thin glassy polymers films such as poly(ethylene terephthalate) (PET), poly(methyl methacrylate) (PMMA), and polysulfone using a QCM. Polymer films in thickness range of 350 - 550 nm were coated on the crystal surface using spin coating method, and the sorption levels of carbon dioxide and other organic vapors associated with these polymer systems compared favorably well with the previous reported values on thick films obtained from conventional methods. Wong et al. [10] developed an isopiestic apparatus using a QCM to measure the solubilities of benzene, toluene and chloroform in poly(styrene) in a concentrated polymer regime.

17

Significant adsorption especially for the polar solvents on the metal electrodes was expected at higher solvent pressures so both faces of the crystal were coated completely using spray coating process. Adhesion of the polymer film to quartz crystal electrode is very crucial factor in sorption studies using QCM, as the changes in inertial coupling of film coated on the quartz crystal leads to hysteresis and might introduce error in the frequency measurements. Equilibration times were reported to be achieved much faster in thin films in these experiments as compared with other techniques. Spin coating has been recommended as the preferred method for coating the polymer film on the surface of the crystal, as it also helps in producing thin and uniform films on the crystal surface[10]. Thermally treating the coated polymer films at 5°C above their glass transition temperature also helps in producing more uniform films, without any cracks and surface irregularities [39].

Rigorous control over the flowing regime of the carrier gas for studying transient and steady state in sorption measurement is described as very crucial as deviations in the flow of the carrier gas can have an effect on the frequency shift resolution of the crystal [40]. Any instability in the flow of the carrier gas will induce fluctuations of the vibrating frequency due to local density fluctuation in boundary layer of the carrier gas adherent to the vibrating surface The carrier gas to be used for carrying the vapors into the flow cell for the sorption experiments should be chemically inert against the electrodes of the quartz crystal and must not react with the deposited layer, as it will block the sites of adsorption for vapors at the layer on the surface of the crystal and will interfere with sorption of vapors of interest.

Another important parameter that affects the stability of the resonant frequency of quartz crystal is the hydrodynamic regime of the carrier gas which sweeps through the cell. Oliveira et al. [11] considered the frequency change due to the injection of gas or solvent into the flow cell housing the coated and the uncoated crystal as a sum of four independent terms, a) ΔF_p – the frequency change to due to hydrostatic pressure b) ΔF_v - change in frequency as a function of properties of gas and crystal, c) ΔF_s frequency change associated with the sorption of vapor on the polymer/crystal interface and d) the frequency change associated with the hydrostatic pressure of the carrier gas. These parameters should be measured using uncoated crystal for each temperature and pressure condition and should be established as a baseline and subtracted from the actual frequency shifts during experimental runs, so as to accurately calculate the frequency shifts associated with mass uptake of vapors on the crystal.

Vogt et al. [41] investigated the frequency and the dissipation factor of quartz resonators coated with poly(4-amonium stryenesulfonic acid) films of thickness ranging from 3 to 205 nm during exposure to saturated water vapors. At some applied layer thickness, viscoelastic nature of the layer becomes a significant part of the response of the quartz crystal, and as the films absorbed more water, they become less rigid allowing for deviations from the Sauerbrey equation. These deviations in Sauerbrey equation were observed for films thicker than 90 nm and were mainly governed by three parameters: film viscosity, thickness and the resonator frequency.

Anomalous shifts in the measured frequency were reported by Banda et al. [42] for quartz crystals coated with glassy polymers, due to non gravimetric effects. Significant errors in mass uptake measurements may arise, if the precautions related with

the film thickness and viscoelastic compliance are ignored. As described above, deviations from Sauerbrey equation were observed for films thicker then 90 nm , similar deviations were observed for film thicker then 100 nm [42].

Vapor phase doping of poly(p-phenylene vinylene) with fuming sulfuric acid was studied by Shah et al. [8] by using a QCM. Mass uptake information derived from Fick's second law was applied to the QCM data to determine the diffusion coefficient, which was found comparable to other studies. However, an unusual frequency response after an initial drop was observed which can be attributed to out of phase resonance behavior of film due to large mass uptake of water on its surface which accounted for the viscoelastic behavior and a deviation from the Sauerbrey equation.

Polymer film coated on the surface of quartz crystal, if thicker than 100 nm should be considered as a viscoelastic media since both its elastic and viscous character contribute to the mechanical compliance [43]. Morray et al. [21] proposed the use of thickness shear mode quartz resonator for determining the polymer mechanical properties, primarily the complex shear modulus. They used the BVD equivalent circuit model of surface loaded quartz resonator to characterize the impedance/ admittance characteristics to extract the film mechanical properties.

For using QCM, as a mass sensing device with polymer films thicker than 100 nm, frequency response should be corrected for viscoelastic effects as the mass uptake then holds its linearity with the change in the frequency as per the Sauerbrey equation. This corrections can be done using the Z-match equation (equation 2-15), which requires the characterization of film's mechanical properties such as shear modulus, which can be determined by using the methodology as explained by Carsten et al. [33].

2.4 Polylactide (PLA)

A major proportion of packaging materials used in commercial packaging applications comprises of synthetic polymers which are derived from non renewable sources, and their consumption rate has been growing steadily. As plastics have low weight to volume ratio, they occupy more space relative to the other materials in landfills. Due to the moisture free anaerobic environment in the landfills, degradation process for the plastic materials is extremely slow. As a result of very slow degradation or no degradation at all in some plastic materials, concerns have been growing regarding the degradability of plastic polymers and the increase of municipal solid waste. Increasing environmental concerns with the depletion of non-renewable sources, degradability of plastic materials, demand for developing polymers which are truly biodegradable has been increasing.

Polylactide, a biodegradable polymer, derived from lactic acid is obtained from renewable sources and presents numerous advantages over conventional petroleum based polymers such as significant energy savings, recyclability and compostability. Extensive research studies have been able to demonstrate polylactide as an economically feasible packaging polymer (43-45).

Widespread availability of PLA in marketplace has helped to develop commercial applications in the packaging industry, initially assigned for petroleum based polymers. Auras et al. [44] reported that PLA showed comparable barrier properties such as CO_2, O_2 permeability coefficients to those of PET and lower than PS. PLA is a very good barrier to d-limonene, ethyl acetate, and its barrier to these compounds can be compared

to PET and Nylon-6. The amount of lactic acid which migrates from PLA to solutions is even lower than current dietary intake of lactic acid values as reported by Food Drug Administration, US Department of Agriculture. These properties of PLA make it a popular choice for replacing traditional polymers in commercial food packaging applications. Now a days, PLA is being used as a primary packaging material in short life food packaging applications for fresh fruits and vegetables such as thermoformed containers, salad trays, and dairy packaging. In addition to that, PLA is also being used in consumer goods and display packaging, threaded containers, bottles and jars. In these short lived food packaging applications for fresh fruits and vegetables, primary containers are exposed to varying relative humidity conditions which might trigger the mass transfer interactions between the primary package and the surrounding environment resulting in deterioration of the product contained inside. To be successfully accepted for these commercial short lived food packaging applications, understanding of water vapor barrier properties of the polymer remains a very crucial factor.

Auras et al. [44] reported that the PLA films stored for more than one week at 5 , 23 and 40 $^\circ$ C and in water activity (a_w) ranging from 0.11 to 0.94 did not absorb measurable amounts of water. These low moisture sorption values in PLA can be described by the difference between the solubility parameter of water and PLA.

Shogren et al.[45] reported the water vapor transmission rate (WVTR) of an as-cast PLLA specimen much higher than that of crystallized PLLA specimen. Tsuji et al. [46] investigated the effects of molecular weight, D- lactide unit content and crystallinity of poly(lactide) on water vapor permeation of PLA and reported that WVTR of films

22

decreased with increasing crystallinity (χ_c) from 0 to 20 %, where as WVTR values leveled off with further increase in crystallinity.

Water vapor permeability coefficient (WVPC) values reported by Auras et al. [12] for PLA films with different lactic acid content were found to be practically constant over the range studied. It was observed that for those films, permeability values were found to increase with decrease in the temperature. Also no significant change in the permeability coefficient values was observed as a function of relative humidity.

Solubility and diffusivity parameters of different gases in PLA were determined using a QCM by Oliveira et al. [11] and a variation in these values is reported when compared with the values determined by time lag method. For measuring these values very thin films of 2.6 µm were used, and it is very likely that deviation from Sauerbrey equation due to the viscoelastic and non-gravimetric effects during frequency measurements might have resulted in the discrepancies in the reported values, so to better understand the water vapor sorption model in PLA using a QCM these non-gravimetric effects should be considered.

3   MATERIALS AND METHODS

3.1   Materials

Polylactide (PLA) resins made with 94 % L-Lactide provided by Nature Works ®

LLC (Blair, NE) were used for measuring the sorption of water vapor on these films.

Quartz crystals of 5 MHz base frequency, crystal holders, and flow cells were obtained

from Maxtek Inc. (Santa Fe, CA). A humidity generator RH-200 used to generate the

required relative humidity for the experimental work previously calibrated was obtained

from VTI Corp (Hialeah, FL). A peltier chamber for controlling the temperature between

5 and 60°C with a precision of 0.1°C and for housing the flow cells with the coated and

uncoated crystal was obtained from Sable Systems International Inc. (Las Vegas, NV).

Tetrahydrofuran (THF) which was used for making the polymer solution was obtained

from Sigma–Aldrich (St. Louis, MO). A spin coating machine for coating the polymer

films on the quartz crystal was obtained from Laurell Technologies Corporation (North

Wales, PA).

3.2   Experimental set up

The system built for measuring the sorption of permeant on the polymer film

using a QCM consists of five parts: a) water vapor activity generation system, b) flow cells,

c) temperature control chamber, d) QCM, and e) data acquisition system. A complete

schematic of the apparatus is shown in Figure 1.
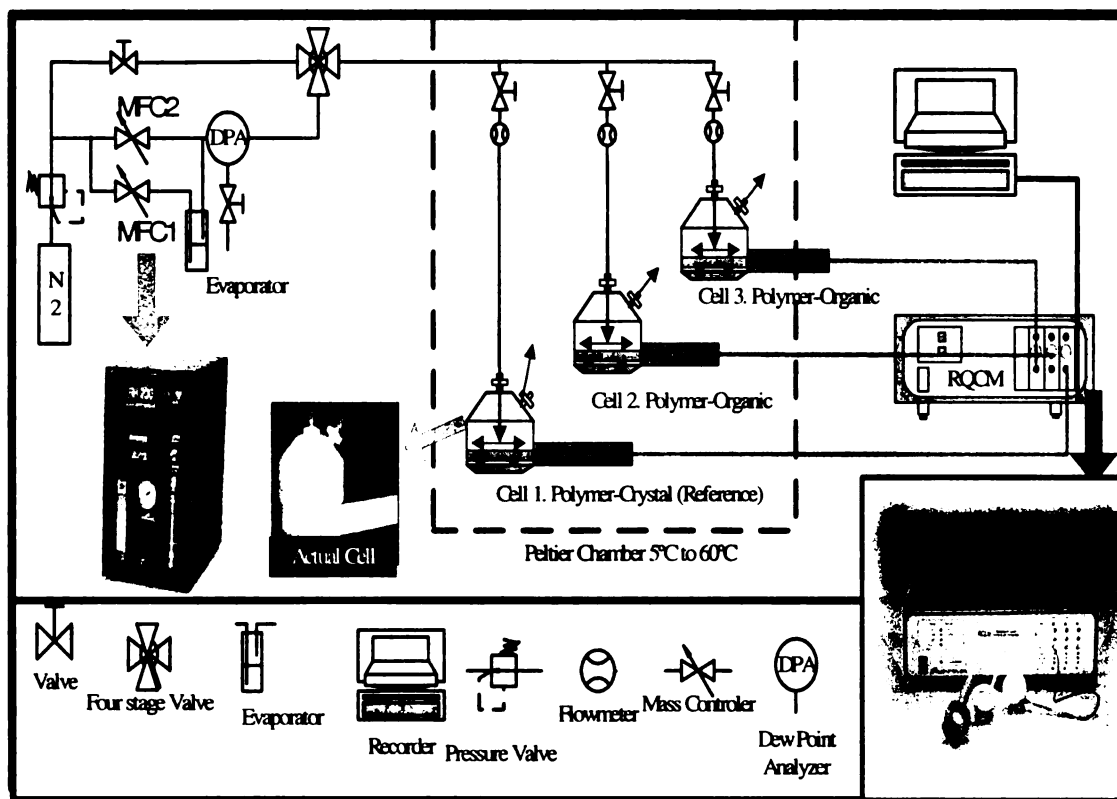
Figure 3-1. Experimental set up for measuring vapor sorption using QCM

3.2.1 Water vapor activity generation system

As the dry nitrogen splits in two parts (see figure 3-1), one entering the mass flow controllers and the other entering the flow cells through the four way valve, the RH generator reduces its pressure to less than 15 psi and is split into branches passing through the wet mass flow controller (MFC1) and the dry mass flow controller (MFC2). Through the wet mass flow controller the gas enters into an evaporator where it becomes saturated with the water vapor. The gas flowing through the dry mass flow controller mixes up the dry gas at the output of the evaporator. The final mixed stream enters into the Dew Point Analyzer (DPA) and flows out to the four way valve from which it is

carried into the flow cells containing the coated and the uncoated crystals. Based on the target relative humidity the software controls the flow of the gas in the wet and dry mass flow controllers. This system can also be used to generate organic vapor at different vapor activities.

3.2.2 Flow cells

The flow cells containing the crystals were made up of Kynar® and two stainless steel inlet and outlet tubes with a .047" I.D. x .062" O.D. A Viton® o-ring provides sealing between the flow cell and the face of the sensor crystal which creates a flow chamber of approximately 0.1 cm^3. The flow cells were connected to the QCM to monitor the change of frequency. Figure 3-2 represents the flow cells used for the study and how the quartz crystals are installed into the flow cells.

Retainer Cover

Crystal Retainer

Crystal

Female BNC
Or SMB Jack

Pogo
Pins

Holder
Housing
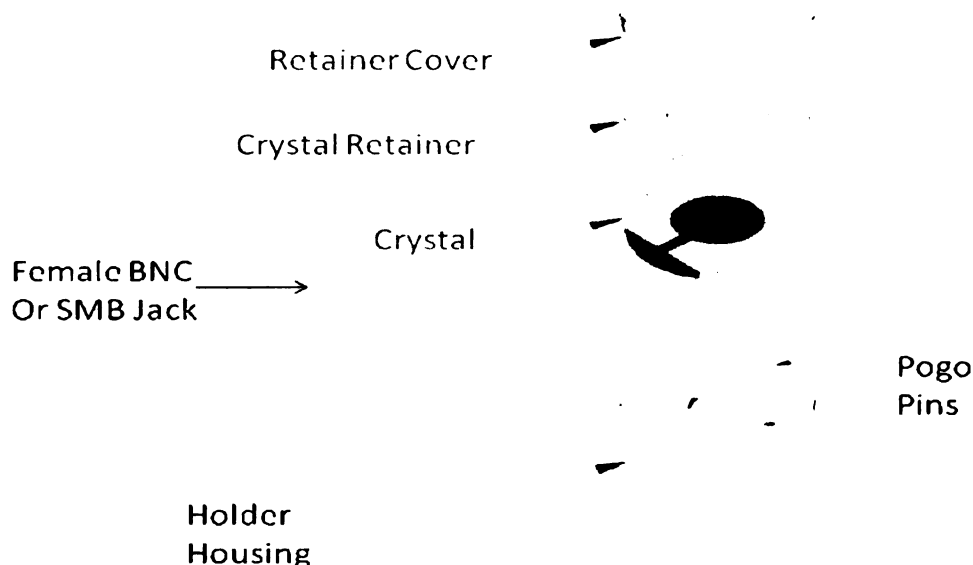
Figure 3-2 Quartz crystal installation in the flow cells. Figure adapted from RQCM Manual [32]

3.2.3 Temperature control chamber

The peltier temperature-controllable chambers have a volume of approximately 8 liters. These cabinets can achieve a temperature control over a range of approximately 5 - 60°C with a precision of 0.1° C and was obtained pre-calibrated from factory (factory information).

3.2.4 QCM system

The QCM system used in this study was equipped with a built in Phase Lock Oscillator (PLO) to support its use in measurement with lossy films and in liquid applications. PLO utilizes an internal Voltage Controlled Oscillator (VCO) to monitor the current flowing through the crystal. At the cancellation of the crystal's electrode capacitance, there is zero phase difference between the current and the voltage which is the exact resonant frequency of the crystal. If the crystal's resonant frequency moves up or down due to the phase differences between the current and the voltage, VCO keeps the frequency of the crystal locked to the crystal resonant frequency through a phase detector. After the frequency is locked to series resonant frequency, the crystal current is demodulated to DC voltage, there by amplifying the voltage, which is further converted into resistance value which QCM outputs to the computer.

3.2.5 Data acquisition system

To support data logging of parameters such as delta frequency, resistance, mass uptake, the QCM was connected to a data acquisition system which transfers the data to a computer. The water vapor activity generation system was also connected to a data acquisition system which controls the flow of wet and dry stream in the mass flow

controllers to generate the desired relative humidity level and storing the data in the computer.

3.2.6 Equipment Run

As the dry nitrogen gas flows into the system it splits in two branches, one flowing into the RH-generator and the other one flowing into the flow cells. As soon as the polymer coated crystals are placed in the flow cells after being thermally treated, the flow cells are purged with dry nitrogen gas for a period of at least 60 minutes for drying the surface of the polymer film coated on the crystal. As the target humidity level in the RH generator is reached the flow of dry nitrogen gas is stopped by closing the four way valve which opens the flow of wet stream of nitrogen gas into the flow cells. Before the wet stream of nitrogen is allowed to enter in the flow cells, it is split into three branches, entering the flow cell at a constant flow of 20 sccm (standard cubic centimeter per minute). With the wet stream entering into the flow cells it results in a frequency change and mass is absorbed on the polymer film. The water vapor sorption on the polymer film is allowed to run until no change in frequency is recorded. The frequency shift and the change in mass associated with the crystals during the experimental run is logged into the QCM and recorded in a computer.

3.3   Experimental set up

3.3.1 System calibration

3.3.1.1   QCM

With the technological developments done on QCM technology, measurements can be done in liquids and viscoelastic deposits. In liquids, the viscoelastic material in

contact with the crystal play an important role in characterizing the resonant frequency and the series resonant frequency of the crystal. Like the decrease in the resonant frequency of the crystal when an additional mass is deposited on its surface, there is also a decrease in the resonant frequency of the crystal when it comes in contact with a liquid. This decrease in the frequency of the crystal in a liquid medium can be calculated from the Kanazawa's equation

$$\Delta f = -f^{3/2} \sqrt{\frac{\eta_l \cdot \rho_l}{\pi \cdot \mu_q \cdot \rho_q}} \qquad (3\text{-}1)$$

where f is the resonant frequency of the crystal, ρ_l is the density of liquid in contact with the crystal, $\acute{\eta}_l$ is the viscosity of the liquid in contact with the crystal, μ_q is the shear modulus of the crystal, ρ_q is the density of the quartz crystal. Before proceeding for any experimental runs the crystals were calibrated to match the accuracy of the crystals with the specified manufacturer limits. Figure 3-2 represents the changes in resonant frequencies measured, when the crystals were dipped in different weight percentage solutions of glycerol in water at 20 °C. The recorded values of the delta frequencies in different weight percentage solutions of glycerol were fitted to a straight line up to 45 wt % of glycerol and were found to agree well with the calculated values. At higher weight percentage values of glycerol, the delta frequency showed higher deviation. Drop in the resonant frequency up to 1500 Hz for crystals when dipped in different weight percentage of glycerol solution was established as acceptable in the calculations as they agreed well with manufacturers specified limits.

29
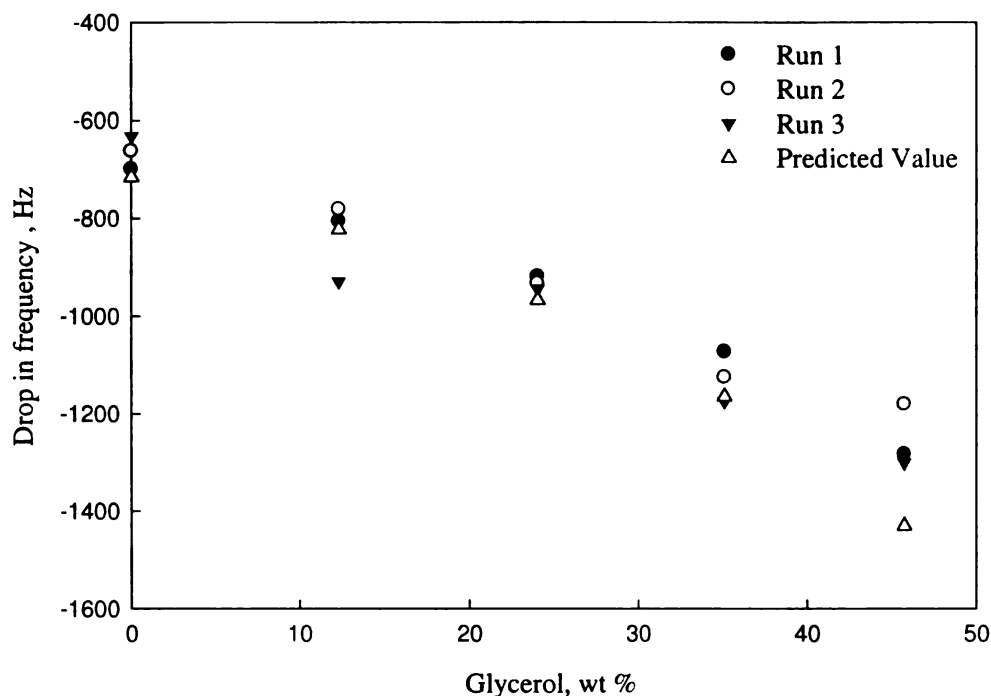
Figure 3-3 Delta frequencies of crystals when dipped in different weight by percentage glycerol solution for three different runs and the predicted values from eq 3-1

3.3.1.2 Flow pressure

For keeping accuracy in measurements in gaseous environment, it was required to maintain a constant gas flow during the experimental runs. To remove the discrepancies associated with the flow pressure of the carrier gas, drop in resonant frequencies of the crystals at different flow pressures of 10, 20, 30 sccm at relative humidity levels of 20%, 40 %, 60 % & 80% to be used in experimental runs was measured. Based on the consistency of the results obtained from three different runs, flow pressure of 20 sccm was selected as the flow pressure for all experimental runs. Figure 3-4 shows the drop in the resonant frequency of the uncoated crystals at a gas flow of 20 sccm. The drop in the resonant frequency for all crystals at this flow pressure was no more than 2 Hz, so this flow pressure of the carrier gas was used to establish a baseline for further experimental work. This baseline shift was subtracted from the drop in the resonant frequencies of the

30

coated crystals during the experimental runs to correct for the actual mass adsorbed/absorbed on the surface of the crystals.
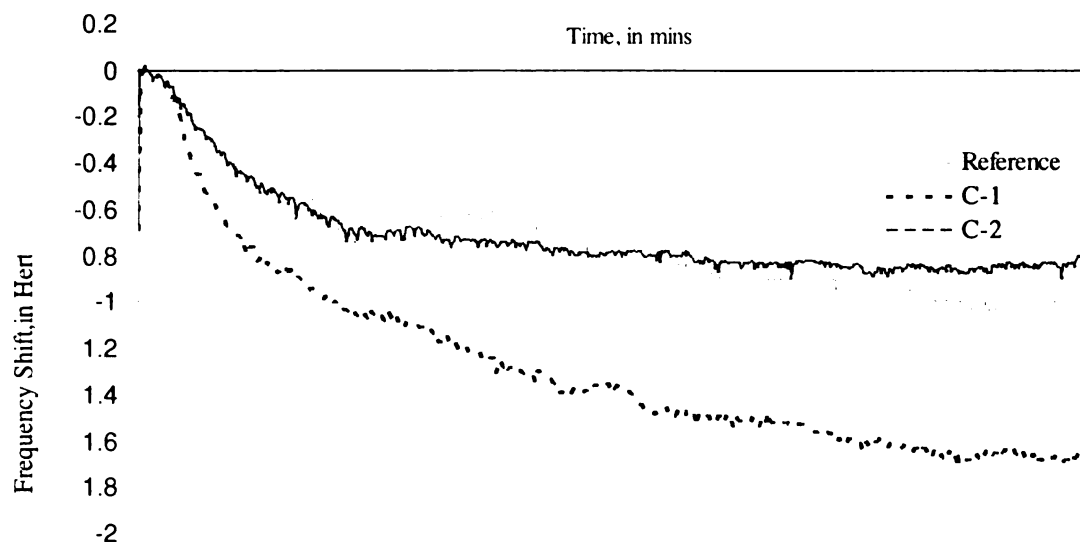
Figure 3-4 Variation in delta frequency at different relative humidity conditions at gas flow of 20 sccm

3.4 Temperature control chamber

The temperature control chamber used for maintaining the temperature was calibrated before performing the experimental runs. Temperature readings were taken after every hour for a period of 8 hours from a thermometer (factory calibrated) dipped in a flask containing HPLC grade water kept inside the chamber at the respective temperatures. A temperature variation of less than 0.5° C was observed during this time.

3.5 Spin coating

A uniform and homogenous polymer film on the surface of the quartz crystal was produced by spin coating. For this purpose polymer resins were dissolved in tetra hydro furan at 35 $^\circ$C and a solution 1 % wt/v was made. Before coating the crystals, they were

31

thoroughly cleaned with acetone to remove any particles on their surface which can have an affect on the resonant frequency of the crystals. Subsequently their resonant frequencies were measured. After washing off the crystals, they were spin coated with the 1% wt/v polymer solution to produce a uniform polymer coating. The spin coating was done in three consecutive steps; a) after properly mounting the crystal on the chuck, they were rotated for 5 seconds at a 100 rpm, and simultaneously starting off the dispensing of the polymer solution on the crystal; b) dispensing of polymer solution was completed within the first 5 seconds. After that, the crystal was allowed to spin over the next 5 seconds at a speed of 200 rpm giving sufficient time and speed for the polymer solution to spread uniformly on the crystal surface; c) In the last drying step, the crystal was rotated for 5 seconds at 50 rpm allowing the solution to evaporate off from the surface of the crystal. After this step, the coated crystals were kept on the stationary chuck for around 10 minutes providing enough time for the solution to evaporate. After this the coated crystals were moved to a vacuum chamber for a period of 5 hours at a temperature of 60° C. This temperature treatment was done for allowing the polymer chains to relax, remove any impurities present on the surface and further drying it producing a uniform polymer film on the crystal. After vacuum drying, the coated crystals were taken out in a desiccator for measuring the thickness of the polymer film. The thickness of the polymer film coated on the crystal was evaluated by measuring the frequency shift associated with the coating of the film on the crystal surface in absent of flow.

$$\frac{\Delta l}{l} = \frac{-\Delta f_o}{f_o}$$

(3-2)

where l is the thickness of the quartz crystal, Δf is the frequency shift associated with the coating of the polymer film on the crystal, and f_o is the resonant frequency of the crystal before coating.

3.6 Thermal Characteristics

A differential scanning calorimeter (DSC) from TA Instruments (New Castle, Delaware) was used to determine the glass transition (T_g) and melting temperatures (T_m) of the polymer films as per ASTM D 3418-97. Crystallinity of the polymer films were determined by determining the enthalpies of fusion (ΔH_f) according to ASTM D 3417-97.

4 RESULTS AND DISCUSSION

4.1 Physical and Thermal Properties

Before producing the polymer films from the actual PLA resin, its physical and thermal properties such as glass transition and melting temperatures and percentage crystallinity were determined by DSC. The physical properties of the polymer films produced by spin coating were also determined during each experimental run. Table 4-1 shows the values of these physical properties of the resin and polymer films.

Table 4-1 Physical and thermal properties of the PLA resin and films

Property	Resin	Film
Film thickness, μm	NA	1.2±0.2
Glass Transition Temperature , °C	66.0±2.0	62.0±2.0
Melting Temperature, °C	148.0±1.0	151.1±2.0
Crystallinity, %	16.0±2.0	21.0±2.0

As diffusion of permeant on a polymer film depends on thickness of the sample, extreme care was taken to produce polymer films of uniform thickness for this study. The thickness of the polymer films were determined by dividing the mass deposited on the crystal before the beginning of the sorption by the density and surface area of the polymer sample. Polymer films produced by spin coating method were found to have a thickness of 1.25 ± 0.29 μm. In addition as the crystallinity of the polymer film greatly affects permeation process, to keep consistency in our experiments, proper attention was

given to produce polymer films of approximately same crystallinity. To do so, polymer solution was allowed to spread uniformly over the crystal surface during the spin coating process and after spin coating, coated crystals were thermally treated. This thermal treatment of polymer films at a temperature 5 °C above their glass transition temperature for 5 hours allowed the polymer chains to relax, thereby obtaining the films of approximately same crystallinity. All the films used in the study had an overall percentage crystallinity of 21 ± 2 %, as shown in table 4-1.

4.2   Moisture uptake

After purging the flow cells containing the coated and uncoated crystals with the dry nitrogen gas for approximately 60 minutes, N_2 with specific relative humidity between 20 and 80 % was allowed to enter into the flow cells. Due to the sorption of the water vapor on the surface of the polymer film on the coated crystal and the bare crystal surface, a drop in the resonant frequency of the crystals occurs. Once the drop in frequency is stabilized, the steady state is achieved. The data generated was used to calculate the mass uptake on the polymer film in accordance to the Sauerbrey equation which can be expressed as

$$\Delta m = -\frac{\Delta f}{C_f} = \frac{(f_q - f)\sqrt{\rho_q \mu_q}}{2nf^2} \qquad (4\text{-}1)$$

where n = number of harmonic at which the crystal is driven

f is the resonant frequency of the uncoated crystal

f_q is the frequency of the coated crystal

ρ_q is the density of the quartz crystal

μ_q is the shear modulus of the crystal

Figure 4-1 shows the drop in the resonant frequency of the coated and uncoated crystals as a function of time. Drop in the resonant frequency is found to be more pronounced for coated crystals as compared to the uncoated crystals, which is due to additional affinity of the film deposited on the crystal towards the moisture.
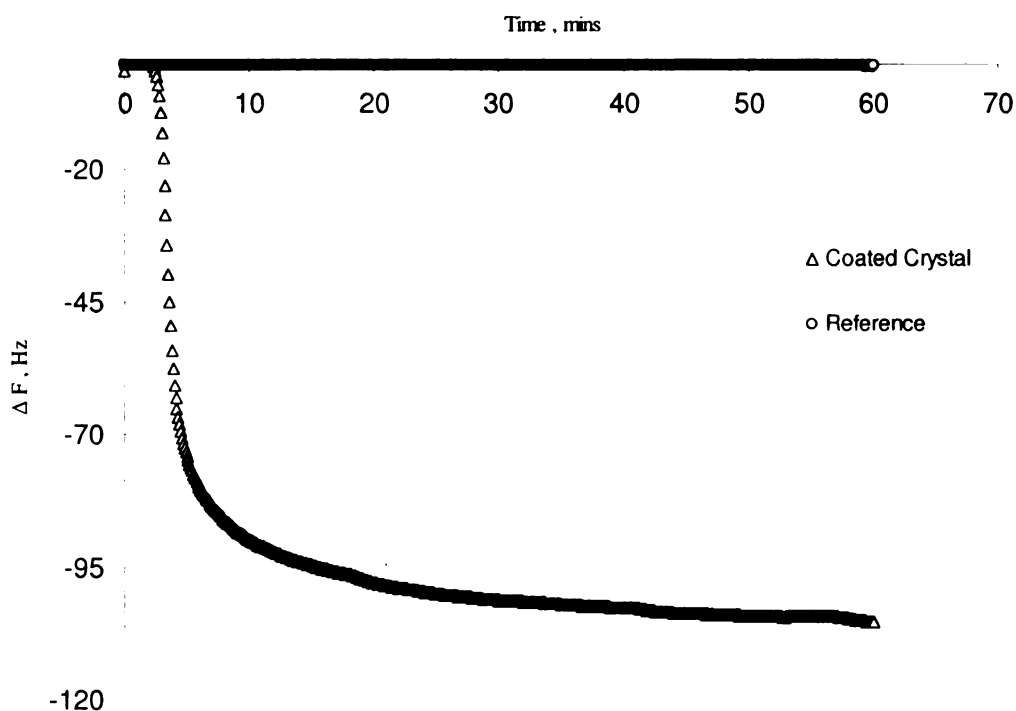
Figure 4-1 Drop in resonant frequency as for a film 1.06×10^{-4} cm at 23 ° C and 20 % RH as a function of time according to the Sauerbrey equation

Sorption of water vapor on the surface of the polymer film was calculated as a function of time, as shown in figure 4-2. The process of mass uptake on the polymer film takes place in two steps; transient state and the steady state. During the transient stage, mass uptake continues to increase with time until it reaches a steady state termed as equilibrium or steady state.
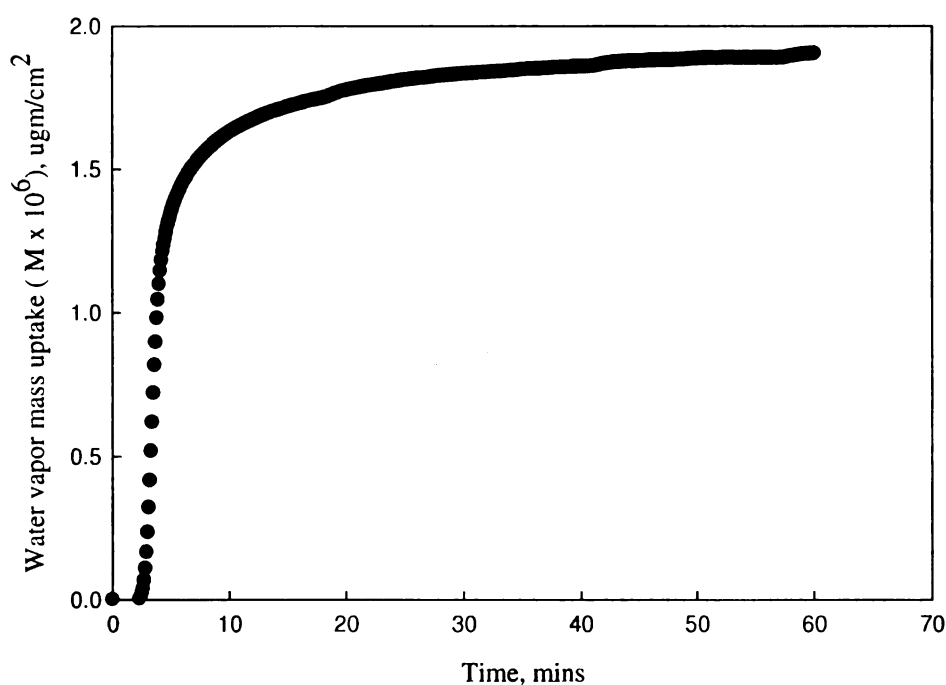
36
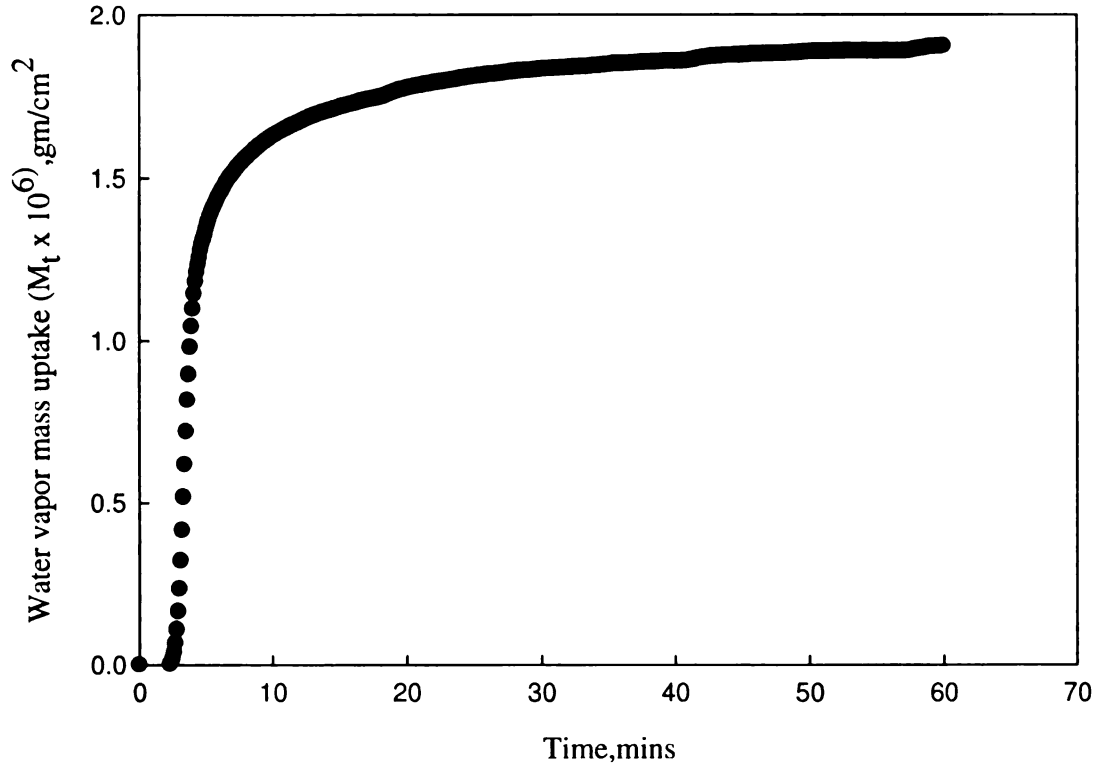
Figure 4-2 Water vapor mass uptake for a film 1.06×10^{-4} cm at 23 ° C and 20 % RH as a function of time

The mass uptake calculated from the Sauerbrey equation (Eq. 4-1) as shown in figure 4-2 represents the water vapor mass uptake on the polymer film coated on quartz crystal.

As the thickness of the polymer films used in the experimental runs had a thickness greater than 100 nm, deviations from the Sauerbrey equation due to non-gravimetric effects have been previously observed in films thicker than 100 nm by Banda et al [42]. Deviations from the Sauerbrey equation may account for some errors in mass uptake measurements. Therefore, in order to check for these errors, mass uptake on the surface of the crystal was calculated from Z- match equation, which can be expressed as

$$\Delta m = \left(\frac{N_q . \rho_q}{\pi . R_z . f} \right) . \tan^{-1} \left[R_z . \tan \left[\pi . \left(\frac{f_q - f}{f} \right) \right] \right] \qquad (4\text{-}2)$$

Where:

Δm is change in mass per unit area expressed in g/cm^2

N_q is the frequency constant for AT –cut quartz crystal

f is the resonant frequency of the uncoated crystal,

f_q is the frequency of the coated crystal,

$$R_z = \sqrt{\frac{\rho_q \mu_q}{\rho_f . \mu_f}} = \frac{Z_q}{Z_f} = \text{acoustic impedance ratio} \qquad (4\text{-}3)$$

ρ_q is the density of the quartz crystal

μ_q is the shear modulus of the crystal in g.cm^{-1}.s^2

ρ_f is the density of the polymer film , g /cm^3

μ_f is the shear modulus of the film in g.cm^{-1}.s^2

To determine the mass uptake on the polymer film from the Z-match equation, the acoustic impedance ratio is required. Quartz crystal can also be used as a tool to extract the mechanical properties of the film such as shear modulus from impedance analysis. For viscoelastic polymer films, generalized impedance Z equals the conventional acoustic impedance and can be expressed as

$$Z = \sqrt{\rho . G} \qquad (4\text{-}4)$$

where:

ρ is the density of the polymer

G is the complex shear modulus of the polymer film.

Behling et al [33] characterized polymer properties such as shear modulus using a quartz crystal resonator by doing impedance analysis. The acoustic load impedance generated from the single film on the crystal surface after taking into account the phase shift difference between of acoustic wave between the quartz crystal and outer coating surface can be described as

$$Z_l = j\sqrt{\rho.G}\,\tan\left(\omega_s h\sqrt{\frac{\rho}{G}}\right)$$ (4-5)

where

ρ is the density of the polymer

G is the complex shear modulus of the polymer film

h is the thickness of polymer coating on crystal surface

ω is the series resonant frequency of the crystal

After considering the gravimetric response corresponding to very small acoustic phase shifts and the non-gravimetric response corresponding to high acoustic shifts, the shear modulus of the polymer film is calculated from the expression

$$G = 16.\rho_f.f_r.d_f^{\,2}$$ (4-6)

where

f_r is the series resonant frequency of crystal

d_f is the thickness of the polymer film coated on crystal

The shear modulus of the film calculated from equation 4-6 is used in equation 4-4 to obtain the conventional acoustic impedance of the material. Conventional acoustic impedance for the viscoelastic film and the crystal obtained from equation 4-4 is used in equation 4-3 to obtain the acoustic impedance ratio, which finally is used in equation 4-2

to predict the permeant mass uptake on the polymer film after considering the non-gravimetric errors induced. Mass of polymer film coated on the quartz crystal is normalized, to calculate actual water vapor mass uptake on the polymer due to the sorption of water vapors on it surface. Figure 4-3 shows the water vapor mass uptake on the polymer film, calculated from the Z-match equation.

Figure 4-3 Water vapor mass uptake for a film 1.06 x 10^{-7}cm at 23°C and 20 % RH as a function of time calculated from Z-match Equation

The water vapor mass uptake calculated from Z-match equation match the water vapor mass uptake calculated from Sauerbrey equation. Figure 4-4 represents the comparison between the water vapor mass uptakes calculated from two different equations. The root mean square difference between the water vapor mass uptake values

on the polymer film predicted from the Z-match and Sauerbrey equation was found to be

less than 3 % , which shows a very good agreement.
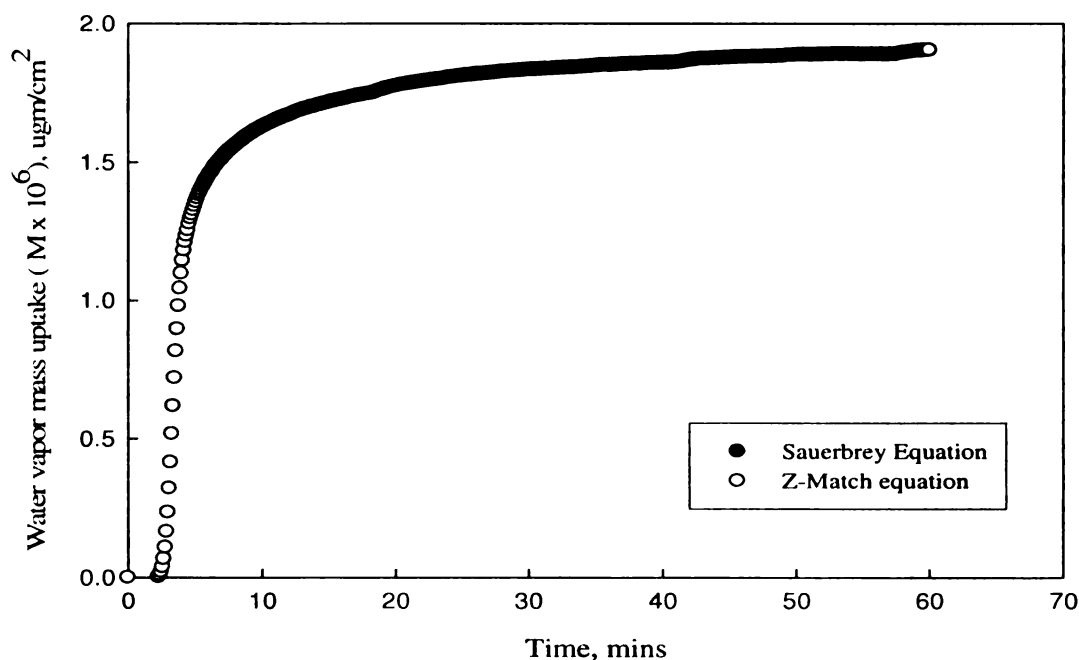
Figure 4-4 Water vapor mass uptake for a film of 1.06 x 10^{-7} cm calculated from
Z-match and Sauerbrey equations

As Z-match equation considers the errors induced in the mass uptake

measurements due to the non-gravimetric errors, but no significant difference in the

measured values was observed by using the Sauerbrey and Z-match equation, to generate

more accurate and reliable measurement data, the Z-match equation was used for all

calculation purposes and data analysis in this thesis.

4.3 Experimental and Predicted Fractional Mass Uptake

Six different films of comparable thickness were used to for each relative

humidity condition at a particular temperature condition to study the water vapor sorption

on polylactide films.

As the water vapors were allowed to enter into the flow cells containing the coated crystals, it usually takes some time for them to get sorbed on the polymer surface. Therefore, it becomes quite necessary to correct for the time at which the actual mass uptake of water vapor started on the surface of the polymer film.

During our experimental procedures, only one side of the polymer film was exposed to the water vapors since the other side was directly in contact with impervious crystal surface. In this case, the permeable surface is at concentration $C= C_o$, whereas the impermeable surface is at concentration $C = 0$. Under these boundary conditions Fick's second law is solved to obtain the following expression. The detail solution of the system is shown in Appendix A

$$\frac{M_t}{M_\infty} = 1 - \frac{8}{\pi^2} \sum \frac{1}{(2n+1)^2} \exp\left(- (2n+1)^2 \pi^2 Dt / 4l^2\right) \qquad (4\text{-}6)$$

Fractional mass uptake was predicted using the equation (4-6) and then compared with the experimental mass uptake for each experimental run at different conditions. Figure 4-5 to 4-6 shows the plot of experimental and predicted fractional mass uptakes for $10°$ C, $23°C$, and $40°C$ at a relative humidity of 20 %.
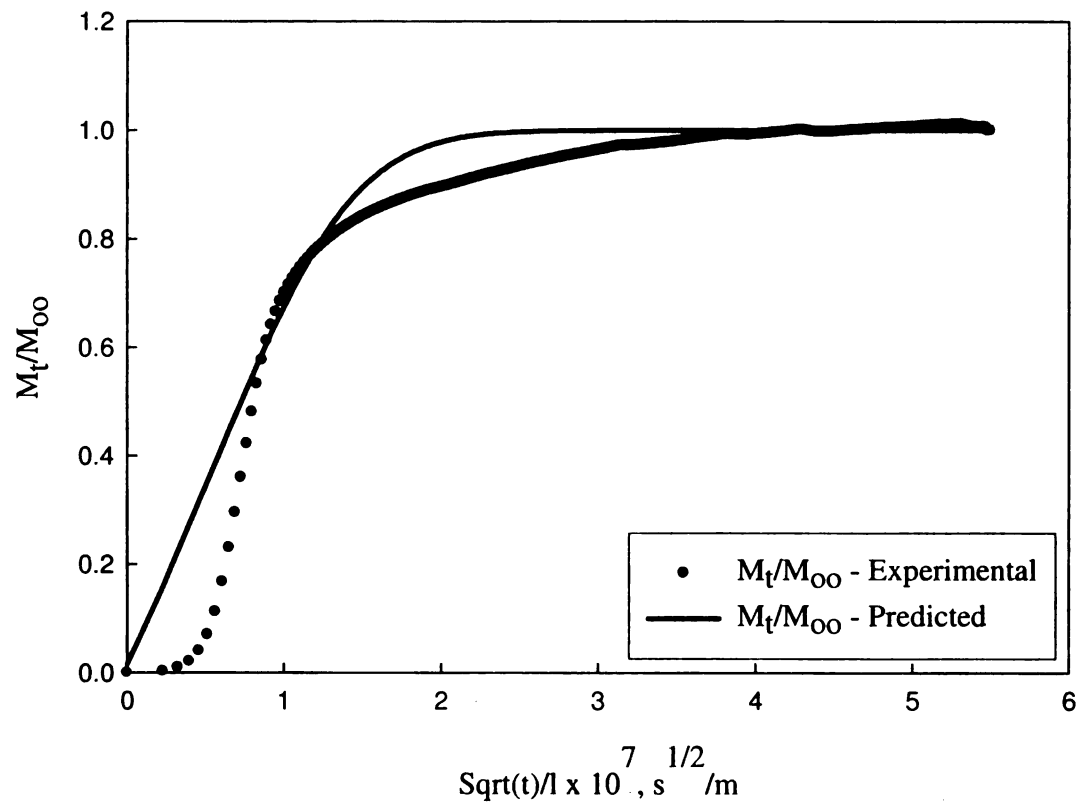
Figure 4-5 Experimental and predicted fractional Mass uptake at 10°C at 20 % RH

1.2

1.0

0.8

M_t/M_{oo}

0.6

0.4

0.2

• M_t/M_{oo} - Experimental

M_t/M_{oo} - Predicted ———

0.0

0   1   2   3   4

Sqrt(t)/l x 10^7, $s^{1/2}$/m
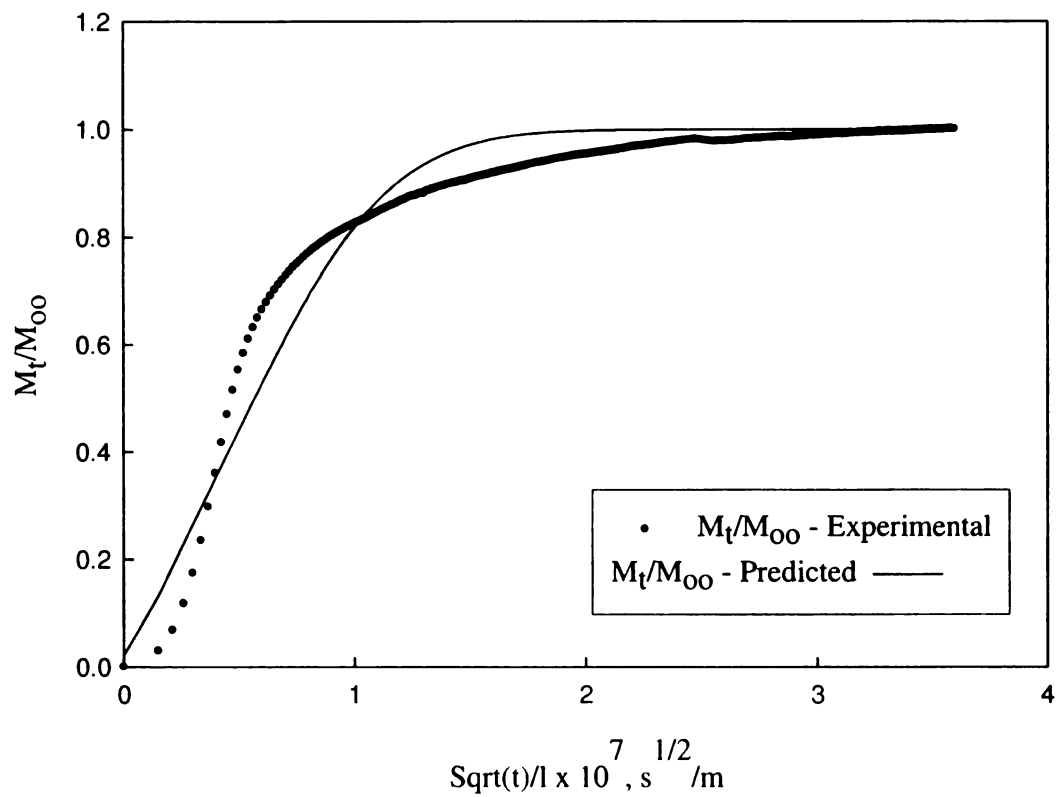
Figure 4-6 Experimental and predicted fractional mass uptake at 23° C at 20 % RH
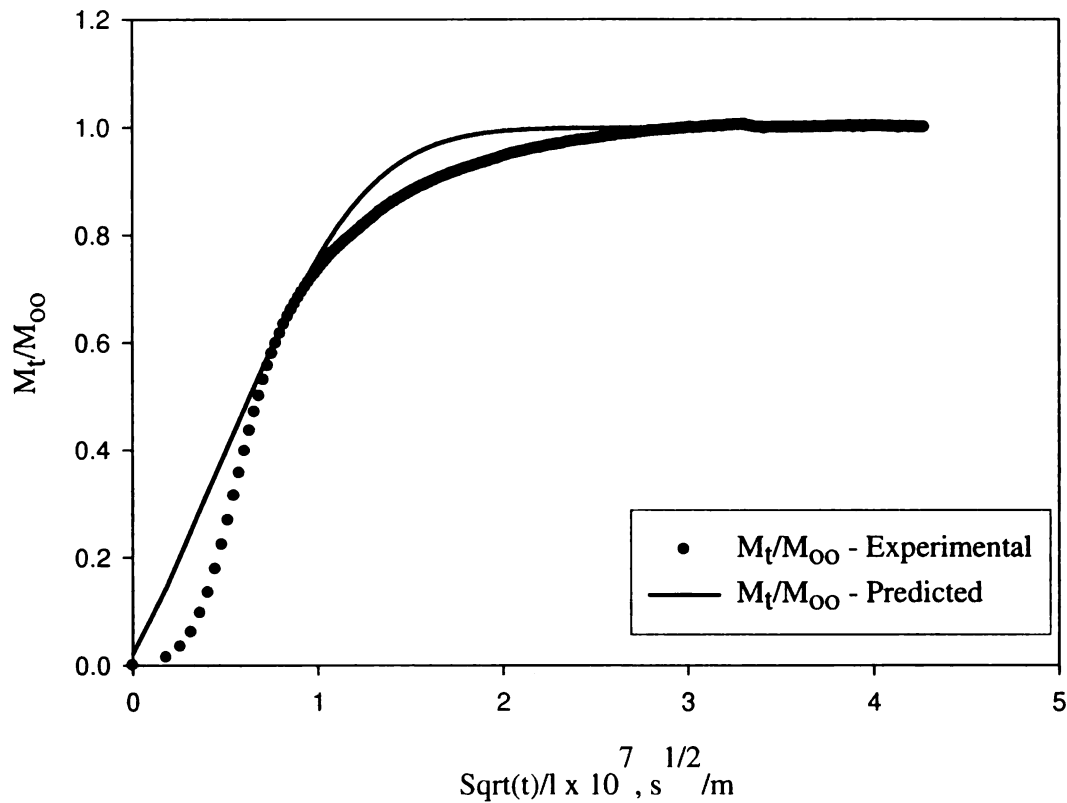
Figure 4-7 Experimental and predicted fractional mass uptake at 40° C at 20 % RH

Root mean square (RMS) values of less than 10 % were found between the experimental and the predicted mass uptake values. Steady state predictions were very closely match, though minor deviations were observed in transient stage. Deviation between the predicted and experimental fractional mass uptake values can be explained with two possibilities. Thickness at different points on the spin coated film can be variable, causing different local diffusion coefficients. It was not possible to measure the thickness of the film at different points. Other possibility of the model not fitting the experimental data in the transient stage may be because of the absence of factor in the model that would compensate the interaction between the PLA and moisture. Earlier

studies have shown that PLA is affected by relative humidity. Probably, a better fit can be obtained if a compensation factor is included in the model equation itself. At steady state, experimental fractional mass uptake values seemed to agree well with the predicted values for all the temperature and relative humidity conditions.

4.4   Determination of Diffusion, Solubility & Permeability Coefficient

Diffusion, solubility and permeability coefficients were calculated under different environmental conditions. Additionally, the effect of different environmental conditions was predicted and compared with the previously reported values.

4.4.1 Diffusion coefficient

Diffusion coefficient determined from the half time method in the sorption range of 35% to 85 % can thus be used to accurately predict the diffusion coefficient of water vapors in the polymer film.

Sum of squares of residual errors (SSE) was calculated for the optimal solution using different values obtained for the diffusion coefficient and the diffusion coefficient corresponding to minimum SSE taken as the best solution. This procedure was followed for each experimental run. Complete code for the QBasic program used for the calculation can be found in Appendix B (Burgess, 2007). The values of the diffusion coefficient ($D \times 10^{15}$, m^2/s) for temperatures 10 °C, 23 °C, 40 °C are summarized in Table 4-2.

Figure 4-8 represents the values of the diffusion coefficient (m^2/sec) at 23 °C and 40 °C for relative humidity values ranging from 20 % to 80 %. Diffusion coefficient values obtained using 23 °C and 40 °C conditions shows large variability though they do

not show statistically significant difference. Determining diffusion coefficient when the sorption reaches 50 % of its extent can also introduce significant errors, if there is any deviation from the ideal conditions.
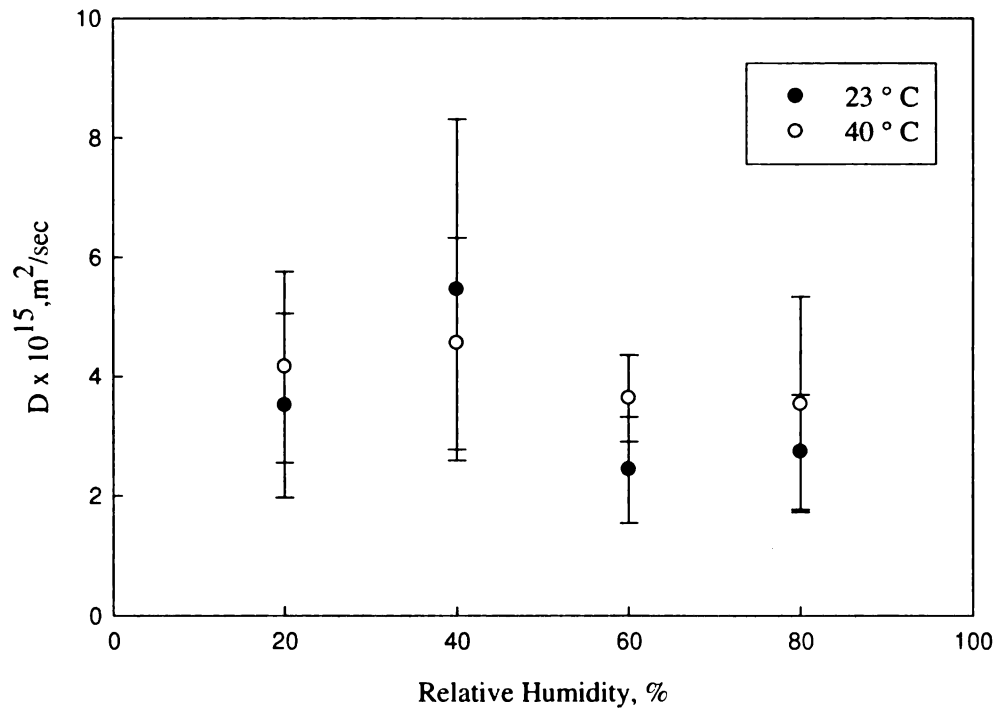
Figure 4-8 Diffusion coefficient as a function of relative humidity

As for deriving the diffusion coefficient, we assume that initially the polymer is in equilibrium with the cell environment and at t=0, the sorbate concentration has a step change to C_0 and is maintained constant during the experiment. In actual experiments, the concentration surrounding the film specimen changes continuously from the initial to the final concentration. Assuming the sorbate concentration in the cell is homogeneous, kinetics of this process might depend on the volume of the cell and the flow rate of the stream. This process also leads to the deviation from the ideal behavior and assumptions; it might have resulted in the high variability in the diffusion coefficient results.

4.4.2 Solubility coefficient

Water vapor mass uptake at equilibrium (M_∞) was used to determine the solubility coefficient. Dividing the mass uptake at equilibrium (M_∞) by the density of the polymer sample and partial vapor pressure, gave the solubility coefficient which can be expressed as

$$S = \frac{M_\infty}{v.p} \qquad (4-8)$$

Values of solubility coefficient (S $\times 10^2$, kg/m^3-pa) for temperatures 10° C , 23° C, and 40° C are summarized in Table 4-2 at the end of the chapter. Figure 4-9 represents the solubility coefficient as a function of relative humidity.
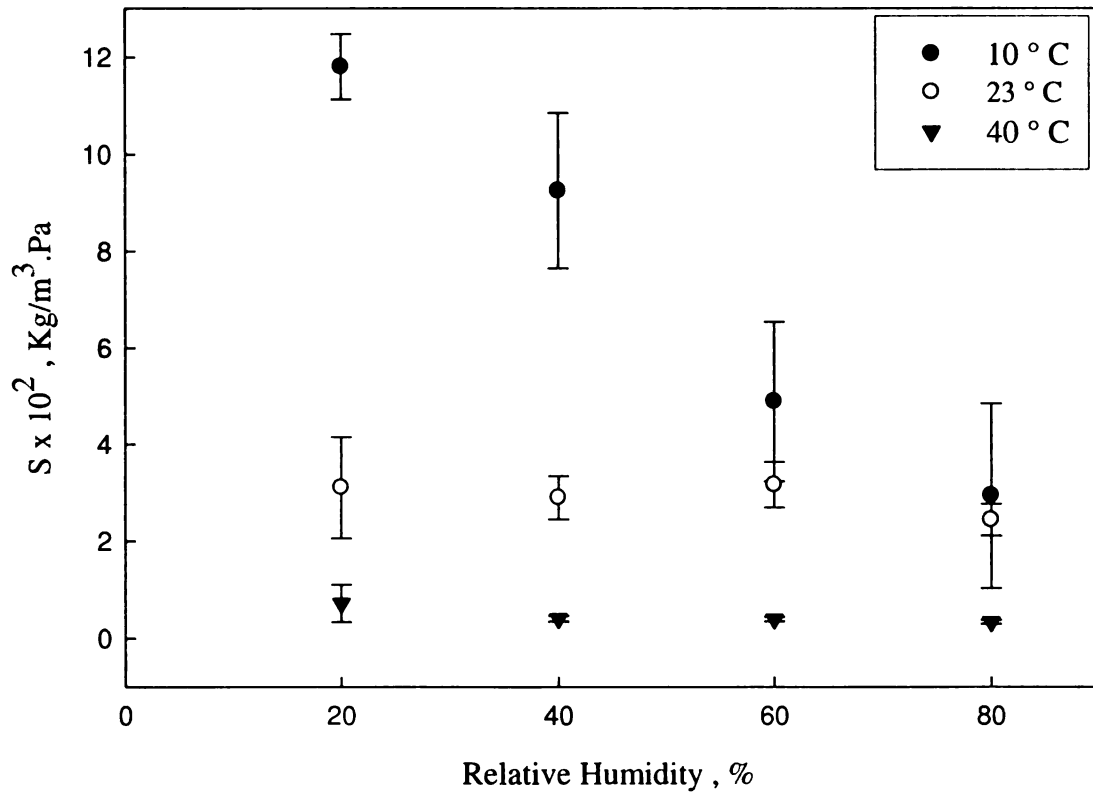
Figure 4-9 Solubility coefficient as a function of relative humidity

Solubility coefficients at 23 °C & 40 °C were found to be independent of the permeant concentration. However, solubility coefficient at 10 °C showed a reduction in the solubility values at higher partial pressures. Solubility coefficient (S) measured at temperature 10 °C, 23 °C & 40 °C for relative humidity ranging from 20 % to 80 % was found to be in the range of 0.72×10^{-2} to 11×10^{-2} kg/m^3-Pa. Large discrepancies exist between the solubility values determined by QCM and the time lag methods.

4.4.3 Permeability coefficient
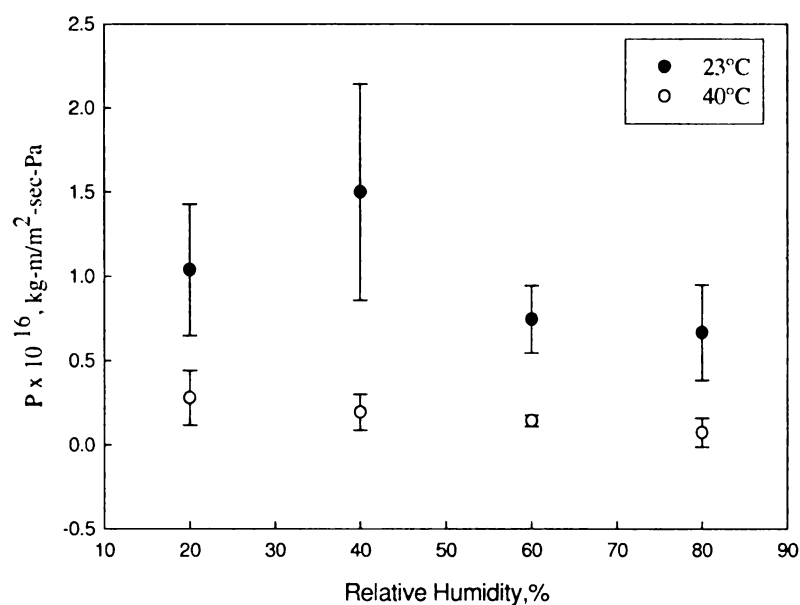
Figure 4-10 Water vapor permeability coefficient as a function of relative humidity

Water vapor permeability coefficient of PLA films at 23° C, 40°C for relative humidity ranging from 20 % to 80 % are shown in figure 4-10. Values of permeability coefficients for different temperature and relative humidity conditions are summarized in table 4-2.

49

No statistical significant change in the water vapor permeability coefficient values was observed with the increasing permeant concentration. So the water vapor permeability was observed to be independent of the relative humidity. Auras et al. [47] also reported the water vapor permeability coefficient values for PLA to remain constant with the changes in relative humidity, despite PLA being a polar polymer.

Analysis of the water vapor permeability coefficient values for polylactide films showed large variability as shown in table 4-2. The values determined using this technique was found to be two orders of magnitude lower than previously reported values. Bao et al. [48] determined permeation properties of poly(lactic acid) which were about one order of magnitude lower then previously reported results and showed considerable disagreement with previously reported values. They indicated non-uniformity of the film thickness as a major source of uncertainty in their results.

As during our experimental runs, we used extremely thin films, which are very hard to handle. There is a possibility of presence of structural defects such as pin holes, cracks in such thin films, which might have contributed to the large variability in permeability values.

Condensation of the water vapors in the flow cells or on the surface of the film at low temperatures such as 10 °C might have also contributed to the high variability in the permeability values at 10 °C . As we know that little amount of permeant such as water is enough to bring in some morphological changes in polymer architecture and lower its glass transition temperature which directly would have affected its permeability coefficient values.

Larger deviations in the water vapor permeability coefficient values during this research can be due to the extremely thin films used in this measurement. With extremely thin films, the possibility of structural defects such as pinholes, cracks in films is increased, which can result in unpredicted behavior during the sorption of permeants.

4.4.4 Effect of Temperature on Permeability Parameters

Temperature dependence of transport parameters is usually described by Arrhenius relationship, and can be expressed as

$$D = D_0 e^{-E_D/RT} \tag{4-9}$$

$$S = S_0 e^{-\Delta H_S/RT} \tag{4-10}$$

$$P = P_o e^{-E_P/RT} \tag{4-11}$$

where

E_d is the activation energy of diffusion

ΔH_s is the enthalpy of sorption

E_p is the activation energy of permeation.

Activation energy of permeation can also be expressed as a sum of enthalpy of sorption and activation energy of diffusion

$$E_p = E_d + \Delta H_s \tag{4-12}$$

3.3.1.1 Activation energy of diffusion (E_d)

Activation energy of diffusion (E_d) was determined for the experiment runs at 10° C, 23° C, 40°C for the relative humidity ranging from 20 % to 80 %. Figure 4-11 represents the plot of confidence interval of activation energy of diffusion. Due to

the higher variability of diffusion coefficient at 10 °C, only the values of diffusion coefficient at 23 °C & 40 °C were used to estimate the energy of diffusion (E_d).
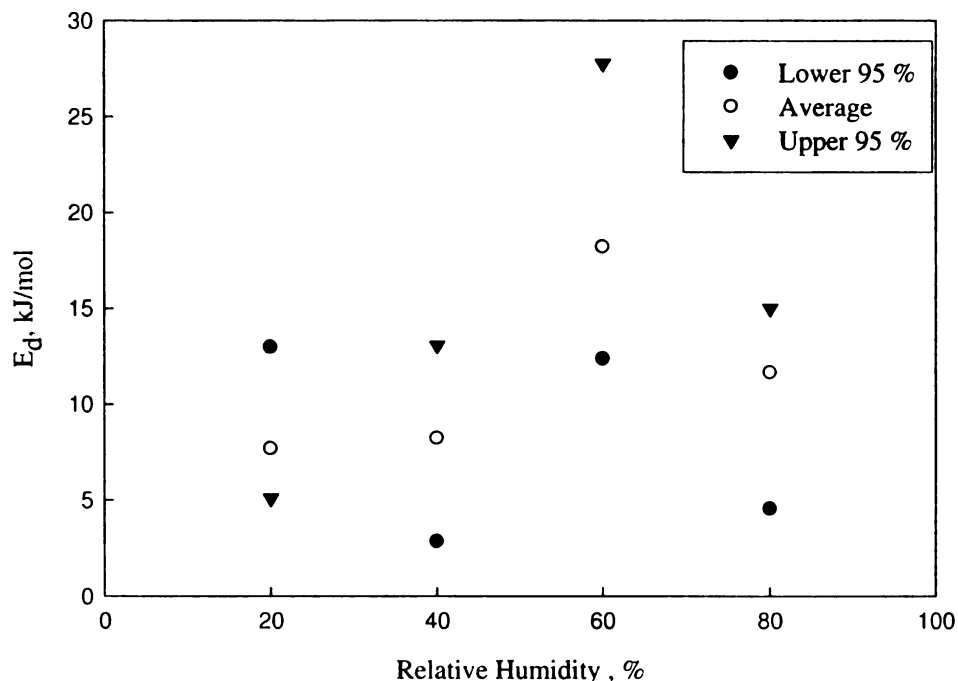
Figure 4-11 Plot of Confidence interval for activation energy of diffusion at different RH

The average values of energy of diffusion (E_d) showed no statistically significant difference as relative humidity increases, however some unpredictable values of energy of diffusion were observed at 60 % RH. Energy of diffusion was found to be in the range of 2.81 kJ/mol to 27.75 kJ/mol in relative humidity range of 20 % to 80 %.

3.3.1.2 Heat of sorption (ΔH_s)

Enthalpy of sorption (ΔH_s) can also be considered as sum of two terms

$$\Delta H_s = \Delta H_c + \Delta H_m \qquad (4-13)$$

where ΔH_c is the enthalpy of condensation of pure gaseous penetrant to the liquid phase and ΔH_m is the partial molar enthalpy of mixing the condensed penetrant with polymer

segments. As the solubility depends on the heat of sorption and unlike activation energy of diffusion, it can take positive or negative values. Figure 4-7 represents the enthalpies of sorption (ΔH_s) and its dependence on relative humidity.
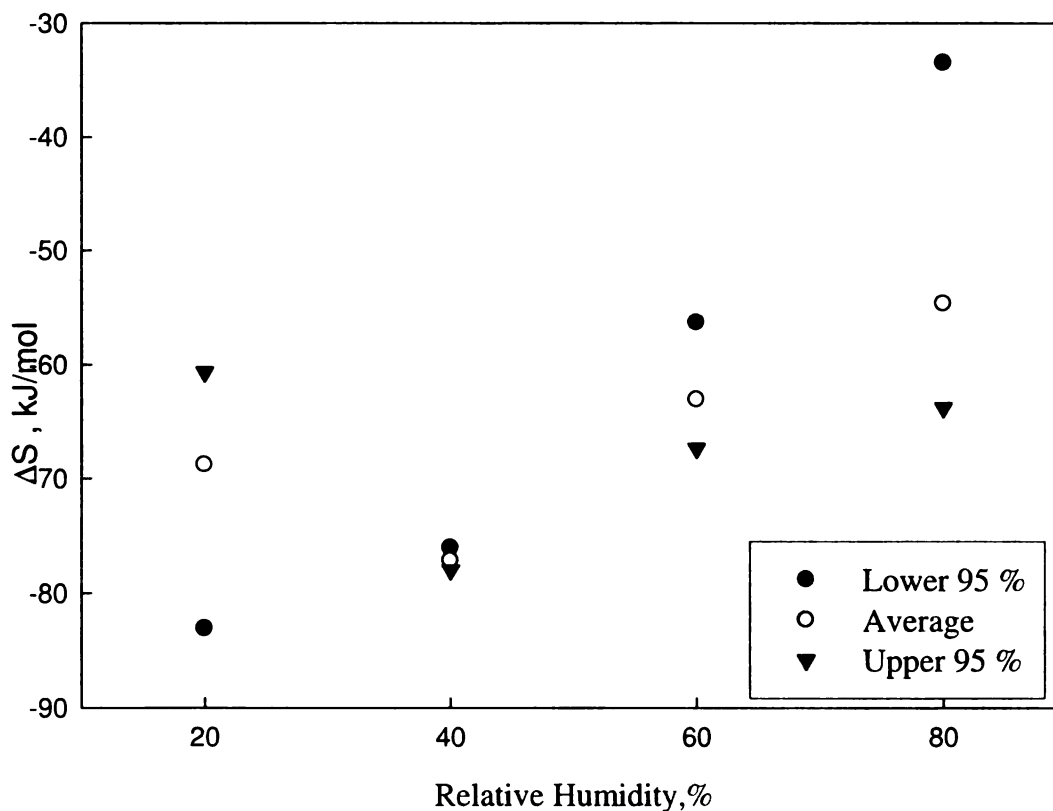
Figure 4-12 Enthalpy of sorption (ΔH_s) as a function of relative humidity s

Heat of sorption (ΔHs) was found to be in the range of -68 kJ/mol to -54 kJ/mol for relative humidity ranging from 20 %to 80 %. For negative heat of sorption, solubility coefficient decreases with increasing temperature.

3.3.1.2 Activation energy (E_p)

Activation energy of permeation depends on relative magnitudes of the activation energy of diffusion and heat of sorption. For $E_d > \Delta H_s$, resulting values of E_p will be positive, which means that permeability coefficient values will increase with the increase in the temperature. Where as for $E_d < \Delta H_s$, resulting values of E_p will be negative, resulting in decrease in the permeability values with the increase in temperature. Figure 4-13 represents the confidence interval on the activation energy of permeation measured at different relative humidity. Activation energy of permeation (E_p) was calculated to be in the range (– 55) kJ/mol to (-85) kJ/mol for relative humidity ranging from 20 % to 40 %.
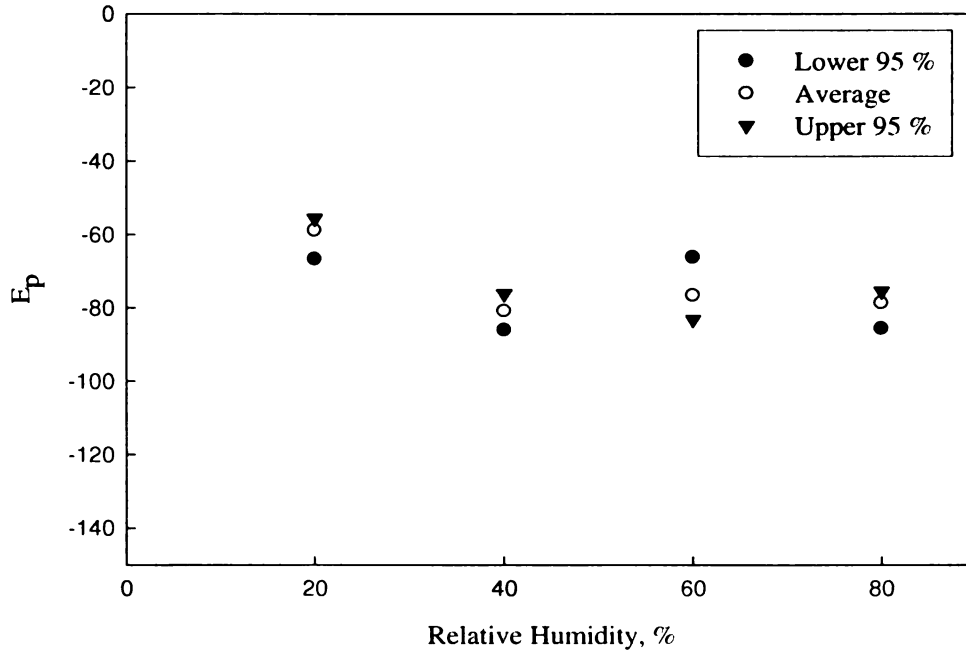
Figure 4-13 Confidence interval on E_p and its dependence on relative humidity

As the energy of diffusivity (E_d) is always positive, negative activation energy (E_p) indicates that heat of sorption (ΔH_s) plays a dominant role in water vapor permeation through PLA. So, water vapor permeation process in Polylactide can be best described by sorption –diffusion model. With the negative values of the energy of activation, permeability coefficient decreased with increasing temperature.

Table 4-2 Summary of P, D, S values (Average +Std Dev)

T °C / RH %		20	40	60	80
10	$Dx10^{15}$(m^2/sec)	2.62±1.01	5.25±2.01	6.19±3.63	5.67±3.75
	S x 10^2(Kg/m^3.Pa)	11.01±0.60	9.00±1.00	4.00±1.00	3.00 ±2.00
	Px10^{16}(Kg-m/m^2.sec.Pa)	2.06±1.87	3.10±2.60	3.16±2.25	1.34±.90
23	$Dx10^{15}$(m^2/sec)	3.51 ±1.54	5.45±2.86	2.43±.88	2.73±.96
	S x 10^2(Kg/m^3.Pa)	3.00±1.00	3.00±0.40	3.00±0.50	2.00±0.40
	Px10^{16}(Kg-/m^2.sec.Pa)	1.04±0.38	1.50 ±.64	0.74±.20	0.66±0.28
40	$Dx10^{15}$(m^2/sec)	4.16 ±1.60	4.55± 0.77	3.63± 0.72	3.53± 1.80
	S x 10^2(Kg/m^3.Pa)	0.72 ±0. 39	0. 41 ±0.06	0.39 ±0.05	0.33 ±0.04
	Px10^{16}(Kg-/m^2.sec.Pa)	2.79±1.62	1.93 ±1.06	1.42 ±0.33	0.07 ±.08

5 CONCLUSION

In this research study, water vapor barrier properties of polylactide (PLA) at 10 °C , 23°C & 40 °C for relative humidity ranging from 20 % to 80 % were determined using quartz crystal microbalance (QCM) technology. This study demonstrates how QCM can be used for determining the barrier properties of polymeric packaging materials. The main findings or the conclusions of this study can be outlined as

1. A complete system using QCM was built, calibrated and used to measure the water vapor sorption of PLA at different temperature and relative humidity conditions.

2. Carrier gas (N_2) flow of 20 sccm was established as the optimal flow rate for the different relative humidity conditions and was used as a baseline in the experimental work.

3. Spin coating conditions for producing extremely thin films were optimized and with those conditions, polymer films with a thickness 1.25 ± 0.29 μm having a crystallinity of 21 ± 2 % were able to be produced.

4. QCM has been found as an effective tool for reducing the equilibration times significantly as compared to other conventional techniques currently in use.

5. This study demonstrated the ability of QCM to measure and obtain diffusivity, solubility and permeability data. Diffusion coefficient (D) in the range of 2.6 to 5.67×10^{-15} m^2 / sec , solubility coefficient (S) in the range of 0.33 to 11.0×10^{-2} Kg/m^3-Pa and permeability coefficient (P) in the range of 0.07 to 3.17×10^{-16} (Kg-m/m^2-sec-Pa) were obtained for temperature at 10 °C , 23 °C & 40 °C and relative humidity ranging from 20 % to 80 %.

6. Even though QCM was able to be used to measure the diffusivity, solubility and permeability data, a large variability was found in the final results , which needs to be looked into in future studies.

5.1 Future work recommendations

- As the variability in thickness of the films used can be a major source of variability in the final results, a more detailed study on the spin coating conditions should be done to determine the best conditions which produce films with lower variability.

- In addition to the variability in thickness of films, there is a need to find out the presence of pin holes, cracks or any other surface irregularities in the surface of films and analyzing them with techniques such as atomic force microscopy.

- Factors such as flow cell volume in the deriving the model with proper boundary conditions should be included for deriving the best suited model.

6 APPENDICES

6.1 Appendix A – Equation for the fractional mass uptake for one sided diffusion

A is the area of the film
L is thickness of polymer film
Using boundary conditions as x = 0 to x = 1
C (x,t) is the concentration is point x in the film at time t
C_0 is concentration at impermeable surface ($C_0 = 0$)
Mt is the mass uptake at time t
M_∞ is mass uptake at steady state
By using Fick's second law

$$M_t = \int_0^l [c(x,t) - c_o] A.dx$$

$$M_T = A\int_0^l \left[(c_1 - c_0) - \frac{4(c_1 - c_0)}{\pi} \Sigma \right] dx = A(c_1 - c_0)\int_0^l \left[1 - \frac{4}{\pi} \Sigma \right] dx$$

$$= A(c_1 - c_0)\left[l - \frac{4}{\pi} \Sigma \frac{(-1)^n}{2m+1} \int_0^l c(\frac{m}{2})\frac{\pi x}{l} e^{-l} dx \right]$$

$$= A(c_1 - c_0)\left[l - \frac{4}{\pi} \Sigma \frac{(-1)^m}{2m+1} e^{s\frac{m\pi x}{2\ l} - \frac{m\pi}{2\ l}} \right] = A(c_1 - c_0)\left[l - \frac{4}{\pi} \Sigma \frac{(-1)^m}{2m+1} e^{-(\frac{2l}{(2m+1)\pi}(-1)^m)} \right]$$

$$= A(c_1 - c_0)\left[l - \frac{8l}{\pi^2} \Sigma \frac{e^-}{(2m+1)^2} \right]$$

$$M_T = (c_1 - c_0)(Al)\left[1 - \frac{8}{\pi^2} \sum_{m=0,}^{\infty} e^{-\frac{(m.1/2)^2 \pi^2 D.T/l^2}{(2m+1)^2}} \right]$$

$$As\ t \to \infty, M_t \to \infty = (c_1 - c_0)Al$$

$$\frac{M_t}{M_\infty} = 1 - \frac{8}{\pi^2} \sum_{m=0,1}^{\infty} \frac{e^{-(2m+1)^2 \pi^2 Dt/4l^2}}{(2m+1)^2}$$

6.2 Appendix B-Code for the QBasic Program, developed by Dr G.Burgess

```
10 Dim T(100), R(100) 'T=TIME,R=MASS RATIO

20 N = 20: For I = 1 To N: READ T(I), R(I): Next I 'EXPERIMENTAL DATA

30 DATA

40 L = thickness of film

50 D1=D1: D2=D2 'search range

70 For D = D1 To D2 Step (D2 - D1) / 10

80 SSE = 0

90 For I = 1 to N

100 Sum = 0

110 For M = 0 To 100: Z = (2 * M + 1) ^ 2 'USE 100 TERMS IN SERIES

120 Sum = Sum + Exp (-Z * 3.14 ^ 2 * D * T (I) / 4 / L ^ 2) / Z

130 Next M

140 SSE = SSE + (R (I) - 1 + (8 / 3.14 ^ 2) * Sum) ^ 2

150 Next I

160 Print "D="; D;" SSE="; SSE

170 Next D
```

Symbols

D – Diffusion coefficient

L – Thickness of the polymer film

T (I) – Time

R (I) – M_t/M_∞

SSE – Sum of squares

Procedure for running the program

1. Input T(I) and R (I) values from the experimental data collected

2. Divide range N based on the data points selected from the experimental data

3. Pick range of diffusion coefficients D1 & D2

4. Input the thickness of the polymer film

5. Save the program for each time new data values are entered

6. After saving the program, run the program by pressing function key F2.

7. Let the program print SSE vs. D for each point

6.3 Appendix C – Complete calculation of determining mass uptake on one film

Table 6-1 Physical dimensions and mechanical properties of film and quartz crystal

Thickness (cm)	0.000105
Thickness (m)	1.05E-06
Nq	166800
Film Density (gm/cc)	1.24
Quartz Density (gm/cc)	2.648
Shear Modulus of film	5357281
Accosutic Impedance of Quartz	883383
Accoustic Impedance of Film	3236619
Impedance Ratio	0.272934
Area	5.064506

Table 6-2 Raw data from QCM used for calculation of determining mass uptake on one film

Time (sec)	Frequency#1 (Hertz)	Frequency#2 (Hertz)	Sauerbrey (gm/cm^2)	Z-Match (gm/cm^2)	Sqrt(Time)/(l)	Mt/Moo (Sauerbrey)	Mt/Moo (Z-Match)
0	5008374.8	4971643.1	0	0	0.00E+00	0.00	0.00
60	5008374.71	4971643.5	1.35392E-06	1.35457E-06	7.41E+06	0.48	0.48
120	5008374.36	4971643.65	1.89362E-06	1.89454E-06	1.05E+07	0.68	0.68
180	5008374.38	4971643.68	2.07986E-06	2.08087E-06	1.28E+07	0.74	0.74
240	5008373.72	4971633.71	2.1856E-06	2.18667E-06	1.48E+07	0.78	0.78
300	5008373.75	4971557.18	2.27066E-06	2.27177E-06	1.66E+07	0.81	0.81
360	5008373.75	4971531.76	2.3267E-06	2.32784E-06	1.82E+07	0.83	0.83
420	5008373.75	4971522.15	2.36914E-06	2.37029E-06	1.96E+07	0.85	0.85
480	5008373.69	4971516.54	2.40666E-06	2.40783E-06	2.10E+07	0.86	0.86
540	5008373.71	4971512	2.44238E-06	2.44357E-06	2.22E+07	0.87	0.87
600	5008373.71	4971508.94	2.46922E-06	2.47042E-06	2.34E+07	0.88	0.88
660	5008373.74	4971506.69	2.49407E-06	2.49528E-06	2.46E+07	0.89	0.89
720	5008373.77	4971504.69	2.51564E-06	2.51686E-06	2.57E+07	0.90	0.90
780	5008373.8	4971502.77	2.53269E-06	2.53393E-06	2.67E+07	0.90	0.90
840	5008373.78	4971501.33	2.5443E-06	2.54554E-06	2.77E+07	0.91	0.91
900	5008373.85	4971500.03	2.56044E-06	2.56168E-06	2.87E+07	0.91	0.91
960	5008373.85	4971498.85	2.57893E-06	2.58018E-06	2.96E+07	0.92	0.92
1020	5008373.81	4971497.94	2.59796E-06	2.59923E-06	3.06E+07	0.93	0.93
1080	5008373.82	4971497.24	2.61392E-06	2.6152E-06	3.14E+07	0.93	0.93
1140	5008373.85	4971496.41	2.625E-06	2.62627E-06	3.23E+07	0.94	0.94
1200	5008373.86	4971495.44	2.63569E-06	2.63697E-06	3.31E+07	0.94	0.94
1260	5008373.89	4971494.36	2.64132E-06	2.6426E-06	3.40E+07	0.94	0.94
1320	5008373.91	4971493.52	2.64259E-06	2.64388E-06	3.48E+07	0.94	0.94

Table 6-2 Con't.

1380	5008373.91	4971492.87	2.65093E-06	2.65222E-06	3.55E+07	0.95	0.95
1440	5008373.86	4971492.3	2.66597E-06	2.66727E-06	3.63E+07	0.95	0.95
1500	5008373.86	4971492.02	2.67703E-06	2.67834E-06	3.71E+07	0.96	0.96
1560	5008373.83	4971491.92	2.68465E-06	2.68596E-06	3.78E+07	0.96	0.96
1620	5008373.9	4971491.45	2.69119E-06	2.6925E-06	3.85E+07	0.96	0.96
1680	5008373.9	4971490.67	2.69772E-06	2.69903E-06	3.92E+07	0.96	0.96
1740	5008373.92	4971490.06	2.69825E-06	2.69957E-06	3.99E+07	0.96	0.96
1800	5008373.92	4971489.68	2.70061E-06	2.70193E-06	4.06E+07	0.96	0.96

6.4 Appendix D - Graphical plots for the water vapor mass uptake on films at 10, 23 & 40°C at relative humidity ranging from 20 % to 80 %

6.4.1 10 ° C – 20 % RH
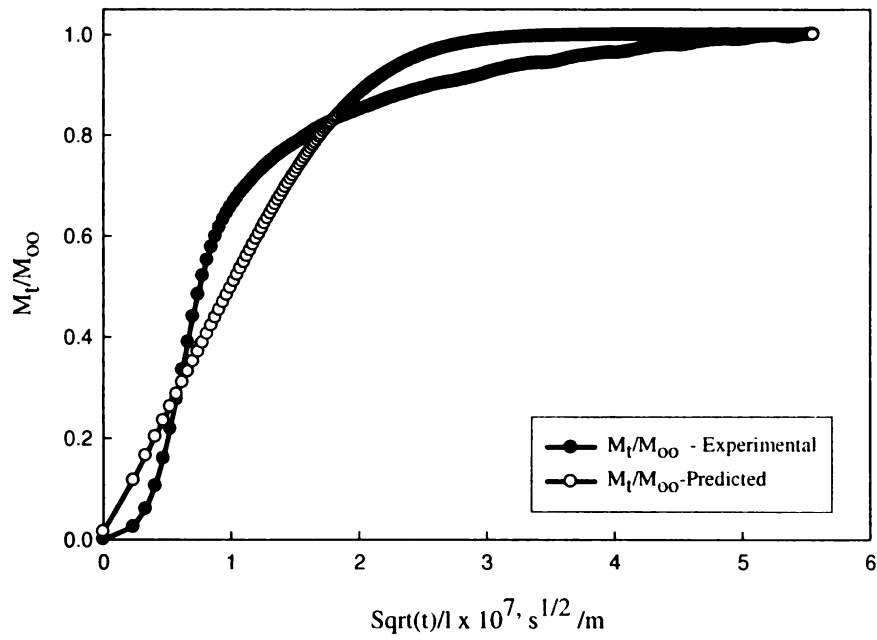
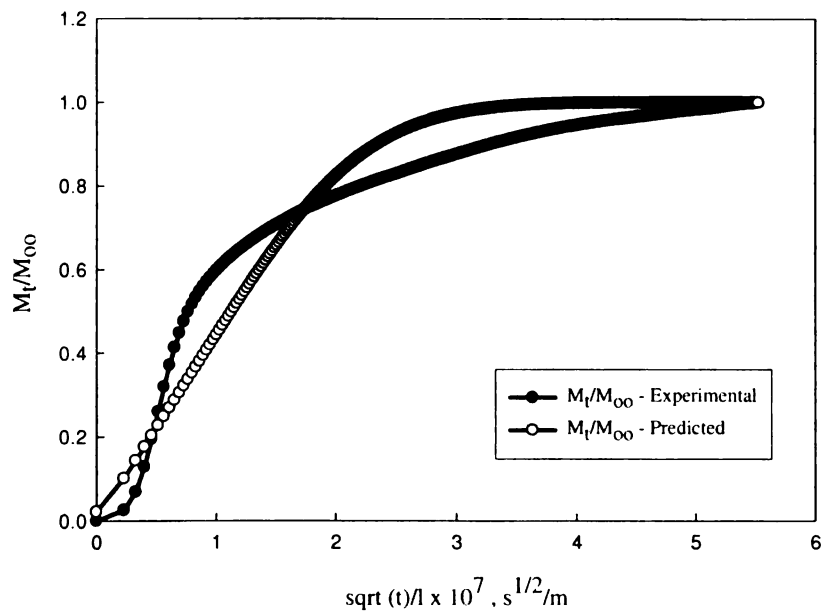Figure 7-1 Experimental & predicted mass uptake for 1.05 x 10^{-6} m at 10°C & 20 % RH
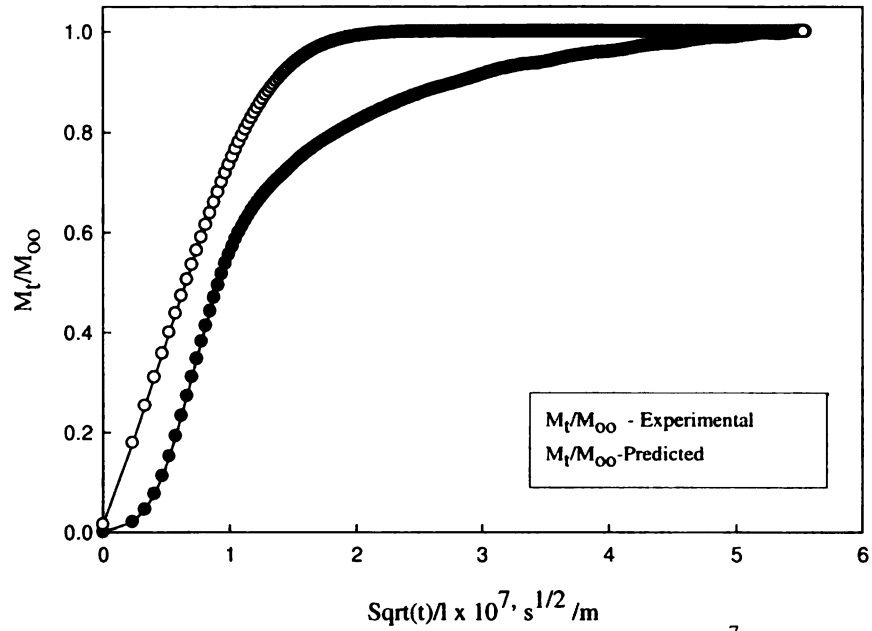
Figure 7-2 Experimental & predicted mass uptake for 6.84×10^{-7} m at 10°C & 20 % RH
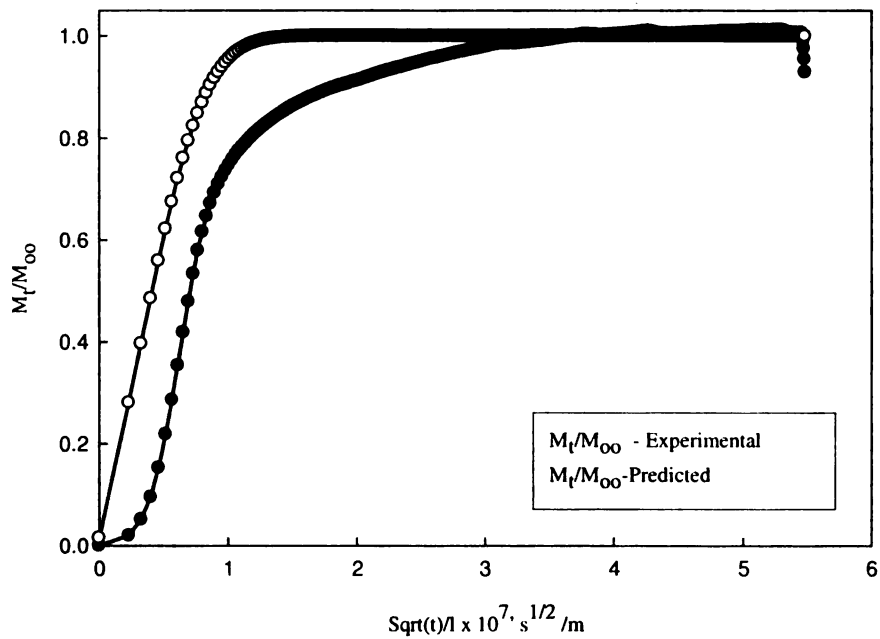
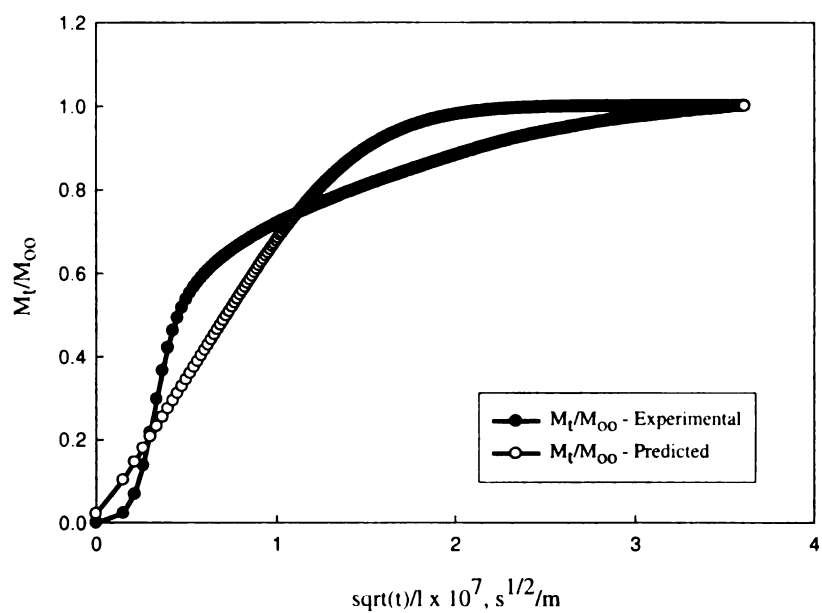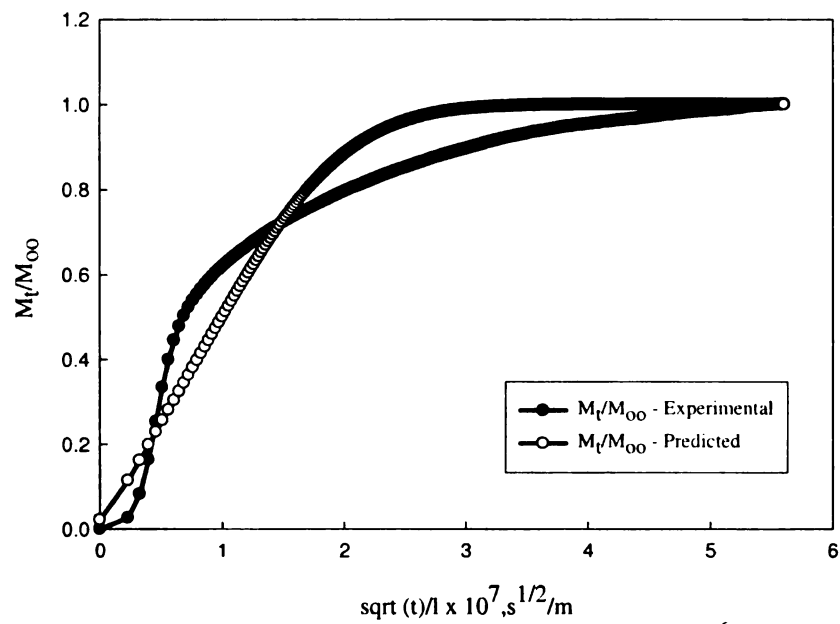Figure 7-3 Experimental & predicted mass uptake for 1.06×10^{-6} m at 10°C & 20 % RH
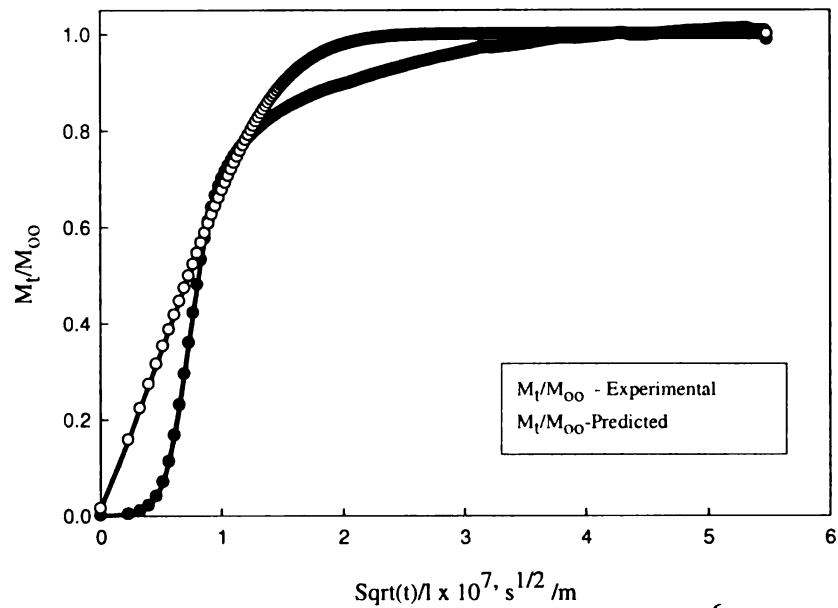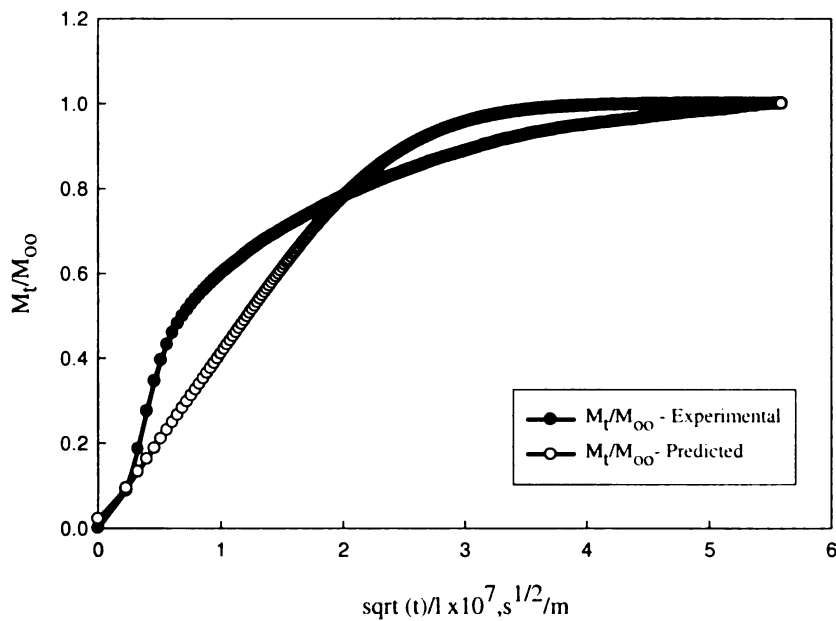
Figure 7-4 Experimental & predicted mass uptake for 1.06×10^{-6} m at 10°C & 20 % RH

6.4.2 10 ° C – 40 % RH
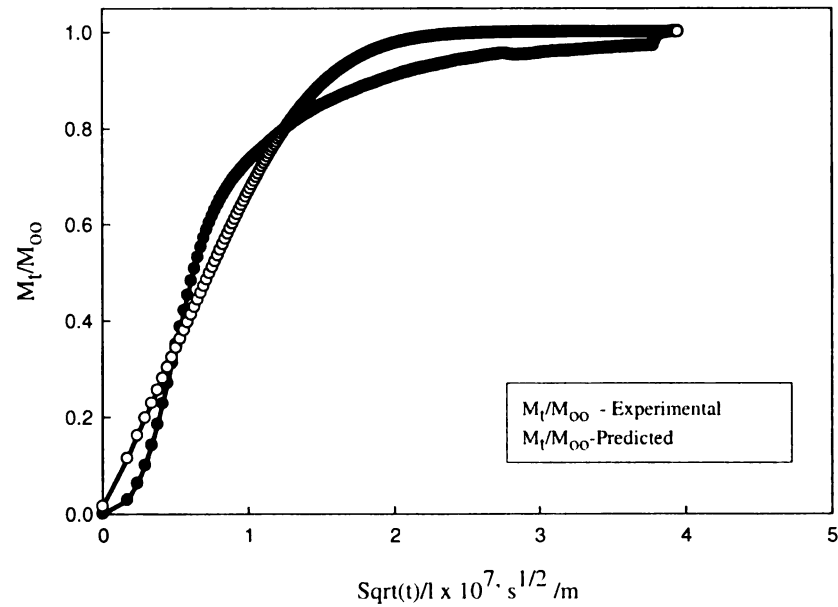
Figure 7-5 Experimental & predicted mass uptake for 1.45×10^{-6} m at 10°C & 40 % RH
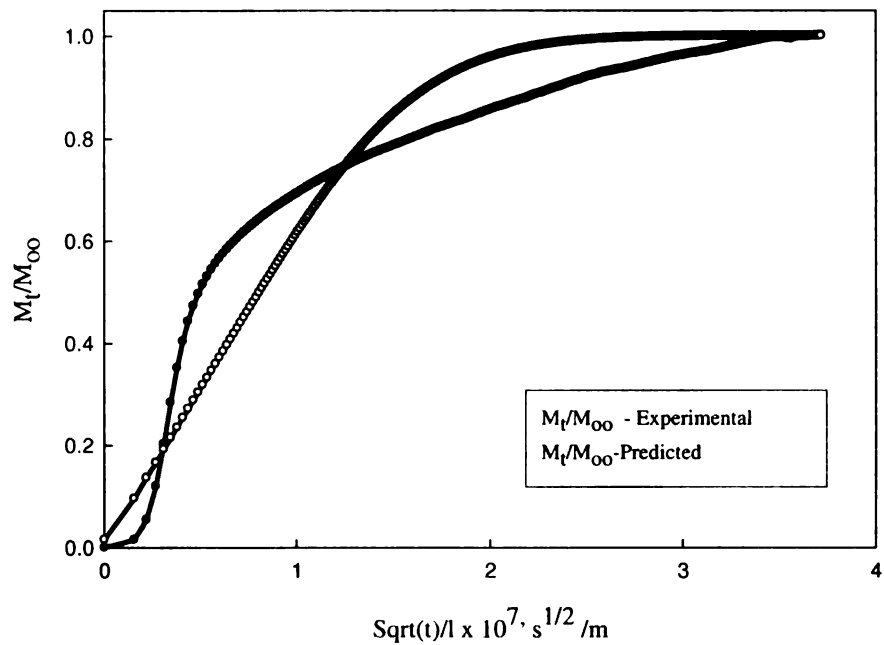
Figure 7-6 Experimental & predicted mass uptake for 1.57 x 10^{-6} m at 10°C & 40 % RH
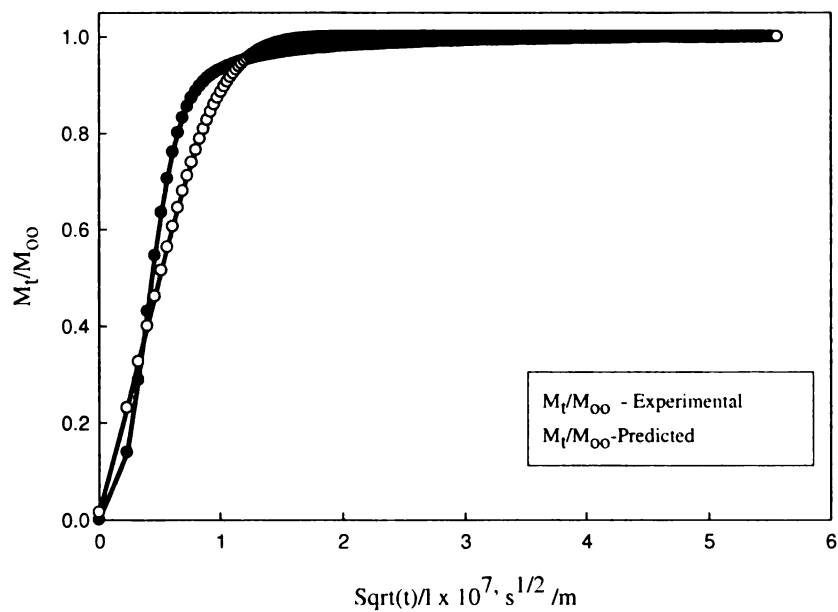
Figure 7-7 Experimental & predicted mass uptake for 1.06 x 10^{-6} m at 10°C & 40 % RH
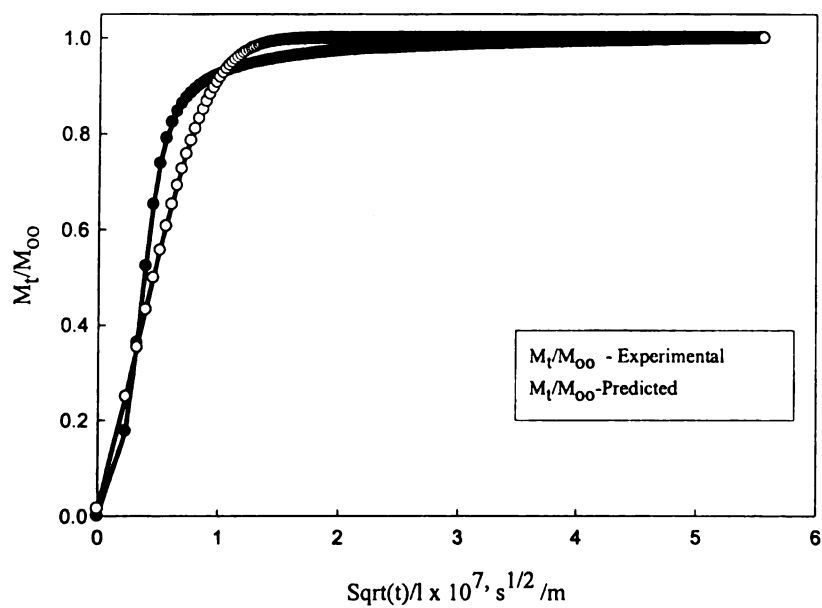
Figure 7-8 Experimental & predicted mass uptake for 1.46 x 10^{-6} m at 10°C & 60 % RH
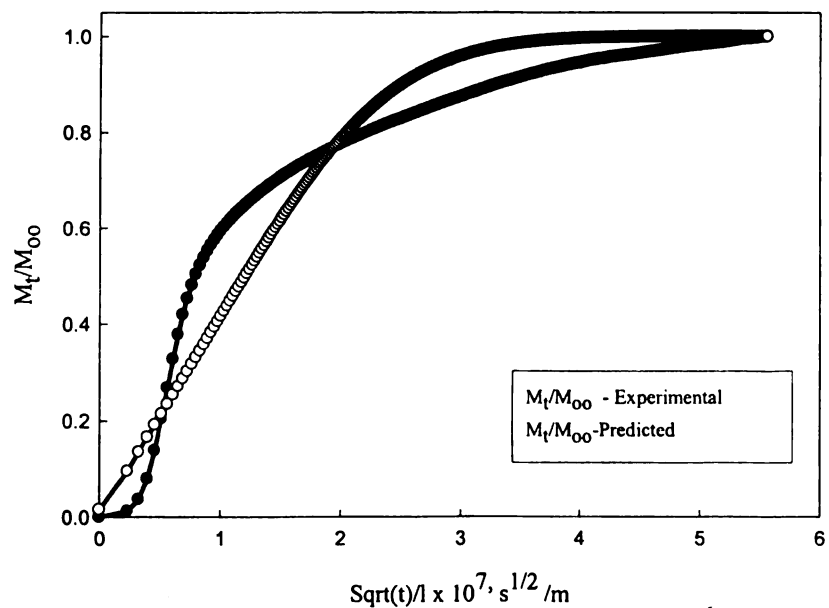
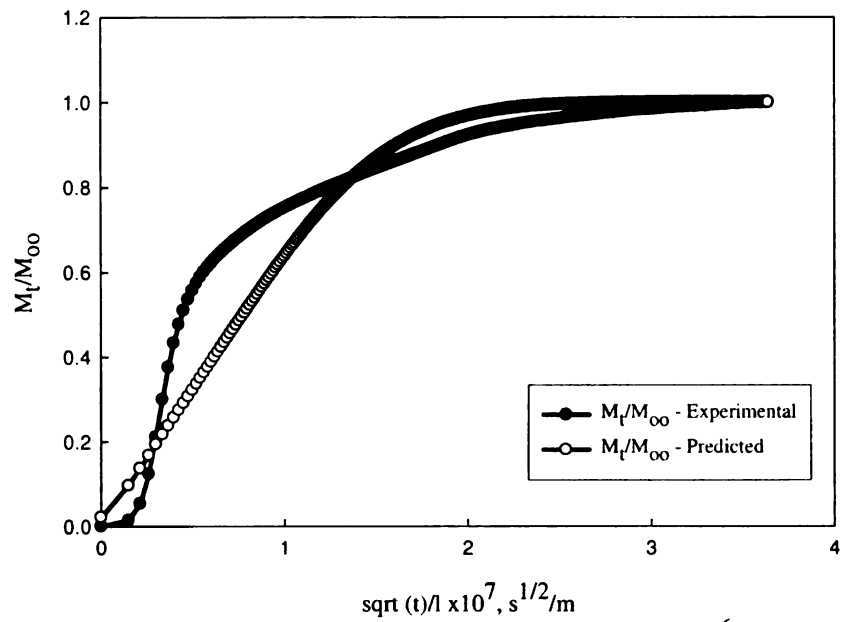Figure 7-9 Experimental & predicted mass uptake for 1.06 x 10^{-6} m at 10°C & 60 % RH
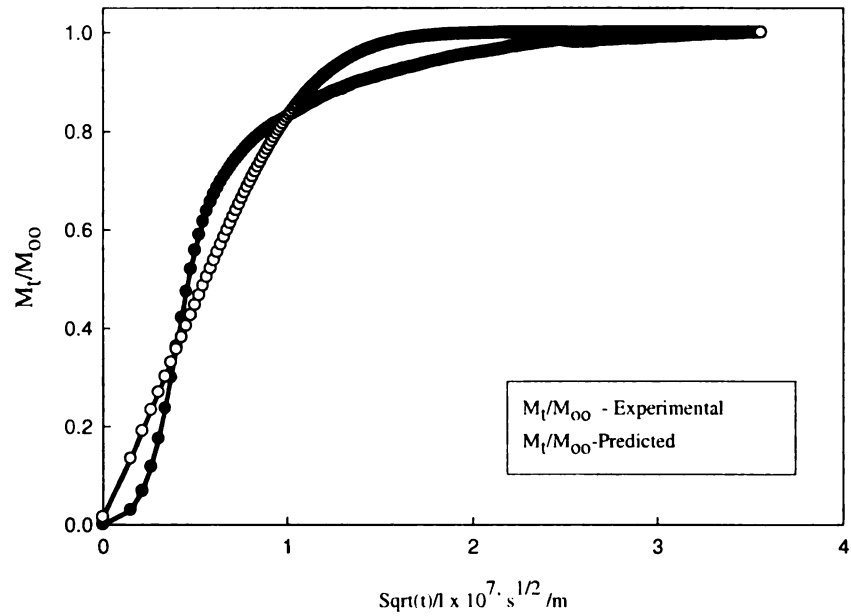
Figure 7-10 Experimental & predicted mass uptake for 1.62 x 10^{-6} m at 10°C & 60 % RH
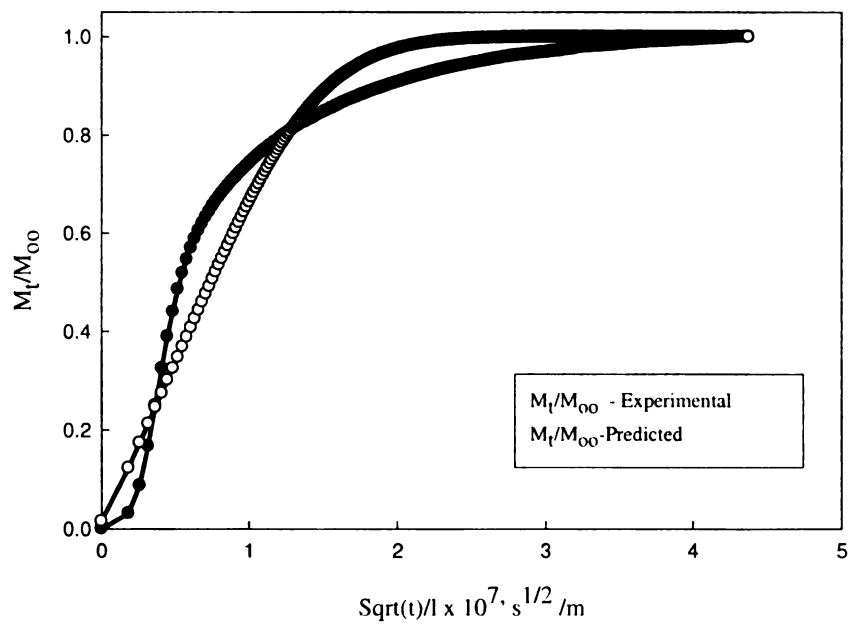
Figure 7-11 Experimental & predicted mass uptake for 1.34 x 10^{-6} m at 10°C & 60 % RH
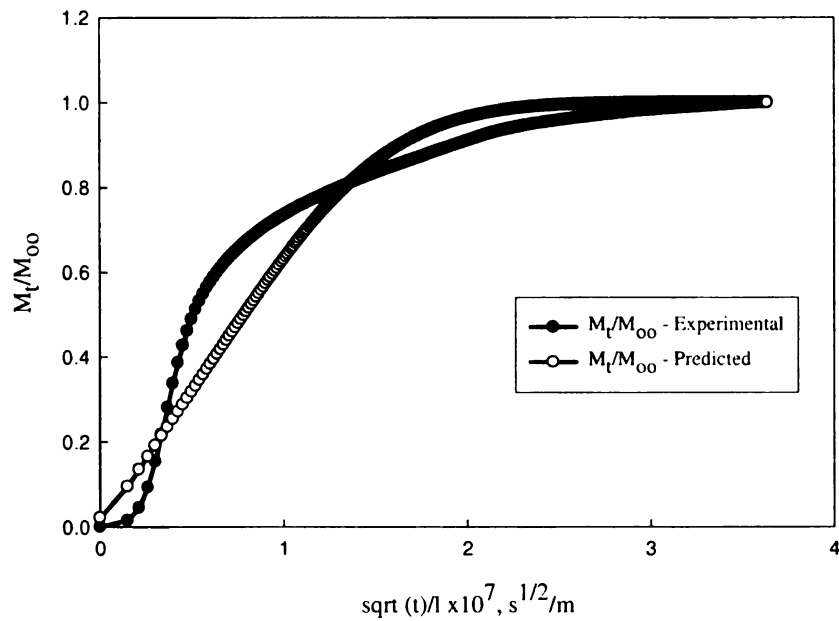
6.4.4   10°C- 80 % RH
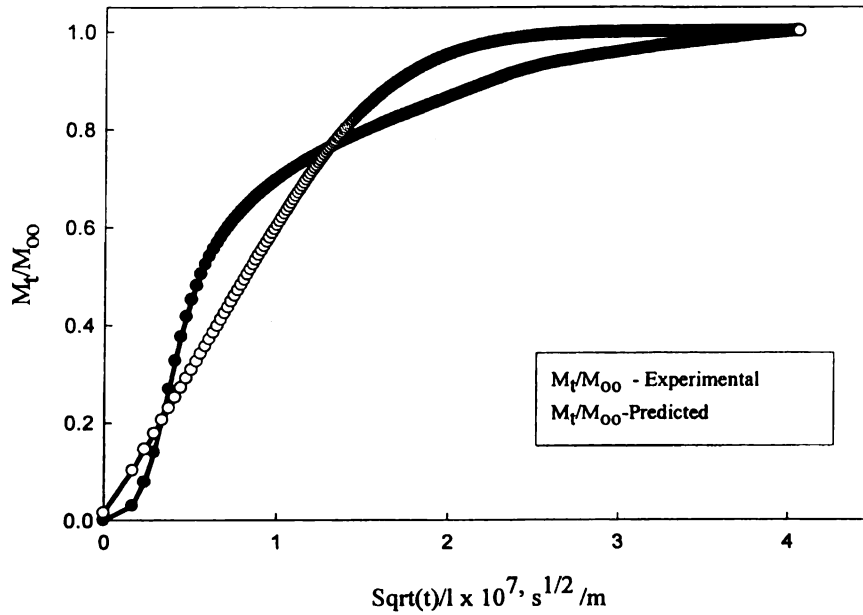
Figure 7-12 Experimental & predicted mass uptake for 1.45 x 10^{-6} m at 10°C & 80 % RH

Figure 7-13 Experimental & predicted mass uptake for 1.47 x 10^{-6} m at 10°C & 80 % RH
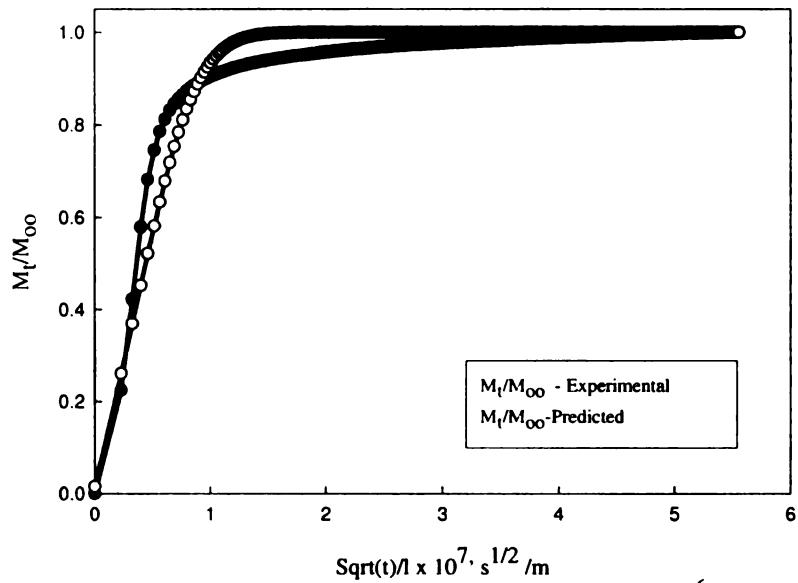
Figure 7-14 Experimental & predicted mass uptake for 1.06×10^{-6} m at 10°C & 80 % RH
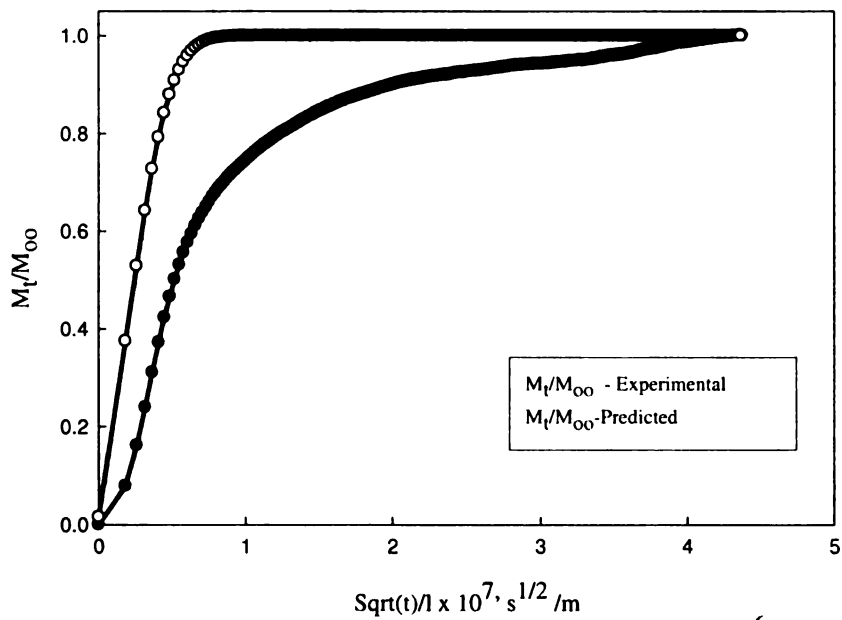
Figure 7-15 Experimental & predicted mass uptake for 1.34×10^{-6} m at 10°C & 80 % RH
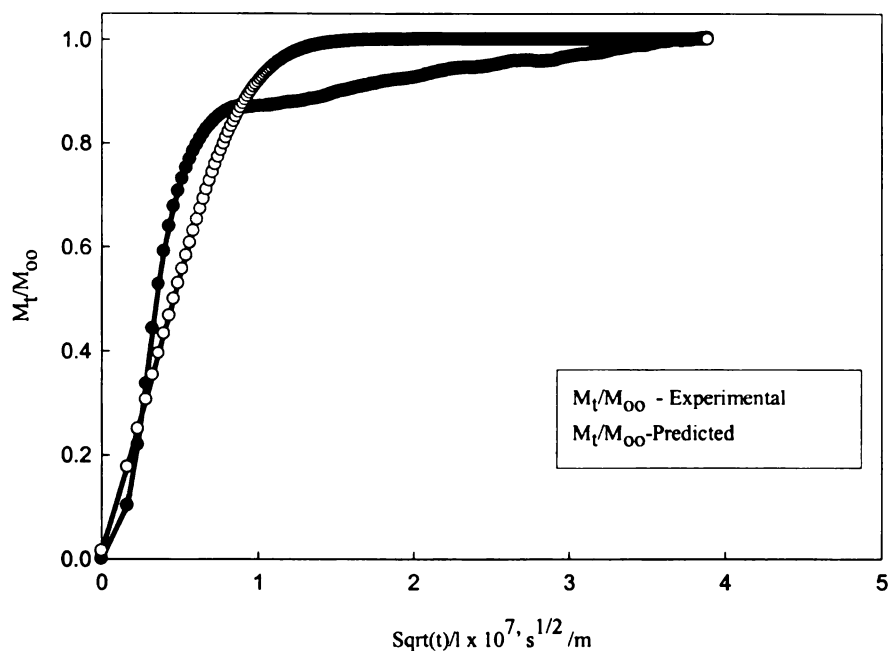
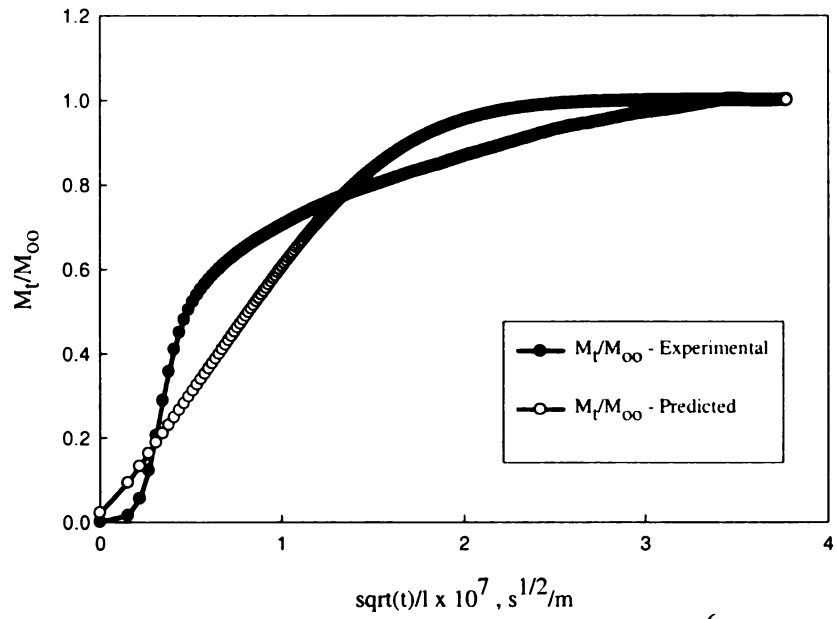Figure 7-16 Experimental & predicted mass uptake for 1.51×10^{-6} m at 10°C & 80 % RH

6.4.5   23 ° C -20 % RH
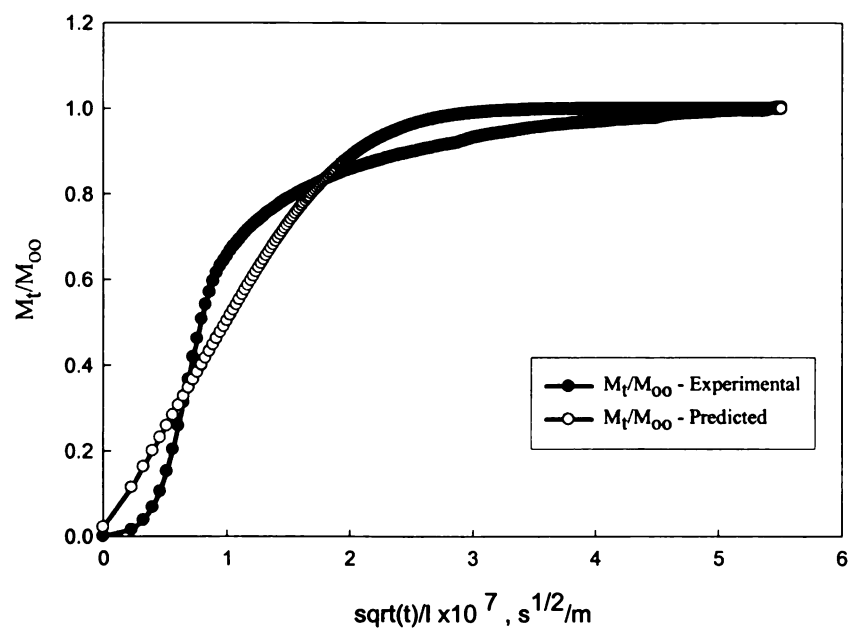
Figure 7-17 Experimental & predicted mass uptake for 1.06×10^{-6} m at 23°C & 20 % RH
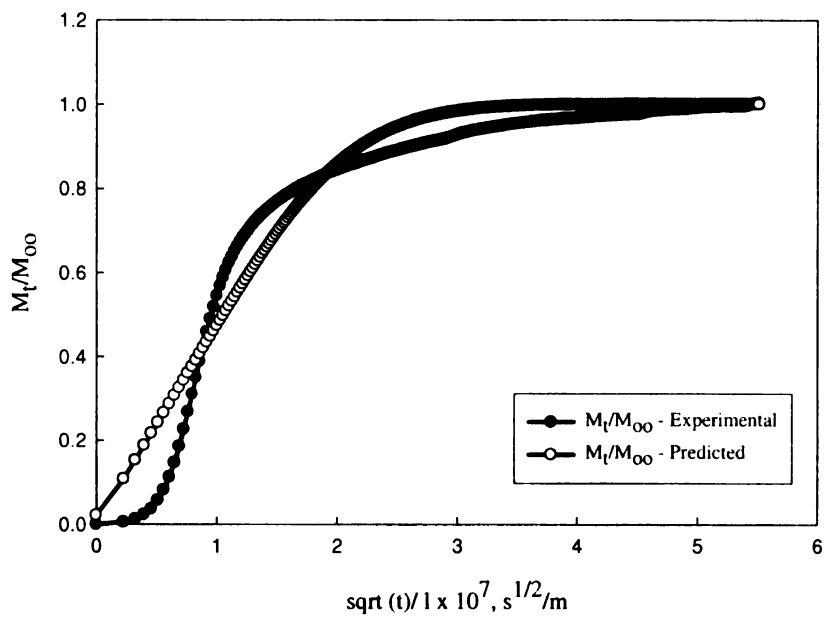
Figure 7-18 Experimental & predicted mass uptake for 1.46×10^{-6} m at 23°C & 20 % RH
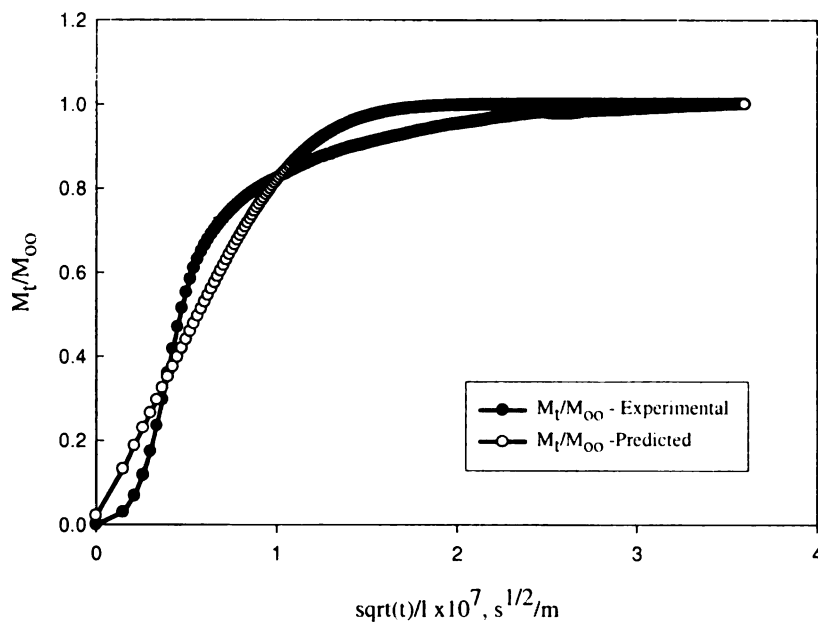
Figure 7-19 Experimental & predicted mass uptake for 1.62×10^{-6} m at 23°C & 20 % RH
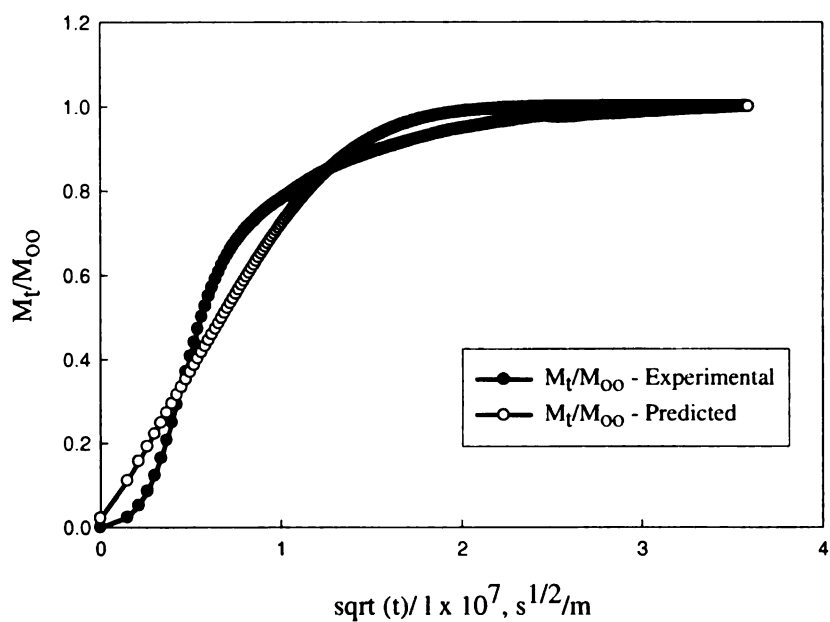
Figure 7-20 Experimental & predicted mass uptake for 1.44 x 10^{-6} m at 23°C & 20 % RH

Figure 7-21 Experimental & predicted mass uptake for 1.04 x 10^{-6} m at 23°C & 20 % RH
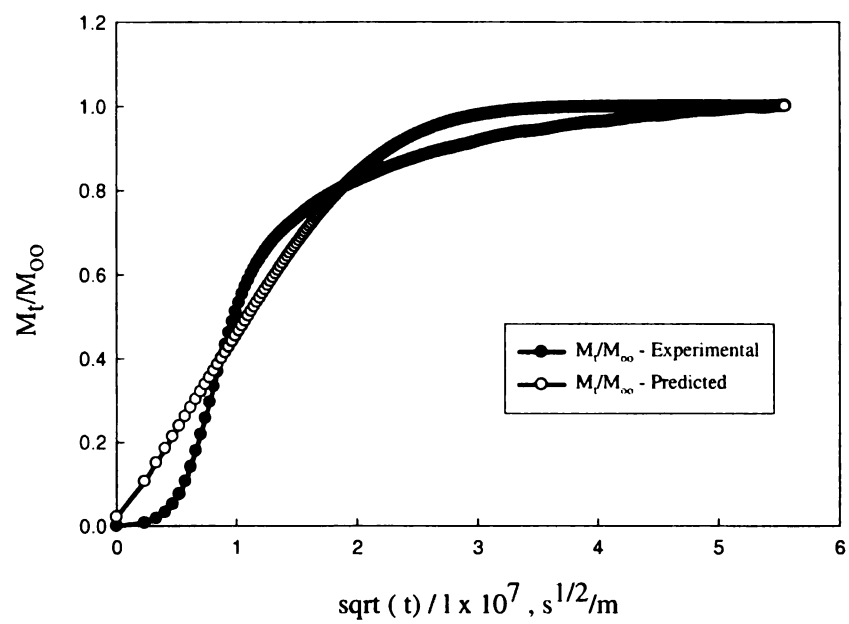
Figure 7-22 Experimental & predicted mass uptake for 6.81 x 10^{-7} m at 23°C & 20 % RH
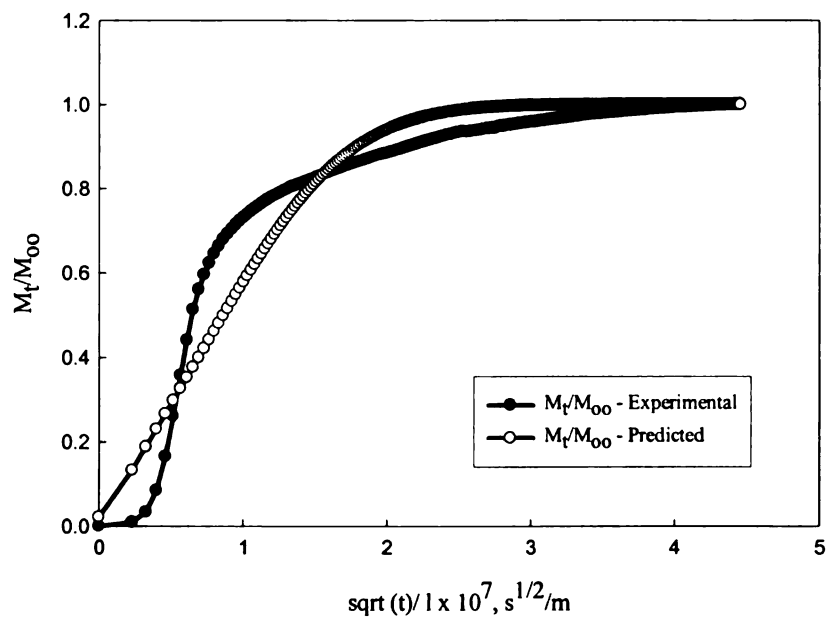
Figure 7-23 Experimental & predicted mass uptake for 1.06×10^{-6} m at 23°C & 40 % RH
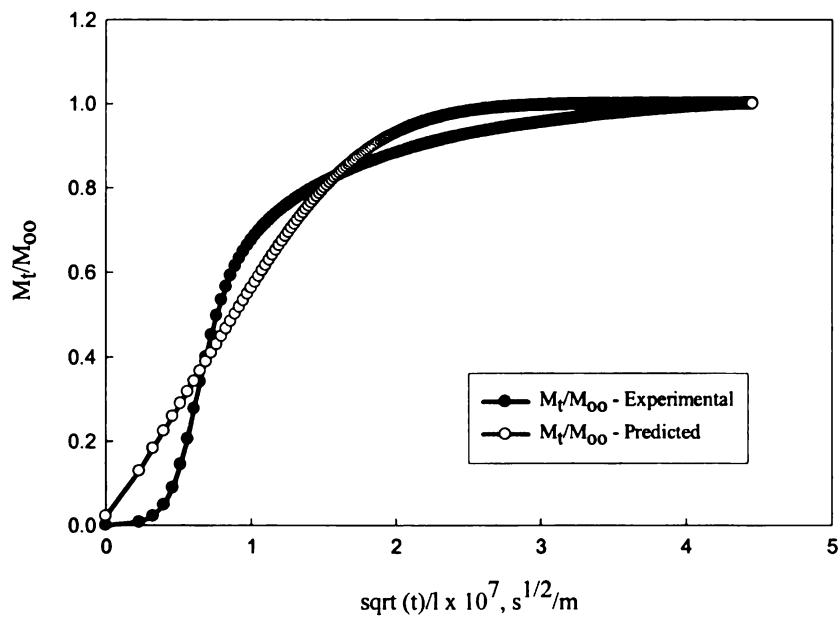
Figure 7-24 Experimental & predicted mass uptake for 1.46×10^{-6} m at 23°C & 40 % RH
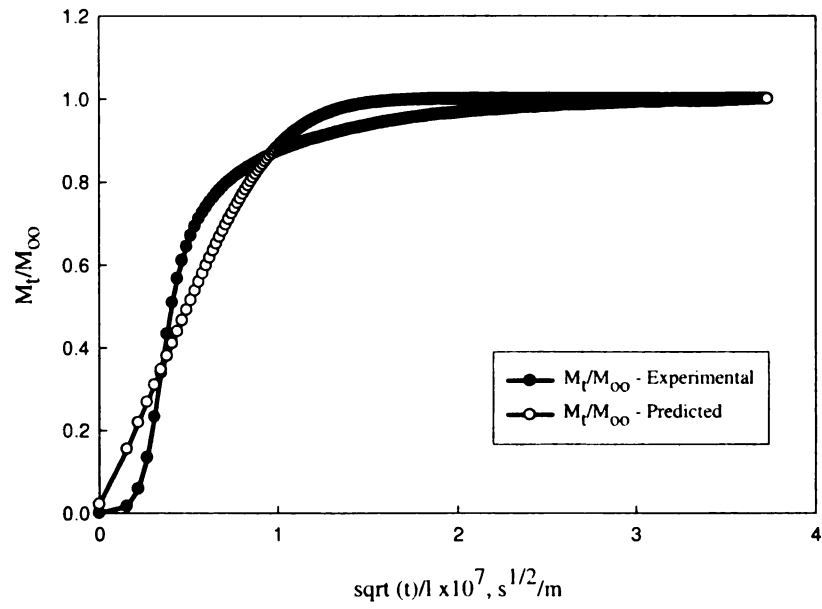
Figure 7-25 Experimental & predicted mass uptake for 1.57 x 10^{-6} m at 23°C & 40 % RH
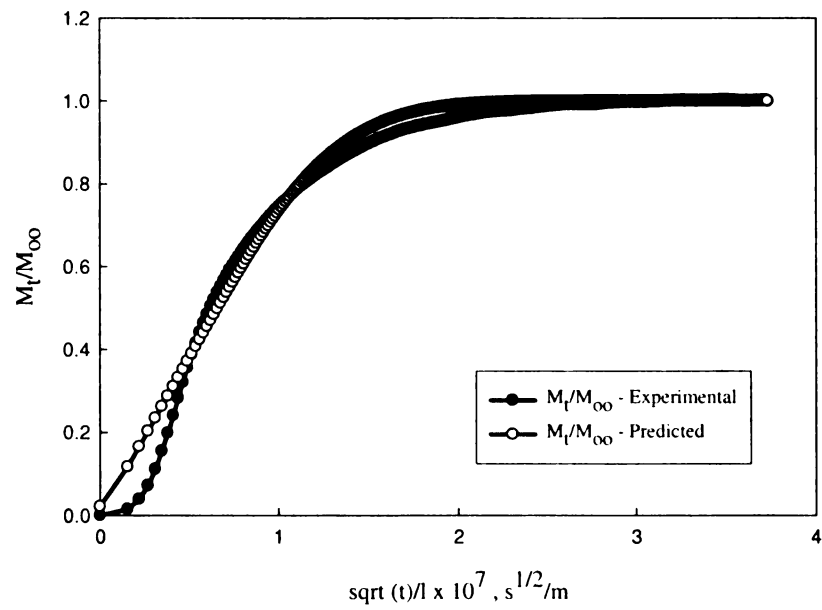
Figure 7-26 Experimental & predicted mass uptake for 1.22 x 10^{-6} m at 23°C & 40 % RH

6.4.7 23° C – 60 % RH
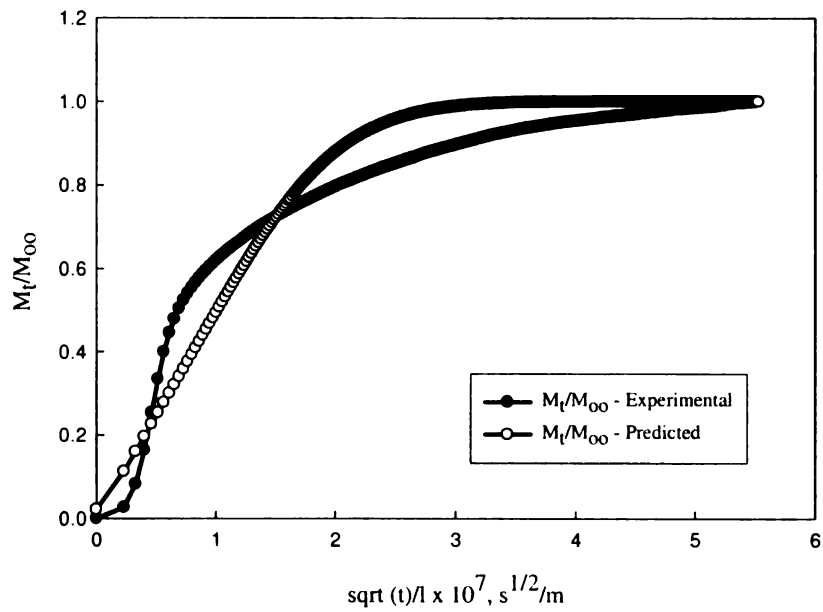
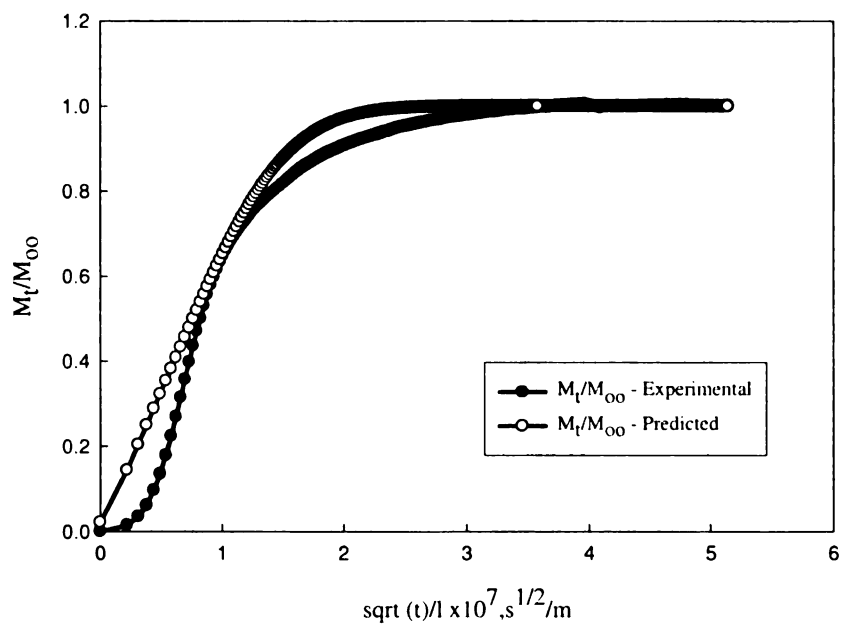Figure 7-27 Experimental & predicted mass uptake for 1.06×10^{-6} m at 23°C & 60 % RH
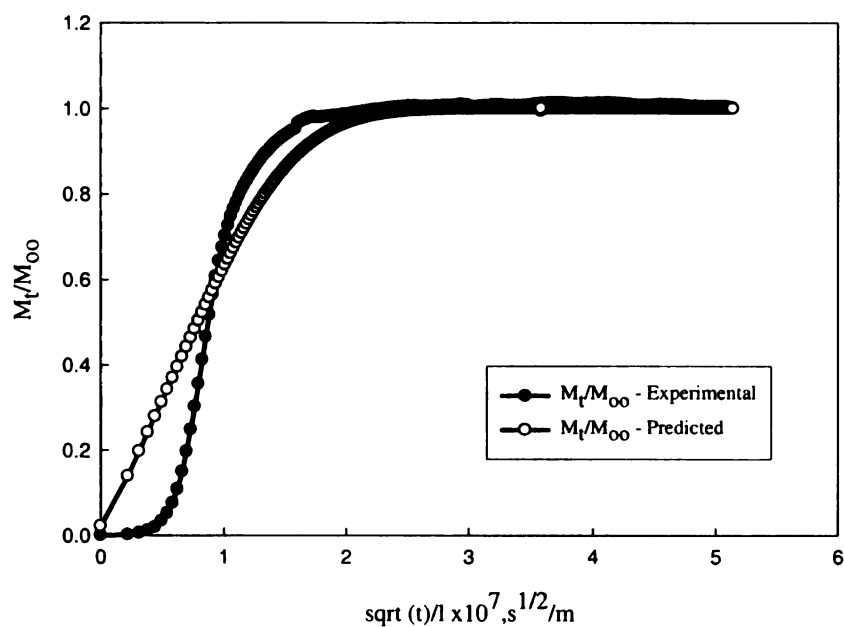

Figure 7-28 Experimental & predicted mass uptake for 1.46×10^{-6} m at 23°C & 60 % RH

Figure 7-29 Experimental & predicted mass uptake for 1.62 x 10^{-6} m at 23°C & 60 % RH
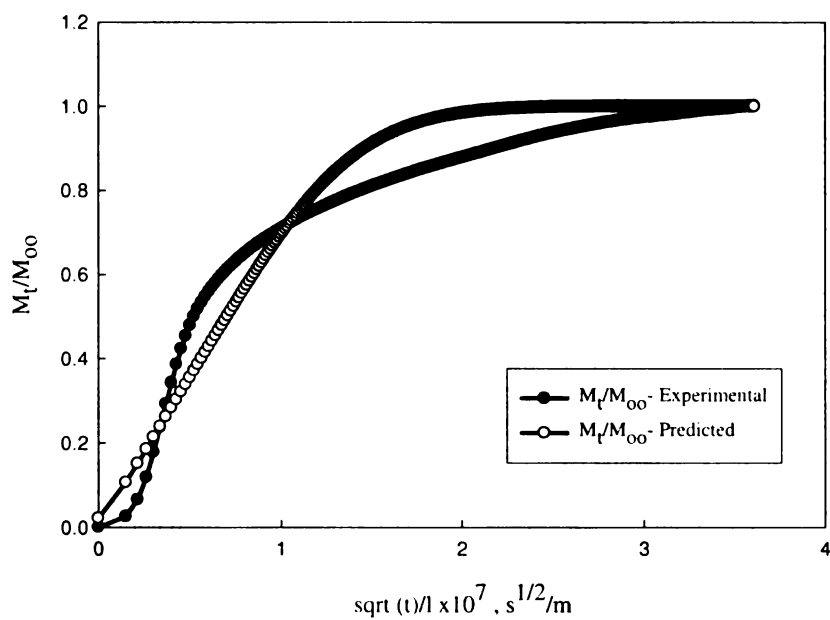
Figure 7-30 Experimental & predicted mass uptake for 1.45 x 10^{-6} m at 23°C & 60 % RH

Figure 7-31 Experimental & predicted mass uptake for 1.06 x 10^{-6} m at 23°C & 60 % RH

Figure 7-32 Experimental & predicted mass uptake for 1.06 x 10^{-6} m at 23°C & 60 % RH
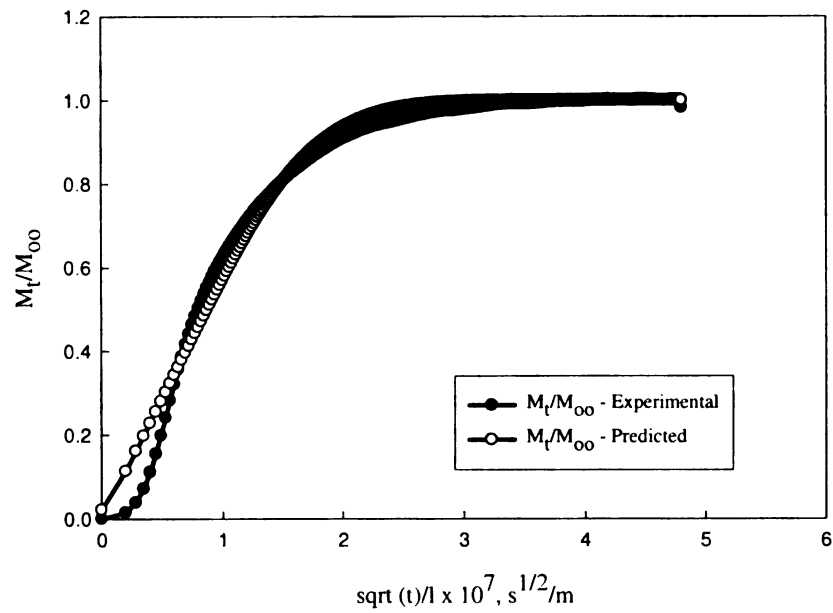
6.4.8 23 °C – 80 % RH
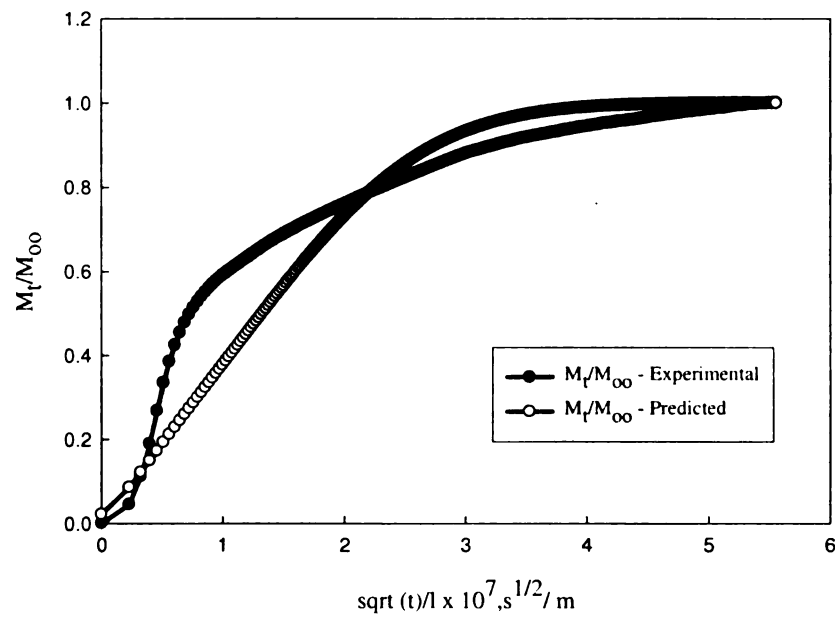
Figure 7-33 Experimental & predicted mass uptake for 1.06×10^{-6} m at 23°C & 80 % RH
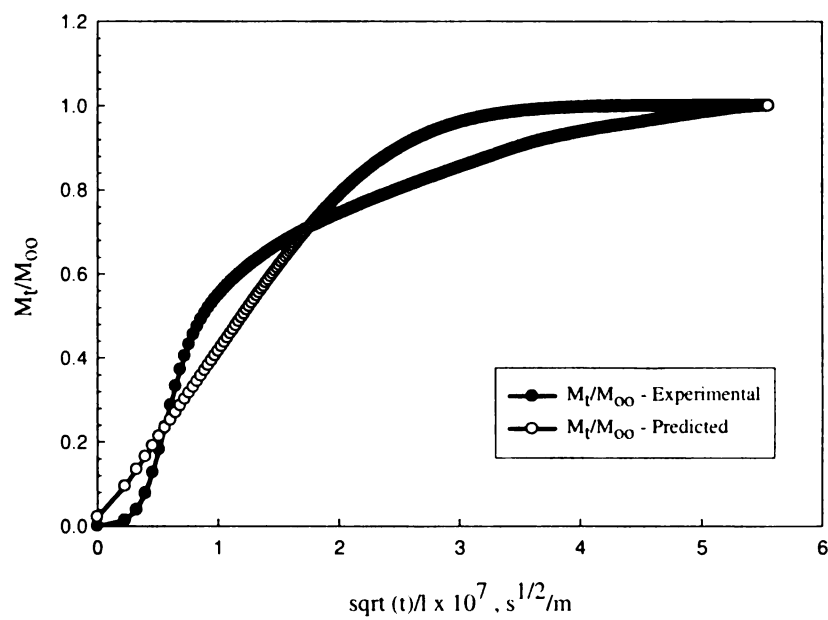
Figure 7-34 Experimental & predicted mass uptake for 1.46×10^{-6} m at 23°C & 80 % RH

Figure 7-35 Experimental & predicted mass uptake for 1.62 x 10^{-6} m at 23°C & 80 % RH

Figure 7-36 Experimental & predicted mass uptake for 1.45 x 10^{-6} m at 23°C & 80 % RH

Figure 7-37 Experimental & predicted mass uptake for 1.57 x 10^{-6} m at 23°C & 80 % RH
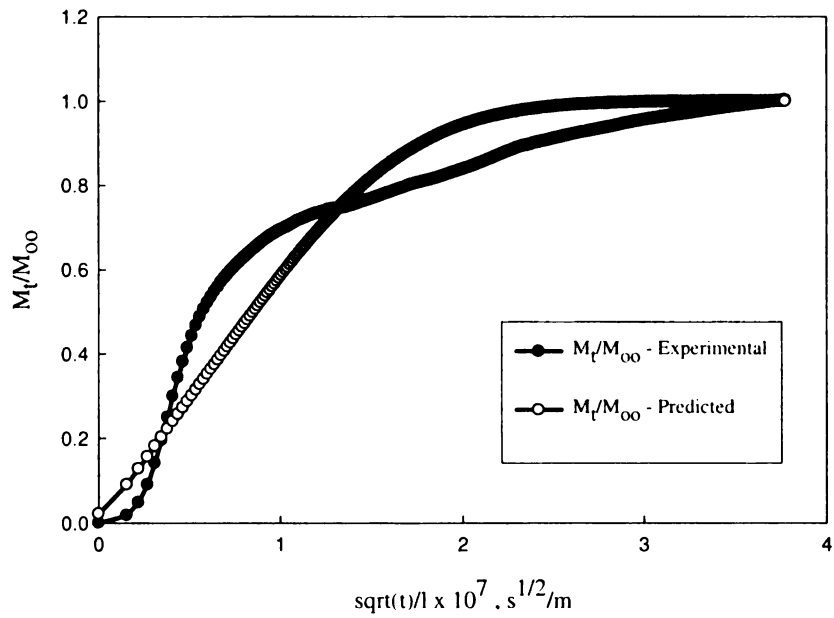
Figure 7-38 Experimental & predicted mass uptake for 1.92 x 10^{-6} m at 23°C & 80 % RH
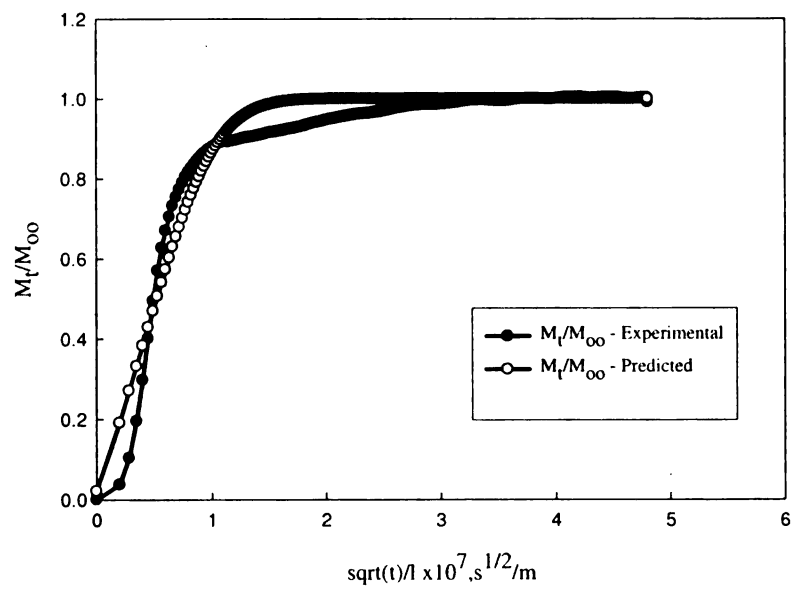
6.4.9 40 °C - 20 % RH
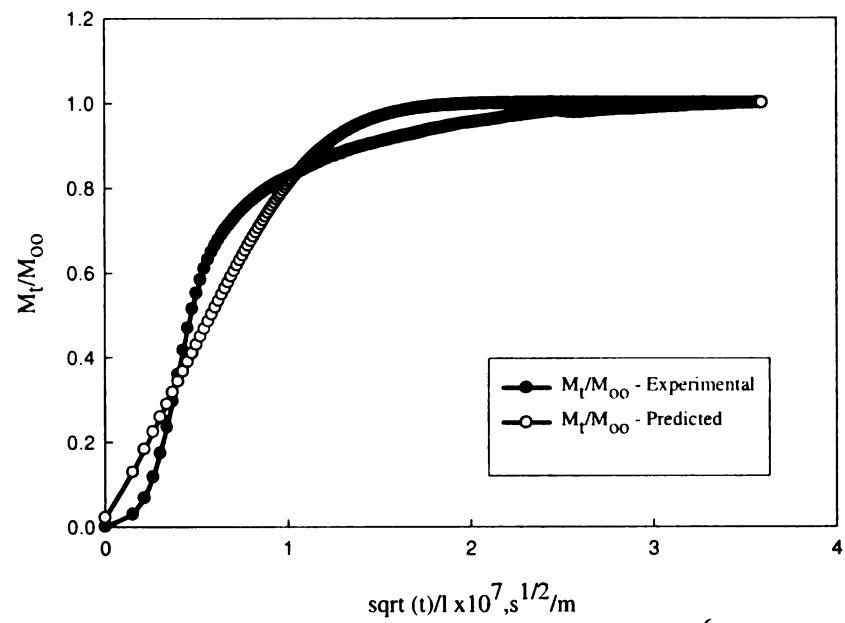
Figure 7-39 Experimental & predicted mass uptake for 1.62×10^{-6} m at 40°C & 20 % RH
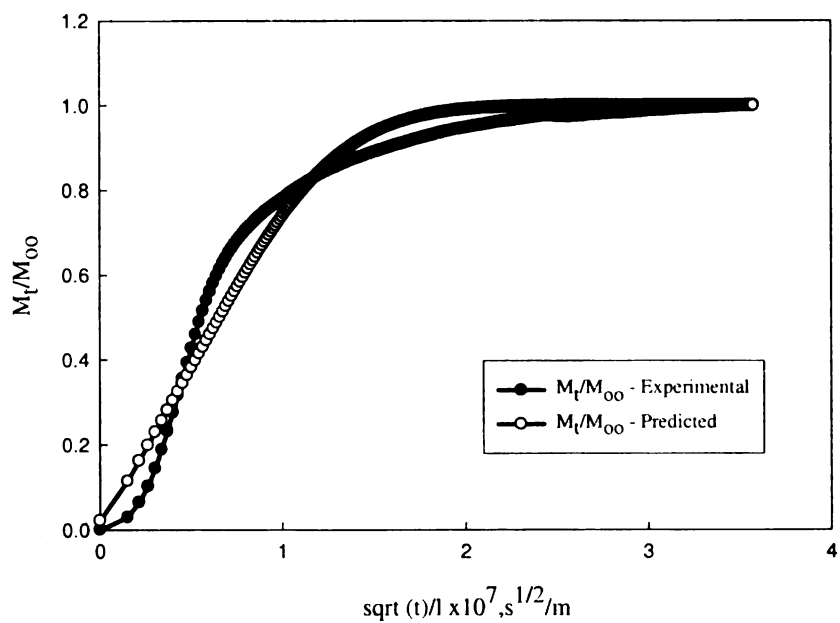
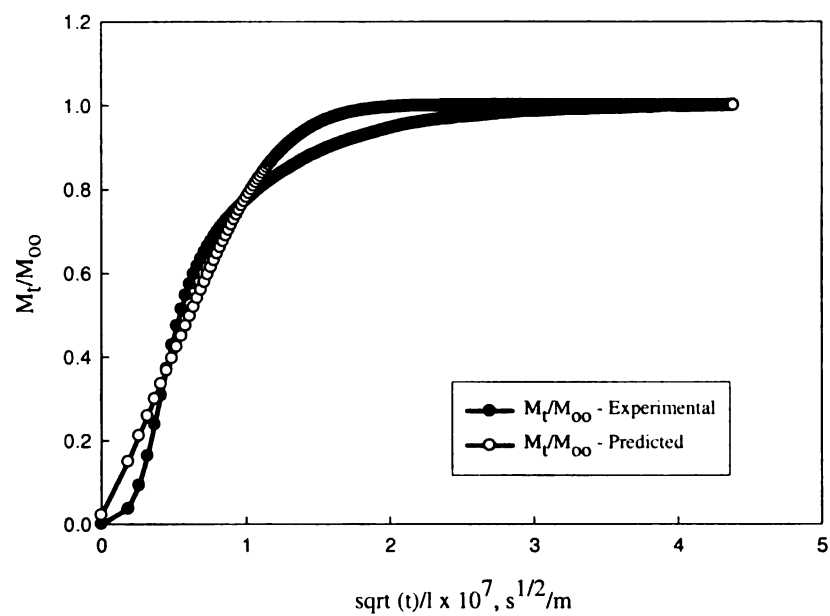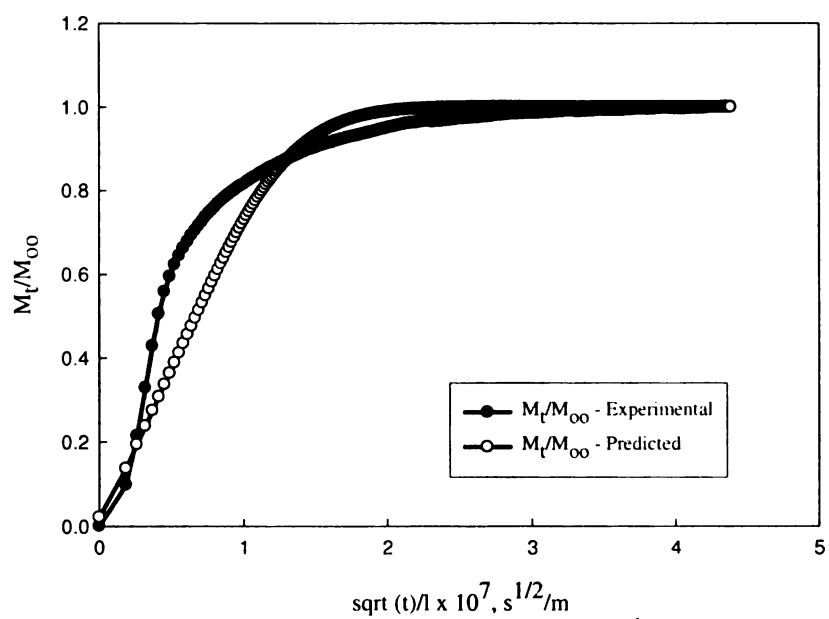Figure 7-40 Experimental & predicted mass uptake for 1.44×10^{-6} m at 40°C & 20 % RH

Figure 7-41 Experimental & predicted mass uptake for 1.11 x 10^{-6} m at 40°C & 20 % RH

Figure 7-41 Experimental & predicted mass uptake for 1.34 x 10^{-6} m at 40°C & 20 % RH

Figure 7-42 Experimental & predicted mass uptake for 1.51 x 10^{-6} m at 40°C & 20 % RH
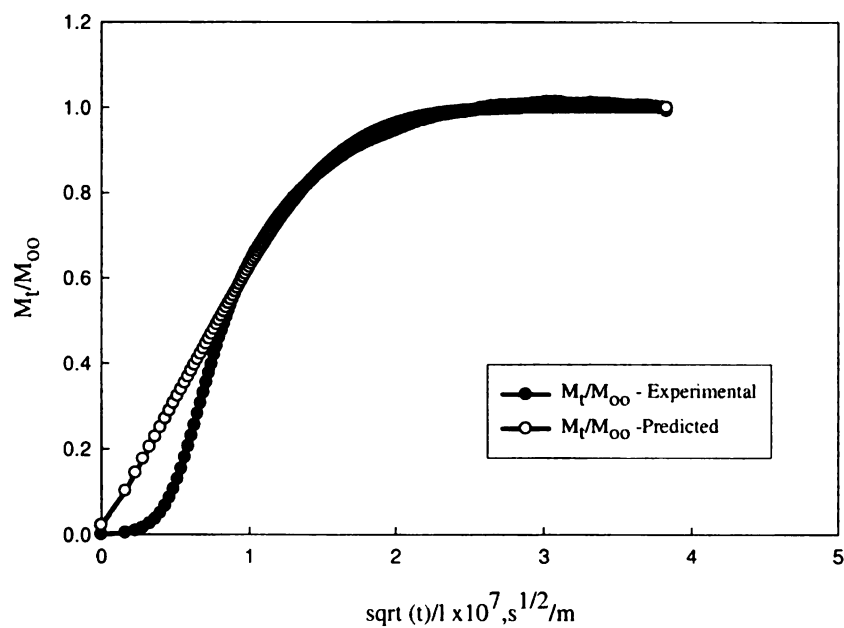
Figure 7-43 Experimental & predicted mass uptake for 1.22 x 10^{-6} m at 40°C & 20 % RH
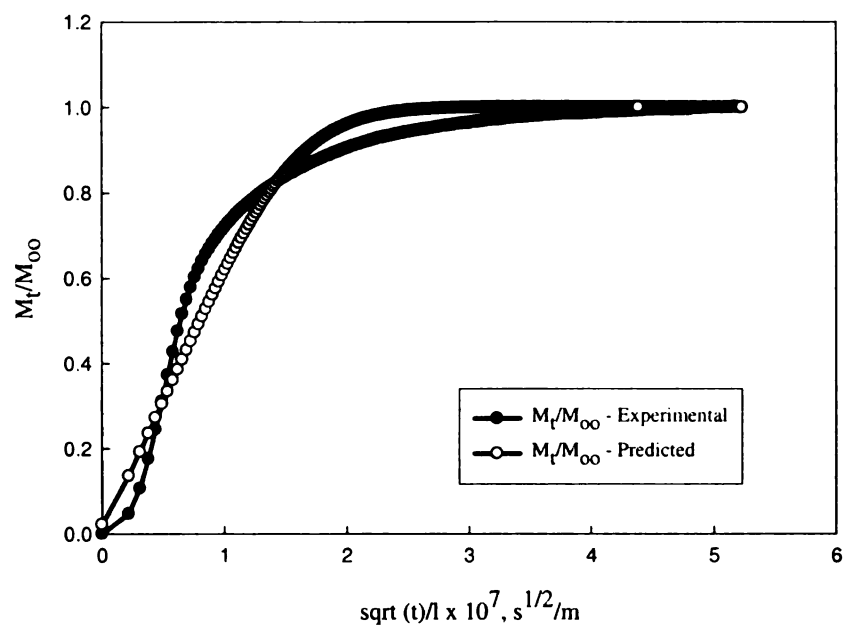
6.4.10 40°C – 40 % RH

Figure 7-44 Experimental & predicted mass uptake for 1.23 x 10^{-6} m at 40°C & 40 % RH

Figure 7-45 Experimental & predicted mass uptake for 1.23 x 10^{-6} m at 40°C & 40 % RH

Figure 7-46 Experimental & predicted mass uptake for 1.34 x 10⁻⁶ m at 40°C & 40 % RH

Figure 7-47 Experimental & predicted mass uptake for 1.11 x 10⁻⁶ m at 40°C & 40 % RH

Figure 7-48 Experimental & predicted mass uptake for 1.12×10^{-6} m at 40°C & 40 % RH

Figure 7-49 Experimental & predicted mass uptake for 1.21×10^{-6} m at 40°C & 40 % RH

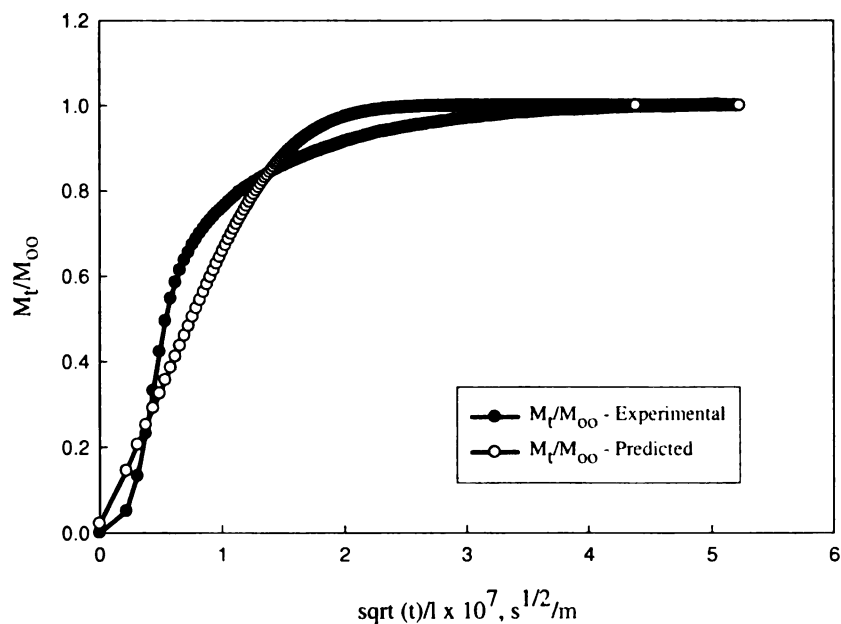Figure 7-50 Experimental & predicted mass uptake for 1.20×10^{-6} m at 40°C & 60 % RH

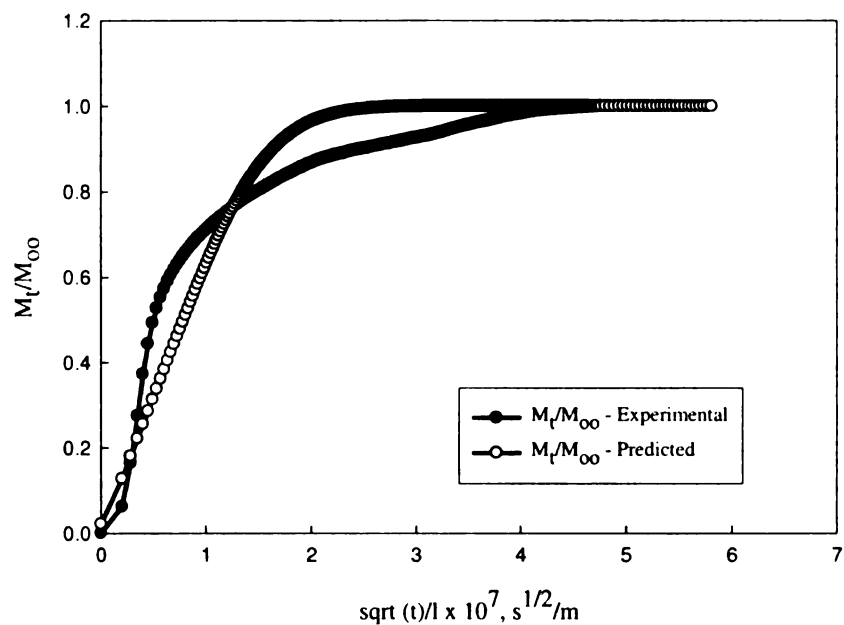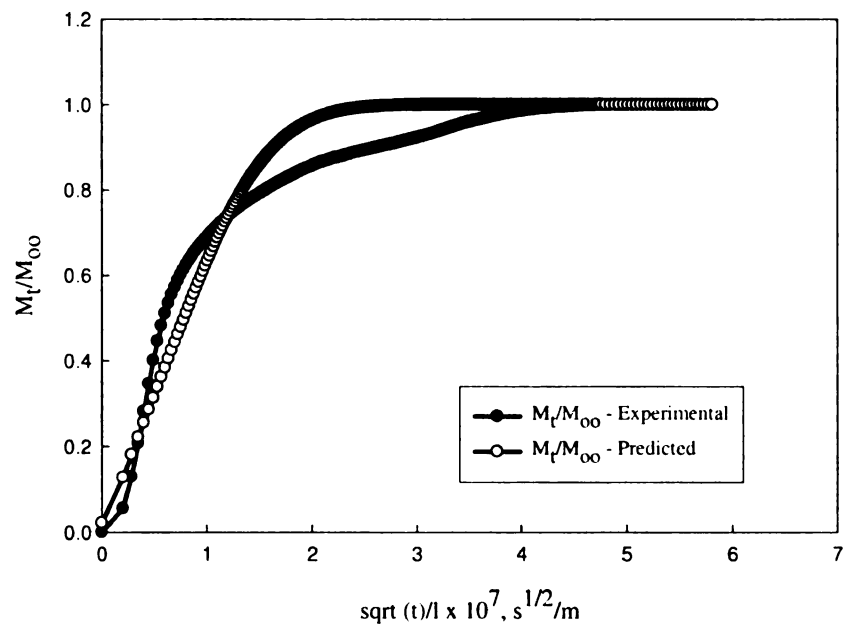
Figure 7-51 Experimental & predicted mass uptake for 1.12×10^{-6} m at 40°C & 60 % RH

Figure 7-52 Experimental & predicted mass uptake for 1.11×10^{-6} m at 40°C & 60 % RH

Figure 7-53 Experimental & predicted mass uptake for 1.34×10^{-6} m at 40°C & 60 % RH

Figure 7-54 Experimental & predicted mass uptake for 1.51×10^{-6} m at 40°C & 60 % RH
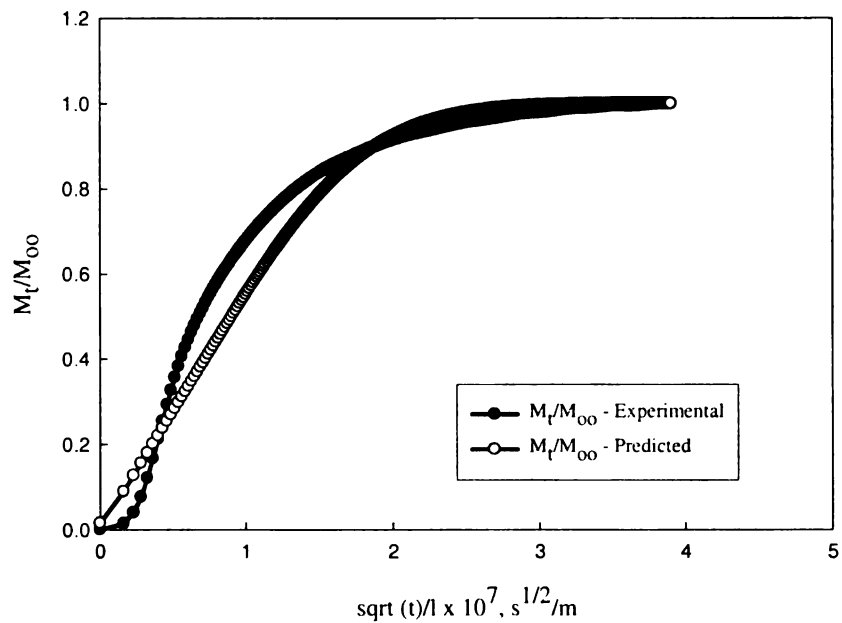
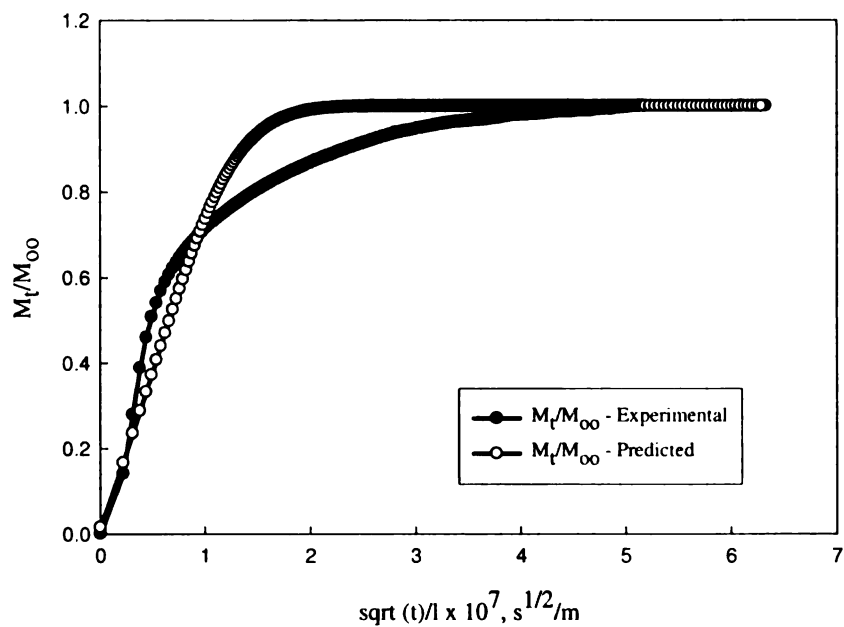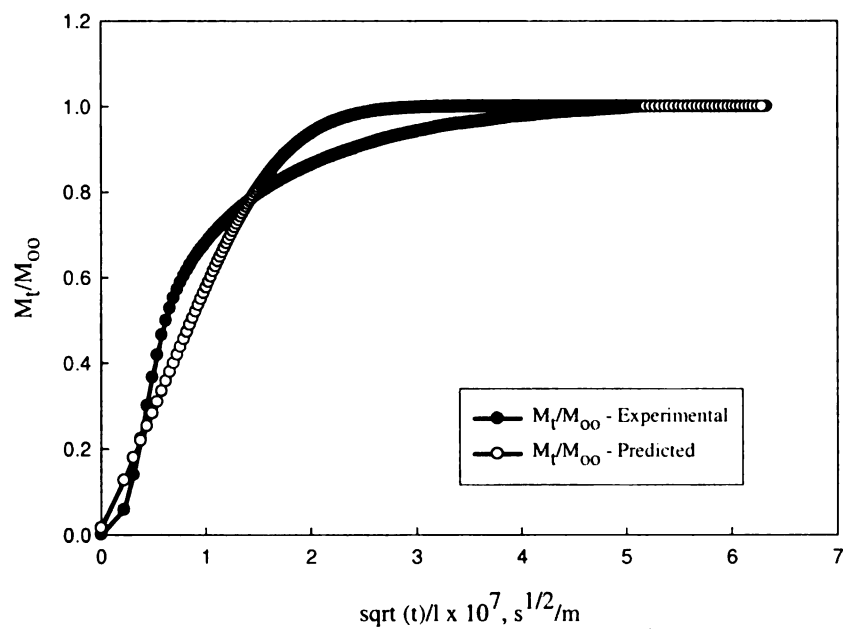Figure 7-55 Experimental & predicted mass uptake for 1.23×10^{-6} m at 40°C & 60 % RH

6.4.12 40°C – 80 % RH

Figure 7-56 Experimental & predicted mass uptake for 1.11 x 10^{-6} m at 40°C & 80 % RH

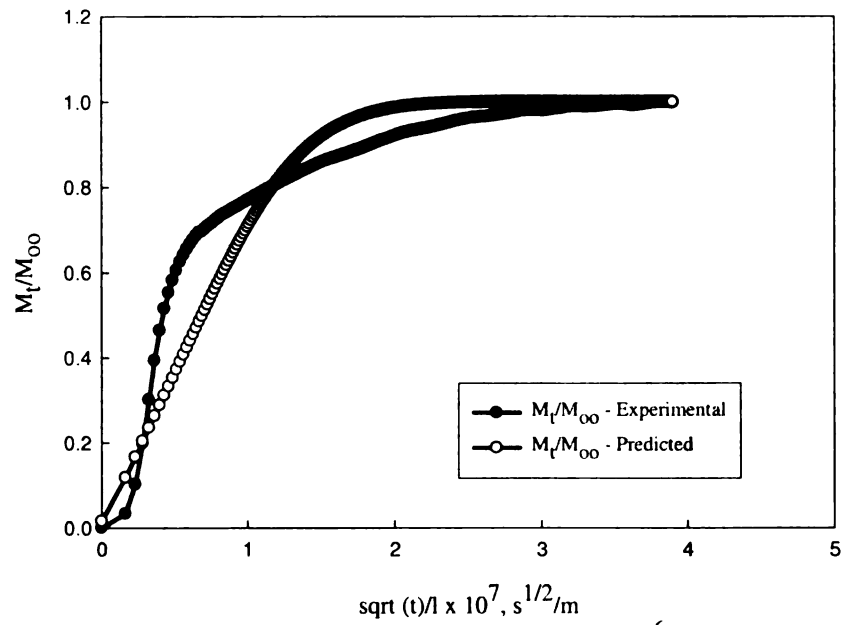Figure 7-57 Experimental & predicted mass uptake for 1.34 x 10^{-6} m at 40°C & 80 % RH
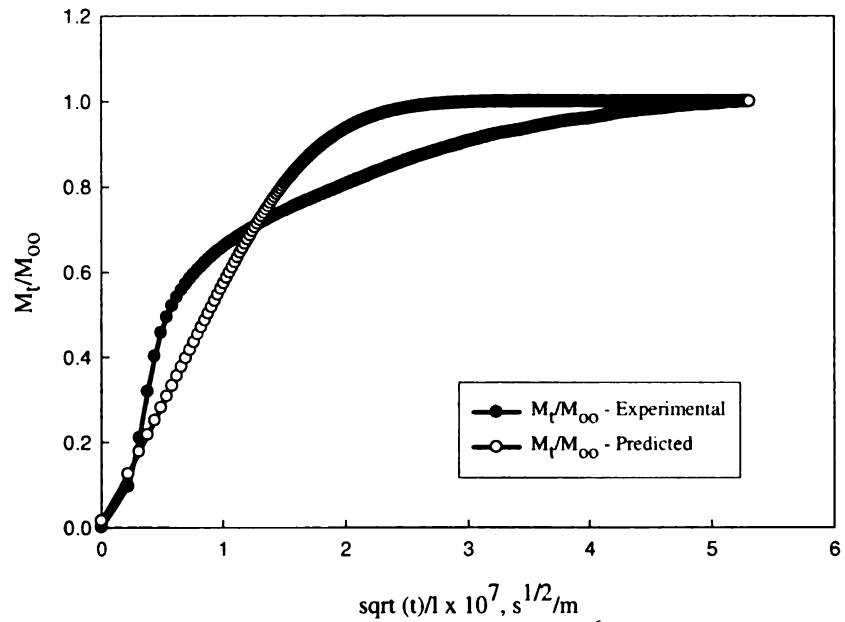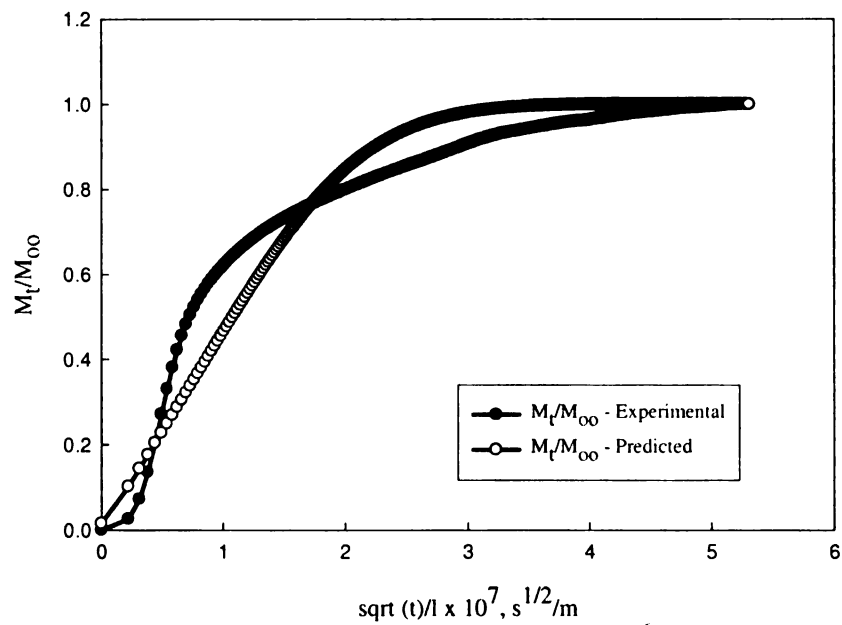
Figure 7-58 Experimental & predicted mass uptake for 1.51×10^{-6} m at 40°C & 80 % RH

Figure 7-59 Experimental & predicted mass uptake for 1.23×10^{-6} m at 40°C & 80 % RH
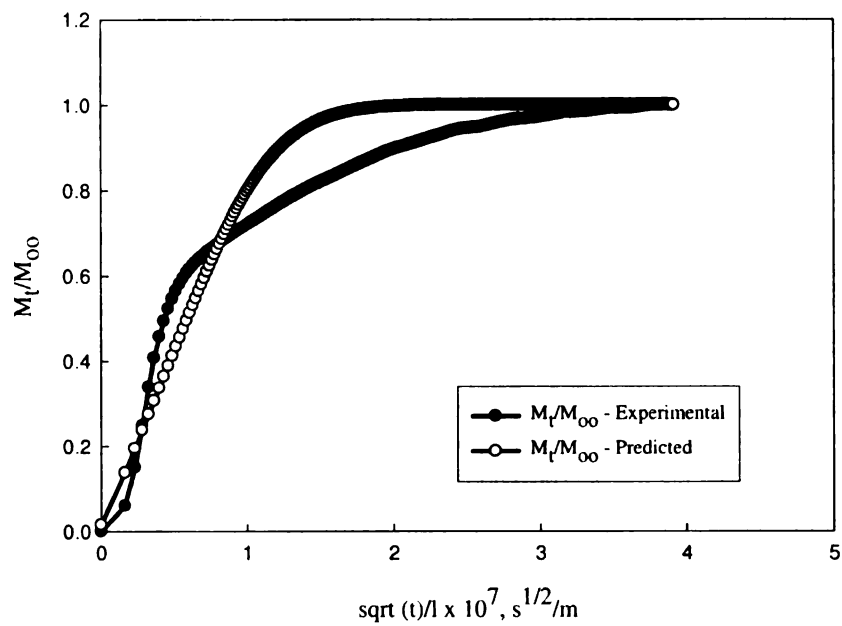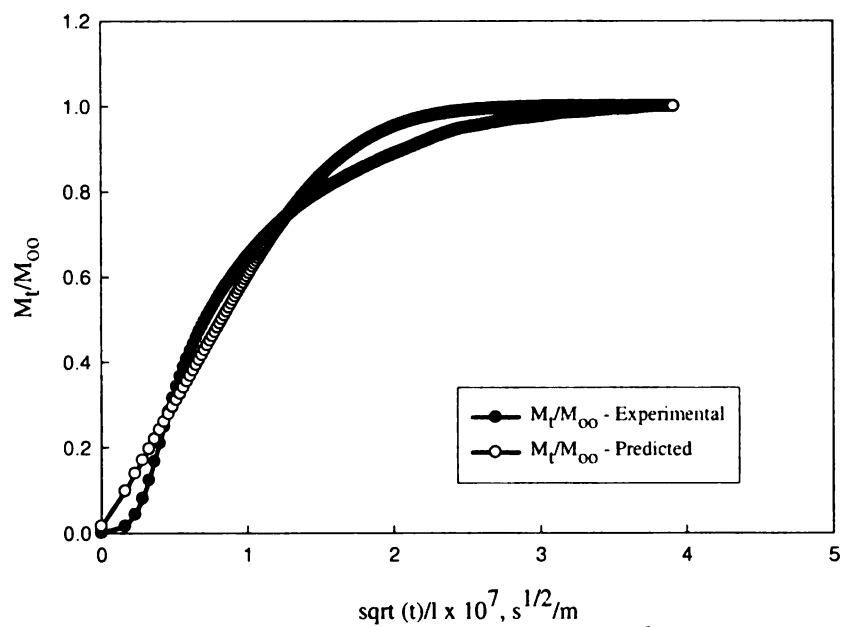
7   REFERENCES

1.   Gavara . R , et al., *Solubility of alcohols in ethylene-vinyl alcohol copolymers by inverse gas chromatography* Journal of Polymer Science Part B: Polymer Physics,, 1996. **34**(127): p. 1907-1915.

2.   Hernandez, R., Selke, S. E. M., Culter, J. D., *In Plastic Packaging.Properties, Processing, Applications and Regulations.* Mass Transfer in Polymeric Packaging Systems:Sorption , Diffusion, Permeation, and Shelf Life 2000, East Lansing: Hanser Publishers. 344-345.

3.   Hernandez-Munoz.P. , G. R., & Hernandez. J., *Evaluation of solubility and diffusion coefficients in polymer film–vapor systems by sorption experiments* J.Membr. Sci., 1999. **154**(195): p. 195-204.

4.   Morales.E. , A.J.L., *Polymer solubility parameters of poly(propylene oxide) rubber from inverse gas chromatography measurements.* Polym . J, 1996. **28**(127-130).

5.   Crank .J *The Mathematics of Diffusion , 2nd ed., Clarendon Press , Oxford,.* 1975.

6.   Wong.H.C , Bhethanabotla.V.R , and Campbell.S.W., *Sorption of benzene,toulene and chloroform by poly(styrene) at 298.15 K and 323.15 K using a quartz crystal microbalance.* Fluid Phase Equilibr., 1997. **139**(371).

7.   Shah.H.V. , H.E.L., & Arcucklee-Keil.G.A, *Vapor phase fuming Sulfuric Acid-Doped poly (p-phenylene vinylene) as a potential humidity sensor.* Journal of The Electrochemcial Society, 2001. **148**(9): p. H120-H127.

8.   Lu.C., *Mass determination with piezoelectric quartz crystal resonators* J Vac Sci Technol, 1975. **12**(578).

9.   Wong.C. H. , Bhethanabotla.V. R. , and C.S. W., *Sorption of benzene, toluene and chloroform by poly(styrene) at 298.15 K and 323.15 K using a quartz crystal microbalance.* Fluid Phase Equilibria 1997. **139**(371).

10.   Oliveira.N.S , et al., *Gas Sorption in poly(lactic acid) and packaging materials.* Fluid Phase Equilibria 2004. **222-223**: p. 317-324.

11. Auras.R, *Ph.D. Thesis , Michigan State University* 2004: p. 268.

12. Best, M.E. and C.R. Moylan, *Diffusion of Water into a Photopolymer Film.* Journal of Applied Polymer Science, 1992. **45**: p. 17-23.

13. Soule, A.D., et al., *Adsorption Modeling with the ESD Equation of State.* Langmuir, 2001. **17**: p. 2950-2957.

14. Hernandez . R , Selke. Susan , and J.D. Culter, eds. *Mass Transfer in Polymeric Packaging Systems:Sorption , Diffusion, Permeation, and Shelf Life* 2000, Hanser Publishers: East Lansing. 322-323.

15. Mikkilineni, S.P.V.N., D.A. Tree, and M.S. High, *Thermophysical Properties of Penetrants in Polymers via a Piezoelectric Quartz Crystal Microbalance.* 1995. p. 750-755.

16. J. L. Duda and J. S. Vrentas *Mathematical analysis of sorption experiments.* 1971. p. 464-469.

17. Barr . C . D *A Comparison of Solubility Coefficient Values Determined by Gravimetric and Isostatic Permeability Techniques,in School of Packaging, Michigan State University , East Lansing, MI.* 1997: p. 116.

18. Lu, Chih-Shun , and L. Owen, *Investigation of film-thickness determination by oscillating quartz resonators with large mass load.* Journal of Applied Physics, 1972. **43**(11): p. 4385-4390.

19. Johannsmann . D *Viscoelastic Analysis of Organic thin films on quartz resonators.* Macromol. Chem.Phys, 1999. **200**: p. 501-516.

20. Morray.B , et al., *PMMA Polymer film chacaterization using thickness shear mode (TSM) quartz resonator.* IEEE International Frequency Control Symposium and PDA Exhibition 2002.

21. Shirzai, H.M., *Quartz Crystal Microbalance/ Heat Conduction Calorimetry (QCM/HCC), a newtechnology capable of isothermal, high sensitivity, mass and heat flow measurements at a solid/gas interface.* A Thesis Submitted to the Faculty of Drexel University 2000.
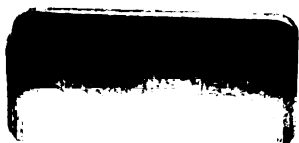
22. Martin, S.J., et al., *Equivalent-Circuit Model for the Thickness-Shear Mode Resonator with a Viscoelastic Film Near Film Resonance*. Anal. Chem ., 2000. p. 141-149.

23. Bandey, H.L., et al., *Modeling the Responses of Thickness-Shear Mode Resonators under Various Loading Conditions*. 1999. p. 2205-2214.

24. Sauerbrey. G Z.Phys., 1959. **155**: p. 206D-222 D.

25. Stockbridge. C . D Vacuum Microbalance techniques edited by K.Behrndt (Plenum, New York), 1966. **5**: p. 193.

26. EerNisse, E.P., *Methods and Phenomena , 7 , Applications of Piezoelectric Quartz Crystal Microbalances:*. Elsevier, 1984: p. 125-149.

27. Behrndt, K.H., *Long-Term Operation of Crystal Oscillators in Thin-Film Deposition* J.Vac.Sci. Technolo., 1971. **8**(622).

28. D.D.R., J.Vac.Sci. Technolo., 1973. **10**(126).

29. Lu.C., L.O., *Investigation of film-thickness determination by oscillating quartz resonators with large mass load*. J.Appl.Phys, 1972. **43**(4385).

30. Mantovani.F , et al., *A combination of vapor sorption and dynamic laser light scattering methods for the determination of the Flory parameter χ and the crosslink density of a powdered polymeric gel* . Fluid Phase Equilibr., 2000. **167**(63).

31. Mantovani.F. , C.I., Grassi.M. , & Lapasin. R., Fluid Phase Equilibr., 2000. **167**(63).

32. Behling .C , Hauptmann .P, and L. R, *Fast Three Step Method for Shear Moduli Calculation from Quartz Crystal Resonator Measurements*, in *IEEE Transactions on Ultrasonics, Ferroelectrics , and Frequency Control*. 1999.

33. King. W. H *Piezoelectric Sorption Detector*. Anal. Chem, 1964. **36**(9): p. 1735-1739.

34. Mikkilineni.S.P.V.N. , High.M.S, and Tree.D.A, *Thermophysical Properties of Penetrants in Polymers via a Piezoelectric Quartz Crystal Microbalance.* J.Chem. Eng.Data, 1995. **40**(750-755).

35. Galla.H-J., J.A., Steinem.C., Angewandte Chemie, Int Edition, 2000. **39**(4004).

36. Bonner . D . C , Holste . J. C , and Saeki . S *Sorption of organic vapors by polystyrene.* J.Polym. Sci.,Polym.Phys.Ed., 1981. **19**(2): p. 307-320.

37. Zhang.C. , et al., *Glassy Polymer-Sorption Phenomena Measured with a Quartz Crystal Microbalance Technique.* Journal of Polymer Science: Part B: Polymer Physics, 2003. **41**: p. 2109-2118.

38. Forest . J. A., Borjesson.L , and Mattsson.J *Using Adhesion to probe viscoelasticity of polymer film surfaces:A quartz crystal microbalance study.* Eur. Phys.JE, 2002. **8**: p. 129-136

39. Mecea.V and Bucur.R.V., *Piezoelectric quartz crystal microbalance (PQCMB) for sorption studies under dynamic conditions.* J.Vac.Sci.Technol., 1980. **17**.

40. Vogt B. D. , et al., *Effect of Film Thickness on the validity of the Sauerbrey Equation for hydrated Polyelectrolyte Films.* J.Phys.Chem. B, 2004. **108**: p. 12685-12690.

41. Banda.L., A.M., & Mckenna.G. B. , *Errors Induced in Quartz Crystal Mass Uptake Measurements by Nongravimetric effects:Considerations beyond the EerNisse Caution.* Joural of Polymer Science :Part B :Polymer Physics, 2006. **44**: p. 801-814.

42. Frye.G. C and Martin. S. J *Dynamics and response of polymer coated acoustic wave devices: Effect of viscoelastic properties and film resonance.* Analytical Chemistry, 1994. **66**: p. 2201-2219.

43. Auras.R., Harte .B., & Selke.S., *An overview of Polylactides as Packaging Materials.* Macromol.Biosci., 2004. **4**: p. 835-864.

44. Shogren, R., *Water Vapor Permeability of Biodegradable Polymers.* Journal of Enviornmental Polymer Degradation, 1997. **5**(2): p. 91-95.

45.   Tsuji, H., et al., *Water Vapor Permeability of Poly(lactide)s:Effects of Molecular Characteristics and Crystallinity.* Journal of Applied Polymer Science, 2006. **99**: p. 2245-2252.

47.   Auras.R., Harte .B., & Selke.S., *Poly(Lactic Acid) Films as Food Packaging Materials.* Macromol.Biosci . 2004.

48.   L . Bao , et al., *Gas Permeation Properties of poly(lactic acid) revisited.* Journal of Membrane Science, 2006. **285**: p. 166-172.